A NOVEL OPTICAL DYNAMIC CLAMP PLATFORM USING IPSC-DERIVED CARDIOMYOCYTES FOR DRUG SCREENING

A Dissertation

Presented to the Faculty of the Weill Cornell Graduate School

Of Medical Sciences

In Partial Fulfillment of the Requirements for the Degree of

Doctor of Philosophy

By

Bonnie Quach

May 2019

A NOVEL OPTICAL DYNAMIC CLAMP PLATFOR USING IPSC-DERIVED CARDIOMYOCYTES FOR DRUG SCREENING

Bonnie Quach, Ph.D.

Cornell University 2019

iPSC-derived cardiomyocytes (iPSC-CMs) are a potentially advantageous platform for drug screening because they provide a renewable source of human cardiomyocytes and can be patient specific. One obstacle to their implementation is their neonatal-like electrophysiology, which reduces relevance to adult arrhythmogenesis. One method to address this problem is to electrically mimic deficient currents in iPSC-CMs using a technique called dynamic clamp. Mimicking the missing inward rectifying potassium current, $I_{K1,}$ in iPSC-CMs via dynamic clamp pushes action potential characteristics to resemble more closely an adult cardiomyocyte. However, this method is technically challenging and low throughput, limiting its practical uses for more high-throughput applications, such as large-scale drug screening. To address this, we aim to create an optically-controlled version of dynamic clamp, which because of its contactless nature, could be high-throughput and not limited to a single-cell format.

The ideal platform would use optogenetics to supplement the deficient current and use a fluorescent voltage indicator to measure the membrane potential. Optogenetic tools are commonly used statically and to either stimulate or

cease electrical activity. This thesis presents a proof of principle of using optogenetic tools in lieu of an electrode by developing an optical dynamic clamp (ODC) platform that uses an LED to dynamically activate a hyperpolarizing opsin, ArchT, to generate an I_{K1}-like current. This ODC platform was verified with the standard electrode-based dynamic clamp (EDC) and gave a similar output, demonstrating a proof-of-concept that optogenetics are able to mimic an electrode. The ODC platform was challenged with E-4031, bayK 8664, terfenadine, and verapamil. The ODC platform was able to detect effects of the drugs on action potential characteristics similar to EDC, but the ODC platform did not consistently yield results identical to EDC. Possible reasons and limitations are discussed. With further development, the ODC platform can possibly be refined to be more precise, but maturation of iPSC-CMs may still be needed to make the platform more relevant to adult electrophysiology. The ODC platform has the potential to expand on the possibilities of dynamic clamp by enabling more relevant formats, such as monolayers, co-cultures or with other engineered platforms.

BIOGRAPHICAL SKETCH

Bonnie Quach is a native New Yorker who attended Bronx High School of Science and Wesleyan University. After graduating, she was a “private English tutor” in France and went to Alaska before she joined the Pharmacology program at Weill Cornell Graduate School in 2012.

She joined the Christini lab in 2014.

DEDICATION

To all the people who gave me coffee and cookies

ACKNOWLEDGMENTS

I would like to thank David J. Christini and Trine Krogh-Madsen for taking a chance on me and saving me when I was lab-less. My wonderful and inspiring former and current lab members, specifically Francis Ortega, Tashalee Brown, Tanmoy Lala Das, Yazhi Yang and Drew Tilley. Thank you all for mentoring me in science and in life.

My support networks:

Quach Family Clan
Outdoor Adventure Club
Pharm (and Affiliates) Delinquents
Wes Golden Girls
My Bronx Science Crew

Thank you is a huge understatement.

This work was financially supported by the Ruth L. Kirschstein Predoctoral Individual National Research Service Award to B.Q. (5 F31 HL134209-02), the PhRMA Foundation Predoctoral Fellowship to B.Q. and NIH RO1 R01EB016407 to D.J.C.

TABLE OF CONTENTS

LIST OF FIGURES

LIST OF TABLES

CHAPTER ONE

BACKGROUND

1.1 Introduction

The goal of drug discovery is to develop a drug to correct an underlying cause of some disease pathology by altering a specific pathway, but off-target effects can be lethal. Prior to a first-in-human trial, researchers extrapolate results from *in vitro* and *in vivo* models to predict whether a therapeutic is safe and effective. Unfortunately, our current assays can only predict about 80% of cardiovascular toxicity seen in clinical trials [1]. Signs of adverse cardiac events in the clinic typically present as arrhythmias, myocardial infarction, congestive heart failure, and coronary heart disease. In addition, cardiovascular toxicity is one of the greatest causes of drug attrition [2]: it is one of the main reasons for project or

Phase	Non-clinical	Phase I	Phase I–II	Phase III/ post-approval	Post-approval	Post-approval	Post-approval
Information	Causes of attrition	Serious ADRs	Causes of attrition	ADRs on label	Serious ADRs	Withdrawal from sale	Withdrawal from sale
Source	Car (2006)	Sibille et al. (1998)	Olson et al. (2000)	BioPrint® (2006)	Budnitz et al. (2006)	Fung et al., (2001)	Stevens & Baker (2009)
Sample size	88 CDs stopped	1,015 subjects	82 CDs stopped	1,138 drugs	21,298 patients	121 drugs	47 drugs
Cardiovascular	27%	9%	21%	36%	15%	9%	45%

Figure 1.1: Percent of drugs that were stopped during different phases of drug development or withdrawn from the market due to cardiovascular toxicity.
Adapted with permission from Ref [1].
ADRs = Adverse Drug Reactions; CDs = Candidate Drugs

clinical trial termination [1] and 45% of drugs withdrawn from the market from 1975-2007 were due to cardiac toxicity [3] (Figure 1.1). False negatives put patients at risk while false positives prevent the development of potentially

effective therapeutics. This is further discussed in Section 1.2. The lack of translation from pre-clinical models to the human population points to a huge unmet need for more sensitive and specific predictive models that better recapitulate human biology.

The lack of translation from *in vivo* safety and efficacy experiments to clinical outcome could be largely attributed to the irrelevance of non-human models that are typically used in experiments to recapitulate human biology [1], [4], [5]. With the advent of human-derived induced pluripotent stem cell (iPSC)-derived cell types, it is now possible to study human cells, which can even be directly derived from patients. By forcing expression of the Yamanaka reprogramming factors, researchers can reprogram adult tissue into pluripotent stem cells and differentiate them into a desired cell type [6]. This revolutionary technology overcomes many research hurdles: first, providing an ethical and unlimited resource of human cells that are difficult to obtain, such as cardiomyocytes, and second, generating an *in vitro* model that is genetically identical to a patient of interest. iPSC-CMs would benefit pre-clinical research by providing an easily-accessible human *in vitro* model for experimental studies. As an additional benefit, patient-derived iPSC-CMs can recapitulate the patient's disease pathology, which is especially advantageous for rare and orphan diseases. Patient-derived iPSC-CMs are useful to assess the efficacy of a drug to treat that disease or identify potential toxic side effects in potentially vulnerable patient populations.

The literature is replete with evidence that patient-specific iPSC-derived tissues possess a similar pathology to those characterized in patients and they respond predictably to well-characterized drugs [7]–[19]. For example, iPSC-CMs derived from LQTS2 patients treated with the currently available therapeutics, nifedipine, pinacidil and ranolazine, demonstrated that these drugs rescued the aberrant electrophysiological phenotype and could be beneficial for LQTS2 patients [7]. Another example is that iPSC-CMs from patients with Pompe disease recapitulated the glycogen accumulation phenotype and treatment with L-carnitine improved bioenergetic markers [8]. With this technology, researchers have access to patient-specific models that they can fully manipulate to thoroughly test hypotheses that would be impossible to test in patients. However, the great potential of this technology is limited by the inability to differentiate these iPSCs into organized and mature adult tissue. With iPSC-derived tissues, including iPSC-derived cardiomyocytes (iPSC-CMs), being phenotypically stuck in a more fetal-like state, there are limitations to using them to reflect adult human behavior. Despite the immature nature of iPSC-CMs, these cells are still an attractive *in vitro* model due to the difficulty of obtaining human adult cardiomyocytes. A greater dissection of the chemical and physical signals that program a pluripotent stem cell to become a structurally and functionally mature cardiac tissue would be needed to produce fully mature cells.

One approach to addressing the electrical immaturity of iPSC-derived cardiomyocytes (iPSC-CMs) is to use a powerful electrophysiological tool, dynamic clamp. Dynamic clamp can be used to supplement deficient currents in iPSC-CMs to make iPSC-CMs appear electrically mature in order to provide results that resemble adult behavior, rather than fetal cardiomyocytes [20]–[22]. This technique will be further described in detail in Section 1.5. Particular focus will be given to the inward rectifier potassium current (I_{K1}) in this thesis. We are developing an optically-controlled platform based on the principles of dynamic clamp and designed to use iPSC-CMs with application for drug screening. The optical dynamic clamp (ODC) system aims to overcome the technical difficulty of obtaining a whole-cell patch to enable high-throughput use of dynamic clamp and improve the biological relevance of iPSC-CMs to human adult cardiac electrophysiology.

The idealized version of the ODC system would use optical tools to replace the function of an electrode: to generate a specified current and to report the membrane potential. Optogenetic tools have been used to generate an unspecified and static current, but this level of control is inadequate for the purposes of dynamic clamp, which will be further explained in Section 1.5. Chapter 2 will demonstrate how we are able to control the optogenetic tool, ArchT, and mimic the missing biological current I_{K1} in iPSC-CMs. This provides a proof-of-concept of using optogenetics to dynamically generate a current and to realize the ODC platform. After establishing the first iteration of the ODC

platform, Chapter 3 will explore the practical application of the ODC platform for drug screening in single cells by using well-characterized ion channel modulators to investigate how the ODC platform performs compared to the standard dynamic clamp platform. Chapter 4 will describe the limitations and future directions of the ODC system.

1.2 The need for more predictive cardiovascular toxicity assays

It is clear that a drug should be deemed as safe before it is approved. However, between 1975 and 2000, of the FDA-approved drugs that were issued new black box warnings, about 24% (11 of 45 drugs) were due to cardiovascular toxicity and 4 out of the 16 FDA-approved drugs withdrawn from the market during this period were also due to cardiovascular toxicity [23]. It turns out that this issue is a lot more complicated than finding a binary safe/unsafe answer, since certain populations that may not be accounted for during pre-clinical and clinical trials may be more susceptible to adverse drug reactions (ADR). This indicates that it is hard for clinical trials to ensure the safety of all patients until it reaches a larger and more diverse population. As more approved drugs were found to be responsible for cardiovascular toxicity, researchers began to identify common features of these drugs and developed assays to identify them earlier in development.

1.2.1 The Classic Paradigm: I_{Kr} inhibition → QT prolongation → Torsade de Pointes → Ventricular Fibrillation

Figure 1.2: Example ECG of a patient with prolonged QT interval
ECG of a patient with QT prolongation (A) that progressed into Torsade de Pointes (B). Adapted with permission from Ref [27].

Torsade de Pointes (TdP) is a polymorphic ventricular tachycardia that produces a particular pattern on an electrocardiogram (ECG), where the QRS axis is twisting around a baseline, hence the name “twisting of points”. The clinical incidence of Torsade de Pointes (TdP) indicates the potential development of a drug-induced arrhythmia and leads to a drug’s withdrawal from the market [24]–[26].

The phenomenon was first described in 1964 in patients with “quinidine syncope” [28]. This was one of the first clinical demonstrations that drugs could induce tachycardia and fibrillation in patients, but it wasn’t understood how. Dessertenne coined the term “Torsade de Pointes” in 1966 to describe the distinct ECG pattern seen in patients with drug-induced tachycardia and fibrillation, after discovering that although the patient had atrioventricular block,

the ECG pattern was produced from episodes of polymorphic ventricular tachycardia (Figure 1.2) [29]. Upon further investigation of these ECGs, it was found that QT interval prolongation, dispersion and alternans increased the risk of TdP by altering the QT interval. Inhibition of the main repolarizing potassium currents, I_{Kr} (hERG/KCNH2 gene) and I_{Ks} (KVLQT gene), has been shown to be one of the main underlying mechanisms behind drug-induced QT prolongation by delaying repolarization of the AP, thereby increasing the action potential duration (APD) (Figure 1.3) [30]–[34]. A lot of emphasis has been placed specifically on the repolarizing current, I_{Kr}, because a lot of toxic non-cardiac drugs have been shown to affect I_{Kr} and the majority of mutations found in patients with congenital Long QT Syndrome (LQTS) were present in KVLQT (75 of 177 mutations) and hERG (80 of 177 mutations) [35], [36]. As a result, I_{Kr} inhibition and QT interval prolongation receives a lot of weight in making a pre-clinical assessment on the safety of a drug.

The issuance of new black-box warnings and the withdrawal of FDA-approved drugs due to cardiovascular toxicity brings into question the extent at which pre-clinical studies predict what happens in the clinic. Verapamil is one of several drugs that has taught us that hERG/I_{Kr} inhibition should not be the sole determinant when assessing for drug-induced toxicity. Verapamil is an I_{Kr} antagonist but has a low arrhythmogenic risk at therapeutic concentrations due to its other ionic effects, which offset the deleterious consequences of I_{Kr} inhibition on the QT interval [37]. Assessing for drug-induced cardiac toxicity

becomes even less straightforward since QT prolongation does not always lead to TdP, and TdP does not always lead to ventricular fibrillation [27], [28], [38]–[42]. This suggests that better predictive markers and more comprehensive assays need to be developed to assess the potential of a drug to induce arrhythmia in patients.

The importance of a predictive cardiovascular toxicity assay is to first and foremost protect patients, but false positives prevent the development of potentially effective therapeutics. A survey to safety pharmacologists, toxicologists and pharmacologists on pro-arrhythmia liability assessment in drug development conducted and published by the Safety Pharmacology Society (SPS) in 2017 revealed that 60% of survey responders would abandon a potentially beneficial drug if it displayed I_{Kr} inhibition at clinically relevant concentrations [43].

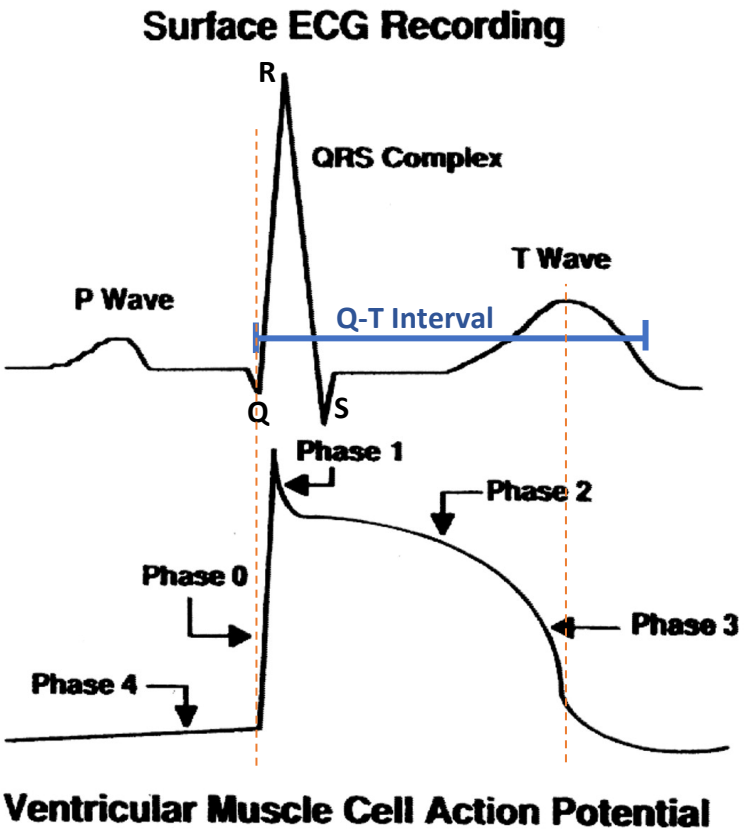

Figure 1.3: The relationship between different phases of the action potential from a ventricular myocyte and features of an ECG.
The QT interval length (blue segment) is associated with action potential duration (dashed orange lines). Adapted with permission from Ref [44].

1.2.2 The CiPA initative: developing a standardized protocol to evaluate pro-arrhythmic risk

Driven by the need for improved predictive cardiovascular toxicity assays and the development of iPSC-derived cardiomyocytes, national and international regulatory bodies have collaborated to create the Comprehensive *in vitro* Pro-Arrhythmia Assay (CiPA) initiative to stimulate research and development of a highly sensitive and selective pro-arrhythmia assay protocol to assess the toxicity of lead compounds prior to entering Phase I clinical trials [45]. The general principle of the CiPA approach consists of two phases: one, to determine the effect of drugs on cardiac ion channels and *in silico* cardiac models, and two, to validate the results from phase one in iPSC-CMs.

Traditionally, assessment of pro-arrhythmia risk is evaluated with assays that measure the effect of a compound on specific ion channels (particularly I_{Kr}) and drug-induced modulation of action potential (AP) waveform or propagation using non-human *in vitro* or *ex vivo* models, or changes in cardiac function of non-human *in vivo* models. Table 1.1 shows that SPS responders rely on different types of assays to judge the clinical potential of drug-induced cardiovascular toxicity, reflecting the lack of standardization across institutions [43]. The survey also showed that among the responders, 51% frequently record drug-induced effects on cardiac AP directly, 46% of responders frequently use iPSC-CMs, 23% of responders frequently use *in silico* studies in assessment of drug safety

and 39% of responders reported that their company never conducted *in silico* studies in the last 5 years [43]. Implementing future CiPA guidelines would require a lot of companies to revamp their drug toxicity screening approach. The SPS survey also illustrates how incongruous the methods to assess cardiovascular toxicity are across different research institutions: which cardiac ion channels are evaluated, which features of an EKG are important, which (if any) positive controls used, temperature at which the experiment was conducted, etc. [43]. The CiPA initiative would establish a clear guideline, thereby standardizing practices across institutions and increasing reproducibility across labs. Also, by designing a multi-faceted approach, the CiPA approach would be sensitive to a greater number of mechanisms behind cardiac toxicity.

Table 1.1: Responders across institutions rely on different models, assays and preparations when assessing drug-induced cardiovascular toxicity. Published results from the SPS survey [43].

Which of the following cardiac/cardiovascular assays has your company used in the last 5 years?			
Answer options	**Frequently used**	**Rarely used**	**Response count**
Cell lines stably expressing ion channels for determination of drug block potency	89%	11%	66
ECG recording using implanted telemetry technology	88%	12%	67
Jacketed External Telemetry (JET)	62%	38%	63
Ion channel binding assays	57%	43%	68
Anesthetized animal models	53%	47%	58
Cardiac action potential recordings (Purkinje fiber, papillary muscle, others…)	51%	49%	61
Human stem cell-derived or induced pluripotent stem cell cardiomyocytes (iPSC-CM)	46%	54%	68
hERG (I_{Kr}) channel trafficking	42%	58%	72
Isolated tissue bath preparations	41%	59%	63
Isolated Langendorff heart	38%	62%	63
Isolated cardiac wedge preparation	18%	82%	51
Proarrhythmia animal models	12%	88%	49
Zebrafish assays	4%	96%	47

1.3 The promises and potential of iPSC-derived cardiomyocytes

With the emerging iPSC technology, researchers without readily accessible human cardiomyocytes are able to derive their own or purchase them. The seminal paper describing the generation of iPSCs was published in 2006 [6]. John B. Gurdon and Shinya Yamanaka received the Nobel Prize in Physiology or Medicine relatively quickly after this publication in 2012, reflecting its importance and paradigm shifting influence [46]. In addition, there has been considerable development in generating pure cultures of chamber-specific cardiomyocytes and other cardiac cell types, allowing for investigation of precise questions [47]–[55]. iPSC-CMs have been shown to recapitulate the disease phenotype of patients *in vitro*, demonstrating its relevancy as an *in vitro* model. Table 1.2 lists some patient-specific iPSC-CM disease models created for studying disease pathology, target identification, and/or drug screening. The following section briefly provides examples in the literature that suggests the utility of iPSC-CM models for drug development.

1.3.1 Ion channelopathies

LQTS1, LQTS2, and LQTS3 are characterized by the gene containing the mutation that disrupts the function of an ion channel and a prolonged QT interval. iPSC-CMs derived from LQTS patients with prolonged QT intervals exhibit the expected effect of ion channel dysfunction *in vitro*, namely prolonged

APD and field potential duration (FPD), and appearance of pro-arrhythmic depolarizations that occur prior to action potential termination, called early after depolarizations (EADs) [7], [56]–[59]. An isoproterenol challenge also increased the appearance of EADs as expected, while clinically-used anti-arrhythmic drugs reduced the number of EADs, demonstrating the potential for drug screening [7], [56], [57]. The patient-derived iPSC-CMs also demonstrated increased sensitivity to cardiotoxic drugs, further implicating their potential in testing for drug toxicity in vulnerable populations [58]. Another great application for iPSC technology to produce well-characterized genetically-based disease models is to induce the known mutation(s) in iPSCs derived from healthy patients and then differentiate the iPSCs into cardiomyocytes [60]. This is especially useful in cases where patient material is not readily accessible.

1.3.2 Congenital Cardiomyopathy

iPSC-CMs derived from patients with congenital cardiomyopathies also reflect the patient's phenotype. One type of congenital cardiomyopoathy, Arrhythmogenic Right Ventricular Cardiomyopathy (ARVC) is caused by a mutation in plakophilin-2 (PKP2), leading to desmosomal abnormalities, fatty infiltration, decreased cardiomyocytes in the right ventricle, and life-threatening ventricular arrhythmias. ARVC patient-derived iPSC-CMs show the anticipated increased lipid accumulation, structural disarray and decreased connexin 43 expression [61]–[63]. Caspi et al. (2013) and Ma et al. (2013) demonstrated

using these patient-derived iPSC-CMs for drug development by showing that inhibition of drug-target candidates can reverse or prevent further progression of the disease phenotype [61], [62]. Kim et al. used these *in vitro* models to dissect the molecular mechanisms underlying the pathology [63]. iPSC-CMs are useful for studying the effects of a mutated protein on cardiac function and screen potential drug candidates.

1.3.3 Multi-system diseases

Patient-derived iPSC-CMs can also reflect the cardiac disease phenotype of diseases that affect multiple tissue and organ systems. For example, Fabry disease where mutation in the *GLA* gene causes accumulation of globotriaosylceramide, particularly in blood vessel cell lining. This causes abnormalities in multiple organ systems, such as skin, kidneys, heart, and nervous system. To design effective therapeutics, it can be fruitful to investigate the effect of the disease on one organ system in isolation, in order to discriminate between if the decline of the organ system is a consequence of distal system failures or if the selected organ system is one of the primary causes of poor patient prognosis. Because of the severity of these multi-organ diseases, such as LEOPARD syndrome, Fabry Disease, and Barth Syndrome, patients tend to die from cardiomyopathy [8], [9], [64]–[66]. Again, iPSC-CMs derived from these patients show the expected phenotype that is observed in patients and can be used for drug screening by studying the molecular

consequences of the mutation and identifying novel therapeutic targets [8], [9], [64]–[66].

Table 1.2: Examples of iPSC-CM disease models created from patient tissue

Disease	Year	Reference
LQTS1	2010	[56]
LEOPARD Syndrome	2010	[64]
Pompe Disease	2011	[8]
LQTS2	2011	[7]
	2011	[57]
	2012	[58]
Familial Dilated Cardiomyopathy	2012	[67]
ARVC	2013	[61]
	2013	[63]
	2013	[62]
LQTS3	2013	[59]
Timothy Syndrome	2013	[68]
T2DM	2014	[9]
Fabry Disease	2014	[65]
Barth Syndrome	2014	[66]

LQTS = Long QT Syndrome
ARVC = Arrhythmogenic Right Ventricular Cardiomyopathy
T2DM = Type 2 Diabetes Mellitus

1.4 The restrictions and reality of iPSC-derived cardiomyocytes

iPSC technology has shown a lot of promise for drug discovery, cell-based therapies, and basic research. However, its actual applicability and use is stunted due to incomplete differentiation protocols causing iPSC-CMs to be in a fetal-like stage of development. Adult cardiomyocytes are rod-shaped and undergo a hypertrophic change after birth where they become 30-40 times their neonatal size [69], [70]. iPSC-CMs are smaller than adult cardiomyocytes and have a circular, triangular or multi-angled morphology, similar to neonatal cardiomyocytes, possibly because they have not undergone the hypertrophic change. iPSC-CMs also lack T-tubules and have disorganized sarcomeres, causing iPSC-CMs to have a decreased contractile force compared to adult cardiomyocytes [71]–[73]. Unlike adult cardiomyocytes, iPSC-CMs rely on glycolysis as their primary source of energy and have less mitochondria by volume [74]–[76]. iPSC-CMs also express more fetal-associated isoforms of certain genes. For example, iPSC-CMs mostly express the fetal troponin I (*TNNI*) isoform, slow skeletal *TNNI* (ssTnI), and express little adult cardiac *TNNI* (cTnI), whereas in adult cardiomyocytes, ssTnI is replaced by cTnI [77], [78]. iPSC-CMs also have abnormal calcium-handling properties, which leads to spontaneous electrical events and disrupts other Ca^{2+}-dependent pathways and voltage-gated channels [79], [80].

It is difficult to fully mimic the conditions of cardiac development *in vitro*, namely extracellular matrix remodeling, hemodynamic load, hormones, and electrical, chemical and physical signals from neighboring cells [81]–[85]. The SPS survey showed that 75% of responders thought that iPSC-CMs are a valuable addition to pro-arrhythmia screening assays but only 21% believe that they are representative of adult cardiomyocytes and provide reliable data as a nonclinical safety assay [43]. Considerable tissue engineering efforts have been able to push maturation of iPSC-CMs, for example via substrate support, constant electrical stimulation, cyclical stretch, co-culturing, and 3D culturing, but more research and development is needed [86].

1.4.1 Electrical abnormality of iPSC-CMs

As described below, the neonatal-like electrophysiological profile of iPSC-CMs is a major barrier for research. On top of that, iPSC-CM AP characteristics (APD_{90}, maximum diastolic potential (MDP), triangulation, upstroke velocity, etc.) vary from lab to lab, making it difficult to compare across the literature. Despite this, iPSC-CMs consistently have decreased I_{K1} (similar to fetal cardiomyocytes) and I_{Ks} as measured by voltage clamp. They also have a “funny current, $I_{f,}$ that is typically present in only fetal and embryonic cardiomyocytes and adult cells from the specialized conduction system of the heart [87]. I_f, also known as the pacemaker current, activates at more hyperpolarized potentials and causes the diastolic membrane potential to slowly depolarize, leading to a

spontaneous action potential. The lack of I_{K1}, an inward rectifying potassium current, depolarizes the membrane potential and increases APD [88]. iPSC-CMs also have immature calcium-handling properties that lead to spontaneous calcium release and spontaneous action potentials [80]. *In silico* models demonstrate that the abnormal presence (particularly Ca^{2+} currents) and absence (notably I_{K1}) of currents have an effect on how other currents activate, such as I_{Na}, NCX and RyR [79], [80], [89]. The depolarized membrane potential, due to the lack of I_{K1}, decreases sodium channel reactivation. Spontaneous calcium release from intracellular stores activates the NCX, causing it to transport more sodium into the cell, and can induce RyR activation. Because of these abnormalities, iPSC-CMs have a slower upstroke velocity, a depolarized MDP, a more triangular AP morphology, and exhibit spontaneous activity (Figure 1.5A and C). With abnormal current activation and behavior, it is difficult to ascertain whether the aberrant effect of a drug resulted from either affecting a critical target that disrupts the system's behavior, or if the aberrant effect was a consequence of the abnormal system that is not applicable to patients. Also, the heterogeneity of channel expression and maturity in iPSC-CMs affects the reproducibility of results to certain clinically arrhythmogenic drugs or ion channel agonists/antagonists [90]–[93]. iPSC-CM electrophysiology can consistently yield predictable results of drug-induced I_{CaL} inhibition and hERG/I_{Kr} inhibition, but the presence or inhibition of other currents are not consistently inhibited across literature [91], [93]. Because of these limitations, researchers must be

wary about extending conclusions drawn from experiments with iPSC-CMs to adult behavior.

1.5 Dynamic clamp is a powerful tool

Dynamic clamp is an electrophysiological technique that utilizes a mathematical model to calculate a desired electrical output (or target current) to be delivered into a target cell and measures the effect of the target current on the cell. The mathematical model can represent a specific current, inhibition of a current, or another cell. The user can adjust the parameters of the model in order to test different hypotheses, such as the effect of a slower inactivation gate, the effect of decrease conductance or amount of coupling to other cell types. Dynamic clamp was first introduced in 1979 and was used to electrically simulate coupling between two cells that were not in contact by measuring the membrane potential of two separate beating cell clusters and injecting a scaled amount of current into the other cell to mimic gap junctional resistance [94]. In the 90s, dynamic clamp was used to study gap junctional coupling between individual cardiomyocytes, and mimic disease states that affected coupling between cells [95]–[97]. The uses and configurations of dynamic clamp have expanded with the increase in computational power, but the principle of the technique remains the same.

1.5.1 Theory and uses of dynamic clamp

In order to execute dynamic clamp, the user needs:

1) Electrical access to a target cell(s) via patch clamp to measure the cell's membrane potential (V_m);
2) A mathematical model describing the target current (I_{target}); and
3) Software and hardware to coordinate measuring the V_m, calculating I_{target}, and injecting I_{target}, in real time.

To answer a research question, a mathematical model is created to reflect an electrical current of interest: an endogenous current, or a modified current, a current flowing through gap junctions, etc. At every timestep, the mathematical model calculates I_{target} based on the measured V_m of a cell and injects I_{target} into another, or back into the same cell (Figure 1.4). The output V_m of the injected target cell is a consequence of adding I_{target}.

Dynamic clamp can be performed in several different configurations. One configuration allows the user to simulate gap junctional coupling by patching two separate target cells or clusters of cells (Figure 1.4A). The V_m of both patched cells would be measured, and the mathematical model would calculate how much current should be injected into one or both cells to simulate unidirectional or bidirectional gap junctional coupling, respectively. The user would define the parameters (e.g., max conductance through gap junctions,

voltage dependence of gap junctions) of the model and could modulate them in the experiment to determine the effect on the cells [97]–[101].

Dynamic clamp could also couple a target cell to a virtual cell or current. Only one target cell would be patched and the V_m would be input into a mathematical model that represents another current, cell, or 2D sheet of cells (Figure 1.4B). The user could determine the effect of the mathematical model on the target cell's electrical output. This could mimic the expression or inhibition of a current in the target cell, electrical coupling to a cell that would be difficult to patch, or the influence of a defined 2D sheet on the cell's activity [22], [90], [100], [102]–[105].

Dynamic clamp can also be used to study channel activity during an AP (Figure 1.4C). The channel of interest, which could incorporate a mutation, would be expressed in a non-electrically active cell. This requires patching the expression system and the target cell. The expression system would be voltage clamped to the V_m of the target cell and the current from channel of interest would be measured. That current would then be injected back into the target cell. This allows researchers to study the effect of the expressed channel on AP characteristics and the activation pattern of the channel during an AP.

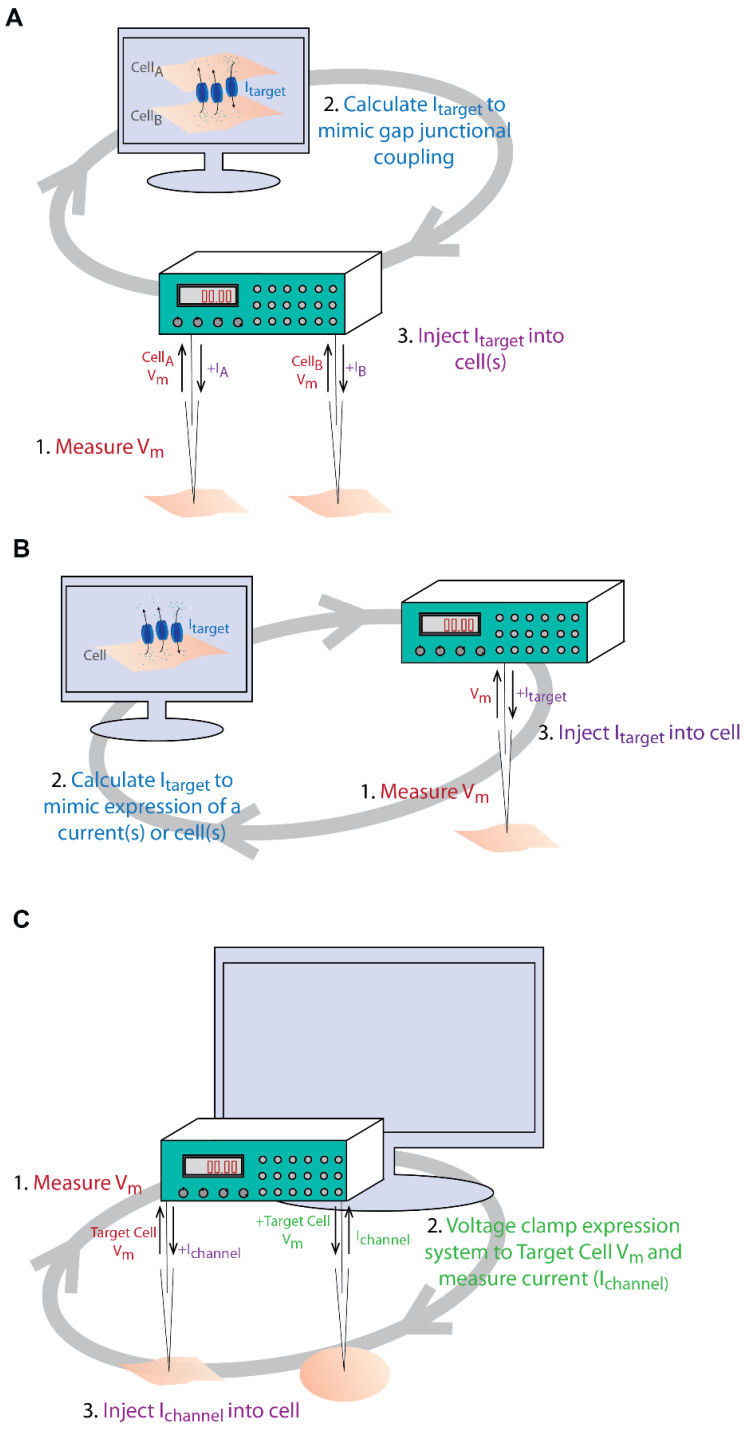

Figure 1.4: Various configurations of dynamic clamp
Panel A demonstrates how dynamic clamp can be used to simulate coupling between two separate cells. Panel B shows the dynamic clamp configuration to couple a cell to a virtual current. Panel C illustrates how dynamic clamp can couple the target cell to a channel expressed *in vitro*.

1.5.2 Using dynamic clamp to mimic I_{K1} in iPSC-CMs

1.5.2.1 I_{K1}: Inward rectifier potassium current

I_{K1} plays a predominant role in stabilizing the membrane potential and in repolarization in ventricular and atrial cardiomyocytes. It is encoded by the *KCNJ* gene subfamily and the channel composition includes Kir 2.x. I_{K1} allows inward currents at potentials more negative than the equilibrium potential of K^+ (E_K) and an outward current at potentials more positive to E_K. As an inward rectifier, at more positive potentials during the plateau phase of the AP, I_{K1} channels are inhibited by divalent cations and polyamines, decreasing the outward current that can be generated and allowing for the plateau phase of the AP. When looking at the current produced at different membrane potentials, the decreasing outward current produced at more positive potentials is described as the negative slope conductance [106].

I_{K1} in atrial cardiomyocytes has different properties from I_{K1} in ventricular cardiomyocytes. I_{K1} in atrial cardiomyocytes has less of a negative slope conductance than ventricular cardiomyocytes and does not rectify completely. I_{K1} is more predominant in ventricular cardiomyocytes than atrial cardiomyocytes. The tissue-specific properties of I_{K1} are reflected in the differences between ventricular I_{K1} mathematical models and atrial I_{K1} mathematical models.

1.5.2.2 Addition of I_{K1} in iPSC-CMs changes AP morphology

Dynamic clamp has been used in iPSC-CMs to study the impact of the missing currents on AP morphology. I_{K1} was electrically mimicked in iPSC-CMs, resulting in a drastic change in AP morphology (Figure 1.5). These dynamic clamp experiments showed that I_{K1} is important for maintaining the resting membrane potential, suppressing spontaneous activity, increasing the upstroke velocity, increasing the action potential amplitude (APA) and shortening the APD (Figure 1.5) [22], [90], [107]–[110]. Using dynamic clamp to supplement the missing I_{K1} current is important to push AP morphology to be more electrically adult-like. Overexpression of *KCNJ2* in iPSC-CMs reduced spontaneous activity and affected AP characteristics similarly to using dynamic clamp to inject I_{K1} [111]. In addition, these iPSC-CMs yielded a clear response to I_{Kr} inhibition, which was masked by further depolarization and reduced AP formation without *KCNJ2* expression [111]. Bett et al. (2013) demonstrated that I_{K1} addition was necessary to observe a measurable effect of Ca^{2+} agonism on AP morphology as in its absence MDP would be too depolarized for AP generation [90]. These experiments demonstrate the importance of I_{K1} expression in iPSC-CMs for drug development. Dynamic clamp could be used to transform the immature iPSC-CM electrical phenotype to resemble that of an adult cardiomyocyte, by correcting for the main electrophysiological abnormality of iPSC-CMs compared to adult human cardiomyocytes.

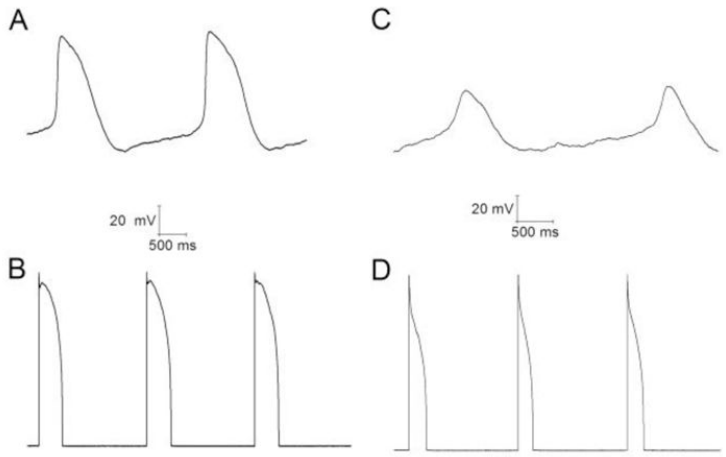

	Resting Potential (mV)	AP Amplitude (mV)	dV/dt_{max} (mV/ms)
Spontaneously beating cells (n=25)	−63±5.8	83±11	15±6
Stimulated cells (n=21)	−63±3.5	90±6	85±6
Stimulated cells with artificial I_{K1} (n=31)	−84±0.1	132±2	147±11

Figure 1.5: Electrically simulating I_{K1} in iPSC-CMs makes its AP morphology resemble a more adult cardiomyocyte AP.
A and C represents APs recorded from a ventricular-like and an atrial-like iPSC-CM, respectively. B and D shows the resulting stimulated AP with dynamic clamp addition of I_{K1}. The table below quantifies the AP characteristics with and without dynamic clamp. Adapted with permission from Ref [90].

1.5.3 Limitations of dynamic clamp

Dynamic clamp is a powerful tool but relies on obtaining a whole-cell patch clamp. This technique requires high technical expertise and is low throughput, making it impractical for large-scale drug screening. In order to obtain a whole-cell patch, a thin hollow glass pipette containing an electrode is carefully placed on the cell membrane and a giga-ohm (GΩ) seal is formed to seal the circumference of the pipette tip with the membrane. The pipette is filled with an intracellular solution that typically mimics the cytosolic ionic composition. The

cell is bathed in an extracellular solution that typically mimics the endogenous extracellular ionic environment. For the electrode to gain intracellular access, the cell membrane could either be ruptured by applying negative pressure, or the membrane could be perforated by antibiotics so that the membrane still is intact, but certain ions can move across it and the electrode can gain access. One antibiotic that is commonly used in perforated patch is gramicidin. Gramicidin allows monovalent cations (e.g., Na^+ and K^+) through, which better preserves the intracellular environment compared to ruptured patch where the cytosolic solution is quickly replaced by the pipette solution. With both types of patch clamp, the volume of the intracellular pipette solution is vastly larger than the cytoplasmic volume, such that the cytosolic concentration of permeable ions is determined by the pipette solution. This prevents endogenous local ionic fluxes and forces the intracellular concentrations to be static, making effects of these endogenous local changes unobservable under whole cell patch clamp. Dynamic clamp can only electrically represent a current, but biologically, the ion channels have an ion specificity and their activation may change intracellular concentrations of these ions [105]. The change in intracellular concentration can have other downstream effects that are not considered. For example, dynamic clamp can mimic a sarcolemmal calcium current but besides changing the membrane potential, the influx of calcium also activates downstream pathways that affect gene expression or phosphorylation of other ion channels. The intracellular sodium concentration activates other exchangers, such as the sodium-calcium exchanger or sodium-hydrogen exchanger. Using whole-cell

patch clamp allows researchers to only measure the instantaneous effect of the target current.

There are several platforms available to study electrophysiology, but there is a trade-off between information content and the throughput of the assay (Figure 1.7) [112], [113]. Manual patch clamp currently provides the highest information content but is the lowest throughput assay. The development of automated patch clamp has made patch clamp higher throughput and overcomes technical barriers, but is best used for expression systems [114]–[116]. For use in the automated patch system, iPSC-CMs need to be dissociated into suspension in order to be placed and adhere onto the platform [109]. However, the dissociation process is thought to disrupt the membrane and ion channels on iPSC-CMs. Ideally, a drug-screening platform would be high throughput and provide high information content. Much effort is currently exerted in developing such assays, for example, platforms that use optical tools to allow for simultaneous pacing and imaging of voltage and/or calcium [117]–[119], video-based assays that analyze contraction, calcium flux, and/or voltage [120]–[122], etc. [113], [120]–[124]. In addition to those approaches, optogenetics is a potential tool that can increase the throughput of assays while retaining high information content because it can be controlled by altering light intensity, its function is versatile, and is genetically expressed. Because of these properties, this thesis aims to build an optically-controlled dynamic clamp platform using optogenetic tools.

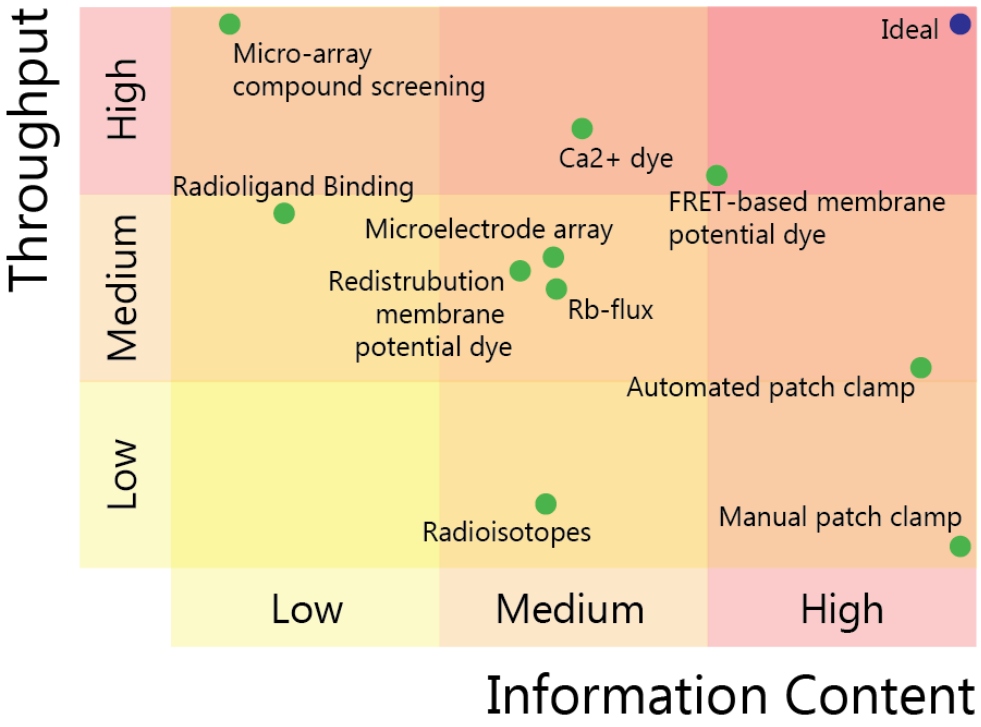

Figure 1.6 Representation of *in vitro* electrophysiological assays to measure the effect of drugs on ion channels arranged relatively by information content and throughput

CHAPTER TWO

OPTICAL DYNAMIC CLAMP: LIGHT-ACTIVATED DYNAMIC CLAMP USING IPSC-DERIVED CARDIOMYOCYTES*

2.1 Introduction

2.1.1 Outline

iPSC-derived cardiomyocytes (iPSC-CMs) are a potentially advantageous platform for drug screening because they provide a renewable source of human cardiomyocytes and can be patient derived. As mentioned in Chapter One, an obstacle to their implementation is their immature electrophysiology, which reduces relevance to adult arrhythmogenesis. To address this, dynamic clamp is used to inject current representing the insufficient potassium current, I_{K1}, thereby producing more adult-like electrophysiology. However, dynamic clamp requires patch clamp and is therefore low throughput and ill-suited for large-scale drug screening. In this chapter, we present the optical dynamic clamp (ODC) method, which uses optogenetic tools to generate target current *in lieu* of an electrode. Furthermore, in the presence of an I_{Kr} blocker, ODC revealed expected AP prolongation and reduced spontaneous excitation.

* A slightly modified version of this chapter is published as Quach, B., Krogh-Madsen, T., Entcheva, E., Christini, D. J., Light-activated dynamic clamp using iPSC-derived cardiomyocytes, Biophysical Journal, (2018)

2.1.2 Optogenetics

Optogenetics was lauded “Method of the Year” in 2010 by Nature Methods because of how it revolutionized neuroscience research by allowing for high spatial and temporal control over specific neural circuits. Since then, the optogenetic toolbox has been improved and expanded. For example, depolarizing and hyperpolarizing opsins have been developed to be activated by different wavelengths and generate a larger photocurrent [125]–[127]. Optogenetic tools have also been developed to be voltage reporters (i.e., ASAP1, QuasAr2) or dual-report calcium and voltage (i.e., CaViar) [128]–[130]. Opsins are also being developed to conduct specific ionic species [131], [132]. As the toolkit expands, so do the possibilities. Besides using opsins to gain control over electrical circuits, there are many efforts to develop optically-controlled methods to simultaneously manipulate electrical activity and measure changes in functional output by combining different opsins. This has a lot of value in cardiac research because of the need for new assays for drug toxicity, as discussed in Chapter One, and to increase the throughput of existing assays. This chapter will focus on the approach developed in this thesis, where the overarching goal is to translate the dynamic clamp method into an optically-controlled version that we name “Optical Dynamic Clamp”.

2.1.3 Optical Dynamic Clamp (ODC)

The ODC platform aims to translate the pain-staking low-throughput method of dynamic patch clamp to an optically-controlled high throughput version. Dynamic clamp provides high-content electrophysiology data, but its use is limited because of very low-throughput and specialized technical expertise. The advent of automated patch clamp with multichannel capabilities works to address some of these barriers to use, but is not without limitation, such as the need for compatibility with cardiomyocytes. In an important step in this direction, Goversen et al. (2018) recently demonstrated using a Nanion Patchliner automated patch clamp device to inject I_{K1} via dynamic clamp into iPSC-CMs [102]. Here, we present a light-controlled approach to this problem. The ODC platform would also allow for many more trials due to its non-contact nature and scalability. In addition, ODC potentially offers more versatility and flexibility over electrode-based methods. These advantages are further elaborated upon in the discussion section of this chapter.

To realize a fully-optically-controlled dynamic clamp, we must first establish the use of optogenetic tools to dynamically inject a target current to observe its effect on AP morphology. First, there would need to be an approach to measure the membrane potential. Second, there would need to be a way to inject a dynamic current. The aim of the thesis is to address the second function first. There are different optical methods present to measure membrane potential,

but there are no published contact-less methods to introduce a specified current into a cell.

Optogenetic tools are a potential solution because they can generate a depolarizing current and a hyperpolarizing current into a cell expressing that opsin. They are typically used to generate a static current to stimulate action potentials or completely inhibit electrical activity. An optical action potential clamp has been used to uncover the dynamic contribution of Channelrhodopsin-2 (ChR2), a depolarizing opsin, during the cardiac action potential [133], [134]. Several computational [133], [135] and experimental studies [136], [137] have used depolarizing and hyperpolarizing opsin to modulate the cardiac AP morphology. For example, activation of ChR2 by static light pulses delivered during different AP phases extended the action potential duration (APD) in neonatal rat ventricular myocytes (NRVM) [137]. Hyperpolarizing anion Channelrhodopsin 1 from *Guillardia theta* (GtACR1) was optically activated by static pulses to shorten the APD in NRVMs via forced hyperpolarization [136]. Static optogenetic manipulation can yield a range of AP responses depending on pulse timing, strength and duration [133]; however, it has inherent limitations when applied to multicellular tissue, where cells are at different phases of the AP at any given time. Computationally, a ChR2 model [134] was used to add a dynamic depolarizing current to simulate short QT syndrome and resemble a target AP, yet no real-time feedback was used [135]. Although this method worked well *in silico*, it would be critical to incorporate a real-time feedback loop

to address inherent cell variability and make the approach AP-morphology-adaptive.

In this study, to demonstrate the use of optogenetics to dynamically tune an AP, we used Archaerhodopsin TP009 (ArchT) [125], [126] to optically generate target outward current I_{K1}, instead of using electronic current injection via a patch electrode. ArchT has proven to be a useful tool to inhibit electrical activity in different excitable cells [125], [138]–[142]. To actualize the real-time feedback loop, the optogenetic tool must have fast kinetics and generate sufficient current. For validation purposes, we compared the use of the ODC platform with the standard electrode-based dynamic clamp (EDC) platform to generate a target current mimicking I_{K1} in human iPSC-CMs. We also investigated whether ODC would be able to uncover, as EDC would, the effects of the hERG channel inhibitor, E-4031, to illustrate ODC applicability to detect the effect of pharmacological agents on electrical activity. Our experiments demonstrate that ArchT can be controlled to generate the target current and yielded results similar to that of using an electrode, even in the presence of an ion channel modulator, corroborating the utility of optogenetic tools in the dynamic clamp setting and in drug testing applications.

In this implementation, we use the outward-current-generating opsin, ArchT, to mimic I_{K1}, resulting in more adult-like action potential (AP) morphology, similar to I_{K1} injection via classic dynamic clamp. The ODC presented here still requires

an electrode to measure V_m, but provides a first step towards contactless dynamic clamp, which will not only enable high-throughput screening, but may allow control within multicellular iPSC-CM formats to better recapitulate adult in vivo physiology.

2.2 Methods

2.2.1 Cell Culture

Cor.4U hiPSC-CMs (Axiogenesis, Cologne, Germany) were thawed, seeded, and maintained according to the protocols provided by the manufacturer. The cells were seeded on 0.1% gelatin-coated 8mm coverslips and plated at 100,000 cells/mL. Cells were incubated for at least 7 days post thaw prior to use for experiments.

2.2.2 Infection and Expression of ArchT

Adenoviral vector was constructed using the Addgene (Cambridge, MA) plasmid pAAV-CAG-ArchT-GFP, deposited by K. Deisseroth's laboratory (plasmid 20940) [143], [144]. ArchT was expressed in iPSC-CMs using MOIs of 250-300, as described in previously published protocols using an adenovirus [143], [144]. Determination of successful infection was confirmed via eGFP fluorescence. Functionality of ArchT was confirmed by illuminating the cells with

an LED (M565L3, ThorLabs) at 595 nm through a 60x objective and observing the amount of hyperpolarization of the membrane potential under current clamp.

2.2.3 Electrophysiology Protocol

Borosilicate glass pipettes were pulled to a resistance of 1-3 MΩ using a flaming/brown micropipette puller (Model P-1000, Sutter Instrument). The pipettes were filled with intracellular solution containing (mM) 10 NaCl, 130 KCl, 1 $MgCl_2$, 10 $CaCl_2$, 5.5 Dextrose, 10 HEPES. For perforated patch, the pipette tip was first dipped into the intracellular solution without gramicidin for 10 seconds. The pipette was then filled with the intracellular solution containing 8 μg/mL gramicidin passed through a 0.25 μm filter. The high calcium concentration in the intracellular pipette solution serves to verify the integrity of the patch as patch rupture under these conditions would lead to immediate cell contracture [88]. The coverslips containing iPSC-CMs were placed in the bath and constantly perfused with an extracellular solution at 37°C containing (mM) 137 NaCl, 5.4 KCl, 1 $MgSO_4$, 2 $CaCl_2$, 10 Dextrose, 10 HEPES. GFP-expressing single cells that were visibly contracting were chosen for experiments. Patch-clamp measurements were made by a patch-clamp amplifier (Model 2400, A-M Systems, Inc) controlled by the Real Time eXperiment Interface (RTXI; *www.rtxi.org*) to coordinate the amplifier via the data acquisition card (PCI-6025E, National Instruments). RTXI was also used to control the LED light intensity. The voltage was corrected for the calculated

liquid junction potential of -2.8 mV. The series resistance was less than 10 MΩ and was not compensated.

2.2.4 Dynamic Clamp Experiments

Figure 2.1A depicts the schematic of the EDC system. At each time step, the electrode measures the membrane potential (V_m), which is then input into a mathematical model of I_{K1} to determine the amount of target current that should be generated at that measured V_m. The amplifier outputs the calculated target current in real-time, simulating the expression of an equivalent current within the cell.

Figure 2.1B illustrates the ODC system. Similar to the EDC system, the membrane potential measured by an electrode is input into the mathematical model of the target current. We used the I_{K1} equations of the human ventricular myocyte model by ten Tusscher et al. (2004). The maximum allowable I_{target} was set to 1.08 pA/pF because that was close to the maximum current that could be generated by ArchT in these cells. ArchT is a proton pump, generating a light- and voltage-sensitive outward current. There is no published validated mathematical model for the ArchT ion current. Instead, we used an empirical

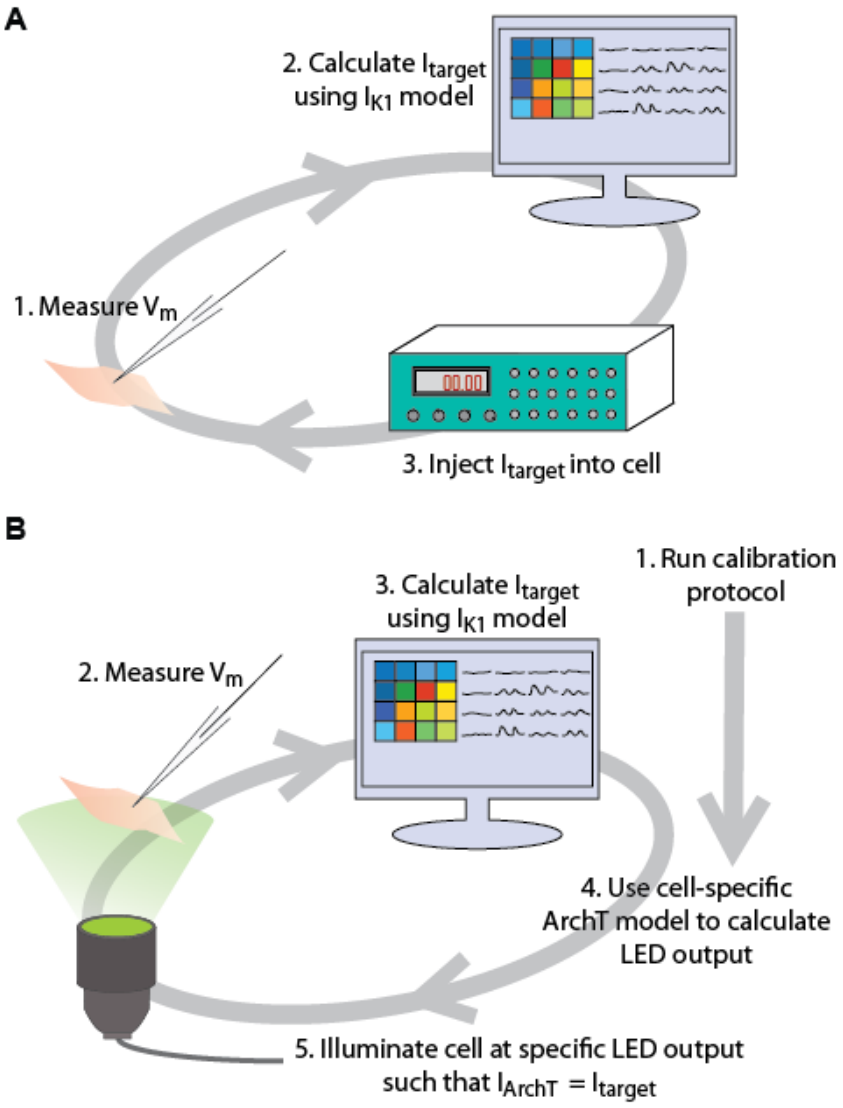

Figure 2.1: Description of EDC and ODC systems
Dynamic clamp is used to simulate the target current, I_{K1}, in iPSC-CMs. (A) The EDC system uses the electrode to measure the V_m and inject a current into the cell. (B) The ODC system utilizes the electrode to measure the V_m, but uses optical ArchT activation to inject the target current. Prior to implementing the ODC system, a calibration protocol is executed to obtain the parameters to generate a cell-specific ArchT model.

equation that was tuned on a per-cell basis to generate the illumination E_e needed to achieve the target current, I_{ArchT}:

$$I_{ArchT} = \frac{a_1 \cdot V_m^* + a_2}{a_1 \cdot V_{rest} + a_2} \cdot b_1 \left(1 - e^{-b_2 \cdot E_e}\right), \qquad \text{(Eq. 2.1)}$$

where the first component describes the voltage dependence, which is linearly affected by the membrane potential, and the second component describes the light intensity dependence of ArchT (Equation 2.1, Figure 2.2). Due to an amplifier calibration error, the V_m used in this calculation by RTXI (V_m^*) was later determined to be of 5% smaller amplitude than the real V_m as recorded by the amplifier. This error affects I_{ArchT} equally in the EDC and ODC systems and simulating its effects in a mathematical iPSC-CM model (Paci et al., 2013) suggests that it has no significant impact on dynamic clamp performance (Appendix A10). The parameter V_{rest} is set to -85 mV, the ideal resting membrane potential. E_e represents the light intensity of the LED. a_1 and a_2 describe the cell-specific voltage dependence while b_1 and b_2 describe the cell-specific light intensity dependence. The values of these parameters are determined for each cell with a calibration protocol prior to running the ODC platform so that the ArchT model represents the characteristics from an individual cell. In about half the cells, inward current events are generated spontaneously even during voltage clamp at -85mV (Appendix A2). These spontaneous events may obscure the recorded current and thus the determination of the cell-specific ArchT parameters. However, cells in which these disturbances did occur were not associated with a reduction in ODC

performance, measured as pre-stimulation potential, fraction of repolarization, and triangulation.

To test the feasibility of using ArchT to inject a target current, stimulated action potentials under the EDC system were compared to those of the ODC platform at three different pacing frequencies: 0.5, 1 and 2 Hz. The cells were stimulated 10 times at 0.5, 1 and 2 Hz sequentially under three conditions (the order of which was randomized): (A) control, in which no additional current was added, (B) addition of I_{target} with EDC, and (C) and addition of I_{target} with ODC.

2.2.5 E4031 addition

After the cells had undergone the aforementioned pacing protocol under the same three conditions, 500 nM E-4031 was perfused into the bath containing the coverslip of iPSC-CMs for 2 minutes. Experiments were again conducted under the same pacing protocol and conditions to measure the effect of I_{Kr} inhibition.

2.2.6 Analysis

APD_X was calculated by determining the time from stimulus to the time point at which the AP repolarized X% of the AP amplitude (AP peak – pre-stimulation

potential). The AP peak was defined as the maximum membrane potential reached during the AP after delivered stimulus. The pre-stimulus potential is defined as an average of the membrane potential in the last 50 ms prior to delivering a stimulus current. The fraction of repolarization, calculated as $(APD_{90}-APD_{50})/APD_{90}$, and triangulation, calculated as $APD_{90}-APD_{30}$, were used as metrics to quantify AP morphology. Data measured at a given pacing frequency in a cell were omitted from the analysis of AP characteristics if they contained more than one spontaneous event under EDC or ODC. This exclusion was necessary because spontaneous activity could affect the subsequent stimulated AP, obscuring the comparison between EDC and ODC.

2.3 Results

2.3.1 Cell-Specific Calibration

Intrinsic cell-to-cell variability of ArchT expression and characteristics necessitated a calibration protocol that determines the cell specific parameters of the I_{ArchT} model (Eq. 2.1). The calibration protocol consists of a voltage-clamp protocol and a light-clamp protocol (Figure 2.2A). The light intensity ramp of the protocol highlighted in blue is used to determine the parameters describing light dependence of I_{ArchT}, while the voltage steps highlighted in purple are used to obtain the parameters quantifying its voltage dependence. Figure 2.2B depicts the example current trace during the light intensity ramp on an extended time

axis and Figure 2.2C shows the current during each of the three voltage clamp steps. These data are used to obtain the cell-specific parameters by determining the best-fit line using a nonlinear least squares analysis. By deriving the cell-specific ArchT parameters, the light intensity can be accurately calculated to activate ArchT and generate the target current in individual cells.

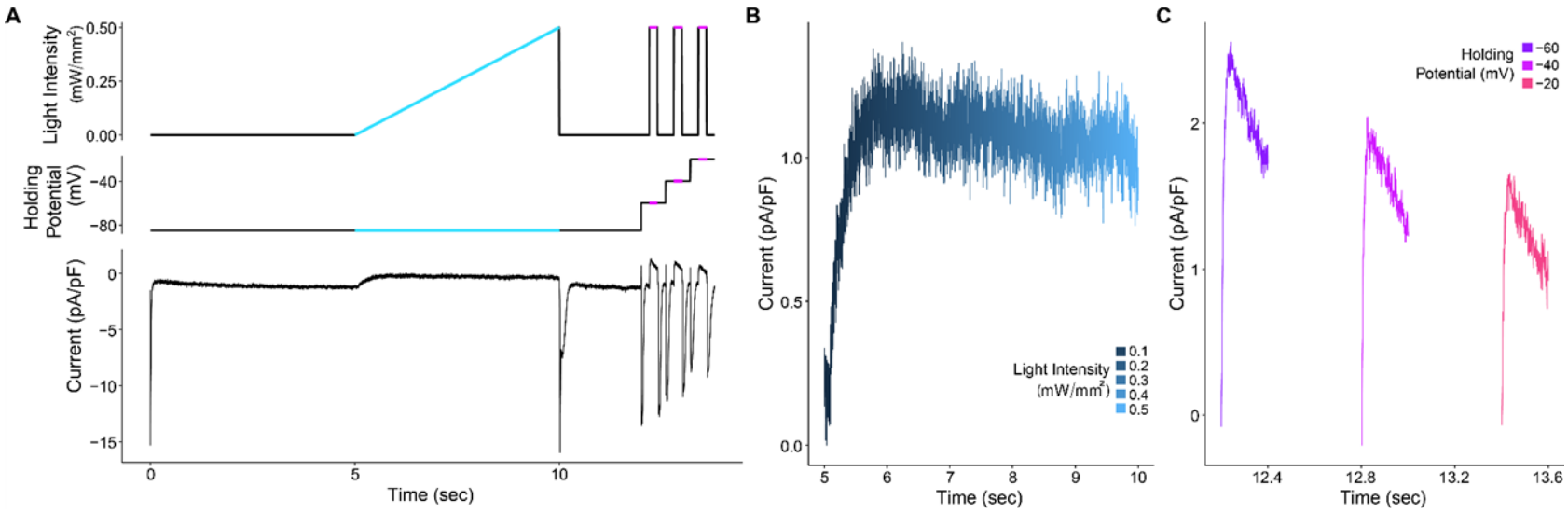

Figure 2.2: Calibration protocol to create a cell-specific ArchT model

(A) The calibration protocol consists of changing the light intensity and the holding potential to determine the ArchT model parameters, i.e., the light dependence (using the blue light-intensity ramp portion of the protocol) and voltage dependence (using the purple voltage-clamp steps in the protocol), for an individual cell. The bottom panel illustrates an example of the current output measured via patch clamp for one cell during the calibration protocol.

(B and C) Current from the example trace in (A) during the light-intensity ramp and voltage-clamp steps, respectively. The currents were subtracted from the baseline, defined as an average of 10 msec prior to illumination.

2.3.2 ODC achieves results similar to EDC

After obtaining the cell-specific parameters for Eq. 2.1, we then used the ODC method and evaluated its performance compared to EDC. Results from one representative cell paced at 0.5, 1 and 2 Hz are illustrated in Figure 2.3. The control yielded a lot of spontaneous activity, making it difficult to trigger a stimulated AP or skewing the subsequent stimulated AP. The EDC and ODC platforms hyperpolarize the membrane potential and inhibit the occurrence of spontaneous events. The stimulated APs in the EDC and ODC conditions are very similar, demonstrating that the EDC and ODC platforms yield nearly identical stimulated APs at different pacing frequencies despite their fundamentally different methods of injecting a current. The EDC target current also overlaps with the ODC target current, as would be expected to generate similar APs. Similar to I_{K1}, the target current is on between APs to maintain the resting membrane potential. During the early phases of the action potential, the target current turns off and then increases during repolarization as I_{K1} would behave. These results indicate that the ODC platform is able to calculate a target current, determine the light intensity needed to generate that target current, adjust the LED output, activate the optical tool, and successfully generate the target current. In short, it demonstrates the feasibility of ArchT to inject a target current analogous to injection via an electrode.

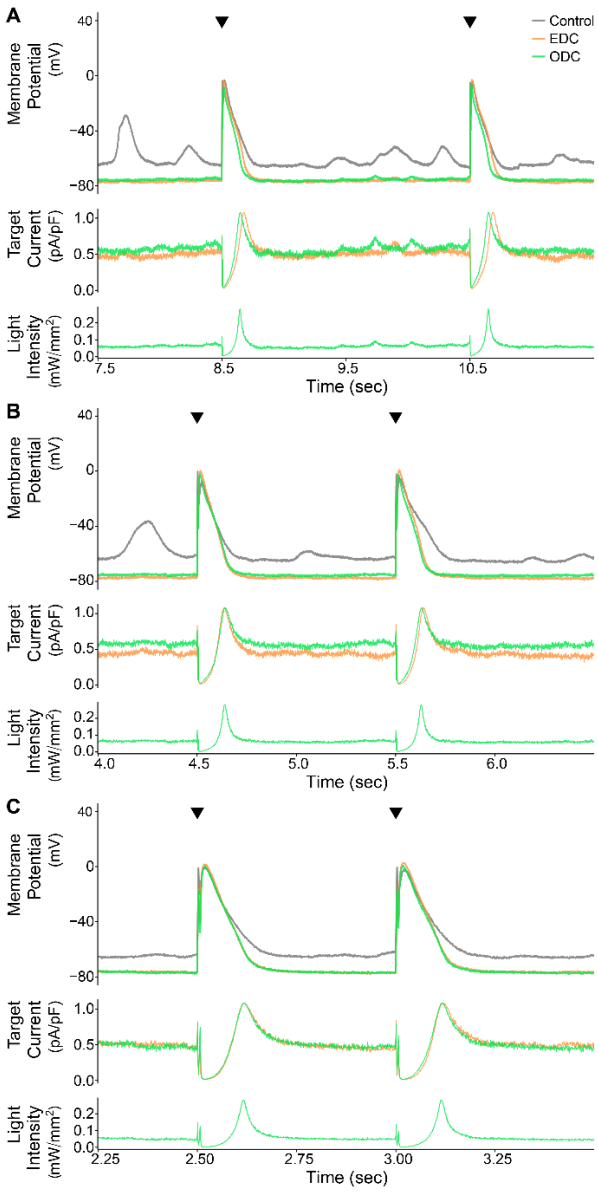

Figure 2.3: Example demonstrating the results of the EDC and ODC platforms

Two stimulated APs from an example cell (cell 1, Appendix A6A and A8) showing the effects of adding I_{target} (I_{K1}) while paced at three different frequencies: (A) 0.5 Hz, (B) 1 Hz, (C) 2Hz. The top panels in each of (A) through (C) overlay the paced APs over time under control and both dynamic-clamp conditions, and the black triangles indicate when a stimulus current was delivered. In the middle panels, the traces represent the calculated target currents for EDC and ODC. The bottom panels show the calculated light intensity used to generate the target current. The time axis corresponds to the time within the full recording shown in Appendix A6A.

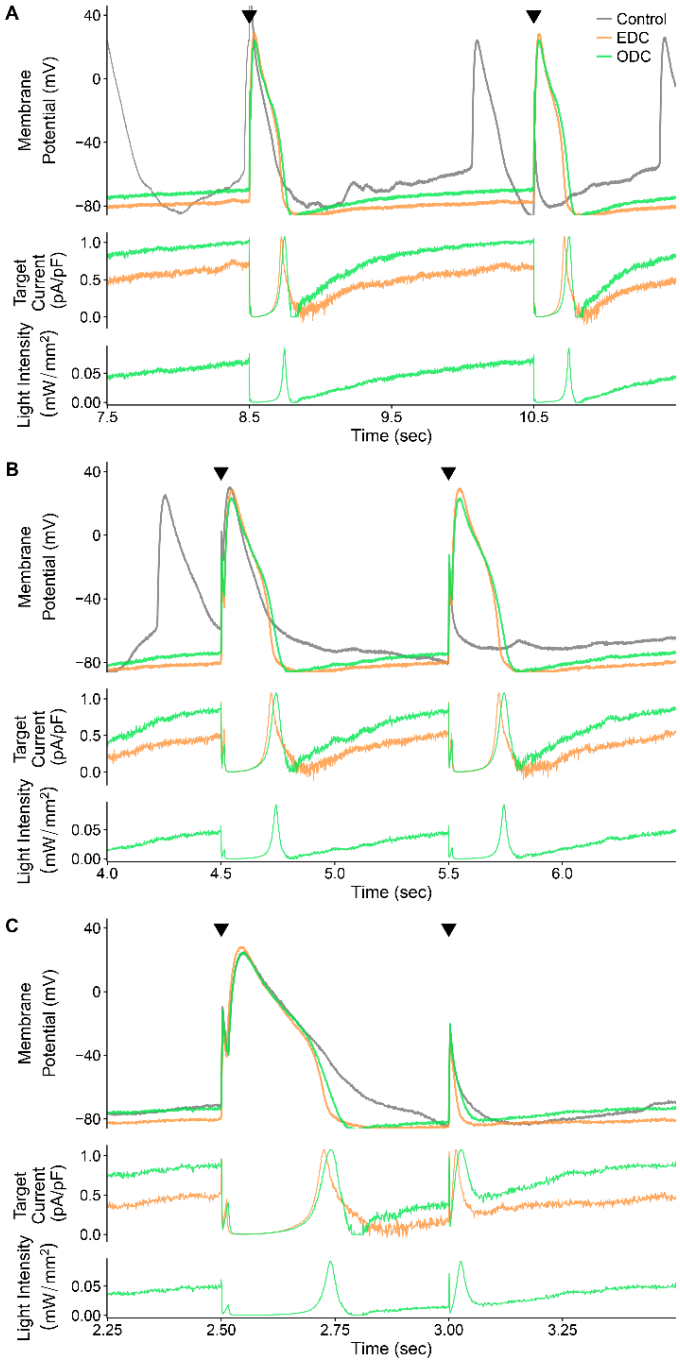

Figure 2.4: Example demonstrating the results of the EDC and ODC platforms

Figure is organized in the same manner as Figure 2.3. This example is from cell 13 (Appendix A6B and A8). The time axis corresponds to the time within the full recording shown in Appendix A6B.

While the cell presented in Figure 2.3 is representative of the most common ODC performance (11 of 16 cells with similar results), in a subset of cells (5 of 16), ODC was unable to maintain the resting membrane potential as well as EDC so that there is a greater than 5 mV difference in the pre-stimulation potential between EDC and ODC. Figure 2.4 shows a cell that illustrates this behavior. The gradual depolarizing drift of the ODC membrane potential led to an increase in the target current (and therefore light intensity) as the ODC attempted to hyperpolarize the membrane potential. Although the light intensity did increase, the membrane potential could not be maintained, potentially because ArchT did not generate the required target current. Despite the difference in the pre-stimulation potential, both dynamic clamp systems had a similar effect on the overall morphology of the stimulated APs, which can be seen by the degree of overlap of the EDC and ODC AP traces. EDC and ODC both inhibited spontaneous activity similarly to the cell in Figure 2.3, allowing for better measurement of the AP waveform whereas without outpacing the intrinsic spontaneous rate, it was difficult under the control condition to measure an AP without a preceding spontaneous event.

Figure 2.5 summarizes the effect of EDC and ODC across 16 individual cells on the pre-stimulation potential (Figure 2.5A), triangulation (Figure 2.5B) and the fraction of repolarization (Figure 2.5C). EDC and ODC have the advantage over the control condition of suppressing the rate of spontaneous activity, especially

when the pacing rate is less than the intrinsic rate (Appendix A3). Both dynamic clamp systems hyperpolarize the pre-stimulation potential compared to the control (Figure 2.5A). Ideally, we would expect ODC to hyperpolarize the pre-stimulation potential to the same value as EDC. In 11 of 16 cells (e.g., cell in Figure 2.3), the pre-stimulation potential in both ODC and EDC were within 5 mV of each other. However, as mentioned above, in 5 of 16 cases, (e.g., cell in Figure 2.4), the pre-stimulation potential of the ODC was depolarized more than 5 mV relative to EDC because ODC did not maintain the membrane potential as well as EDC did. This is reflected when comparing the average pre-stimulation potentials across conditions (Figure 2.5D). Despite the more depolarized pre-stimulation potential, ODC had similar effects as EDC on the overall AP morphology. As one marker of AP morphology, we used fraction of repolarization, which quantifies the fraction of the AP that is spent in the repolarization phase. We expect the fraction of repolarization to decrease with dynamic clamp, given that I_{K1} contributes to late repolarization. The ODC affected the fraction of repolarization by the same magnitude as EDC on average (Figure 2.5D) and this is also seen on an individual basis (Figure 2.5C). Triangulation provides another marker of the overall shape of the AP. In most cells, ODC altered triangulation by similar magnitudes as EDC (Figure 2.5E). The overall average across all pacing frequencies also demonstrates that ODC had a similar effect on triangulation as EDC (Figure 2.5F). Further AP characteristics are provided in Appendix A.13. In summary, comparing the AP

characteristics under EDC and ODC reaffirms that ArchT is able to recapitulate similar effects as an electrode on AP morphology.

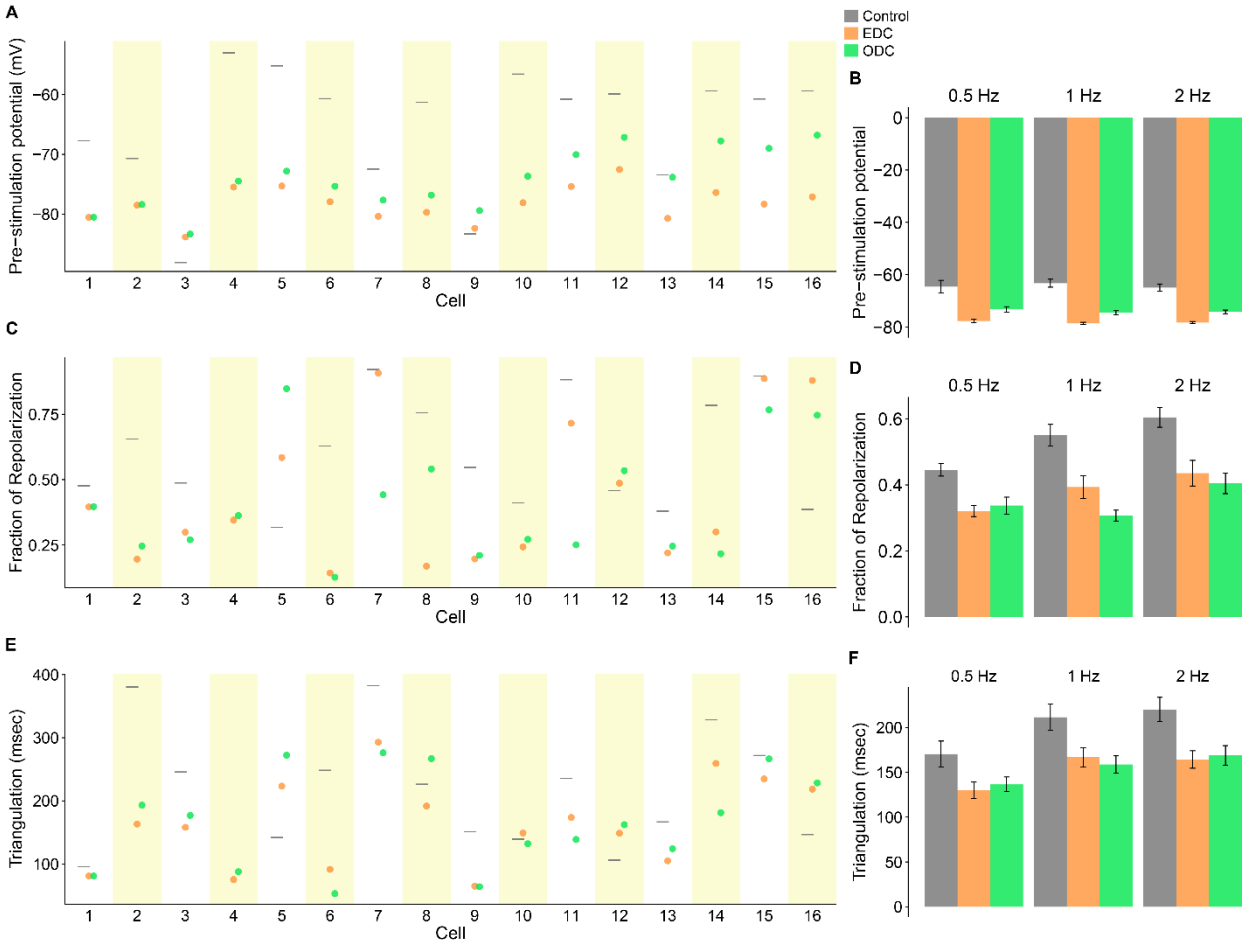

Figure 2.5: Summary of the effects of EDC or ODC on AP morphology

Pre-stimulation potential (A), fraction of repolarization (C) and triangulation (E) of individual cells at 2Hz pacing in control (gray) and after adding an I_{K1} target current via EDC (orange) or ODC (green). The results of individual cells at 0.5Hz and 1Hz are displayed in Appendix A8. Average of all cells and standard error mean (SEM) of the pre-stimulation potential (B), fraction of repolarization (D) and triangulation (E) by pacing frequency. No stimulated action potential could be measured for the control condition of cell 16 due to the high rate of spontaneous activity.

2.3.3 ODC platform detects effect of I_{Kr} inhibition similar to EDC

To investigate the feasibility of using the ODC platform for drug screening, it is important to determine if ODC can detect changes in AP morphology similar to EDC in the presence of an ion-channel modulator. We used an I_{Kr} inhibitor, E-4031, because I_{Kr} is a dominant repolarizing current in iPSC-CMs and I_{Kr} inhibition assays are commonly used as drug toxicity assays. Figure 2.6 shows an example after E-4031 treatment, demonstrating that the ODC platform mimics the effects of EDC on AP morphology. With E-4031 addition, the APD increases in the control, EDC and ODC conditions, as expected with I_{Kr} inhibition (Figure 2.6A-C). Importantly, it is easier to observe the E-4031 induced AP prolongation under EDC and ODC compared to the control because there is less spontaneous activity (Figure 2.6A-C). That said, like in Figure 2.4, ODC does not maintain the membrane potential as well as EDC between APs, which can be seen in the different pre-stimulation potentials (and non-overlapping target currents) (Figure 2.6D). However, the overlapping EDC and ODC stimulated APs and target currents during the AP indicate that ArchT achieved a similar effect as the electrode on AP morphology even if the same pre-stimulation potential was not achieved (Figure 2.6D, E). Thus, the ODC platform behaves like EDC in illuminating the expected changes on AP morphology and APD prolongation with E-4031 addition.

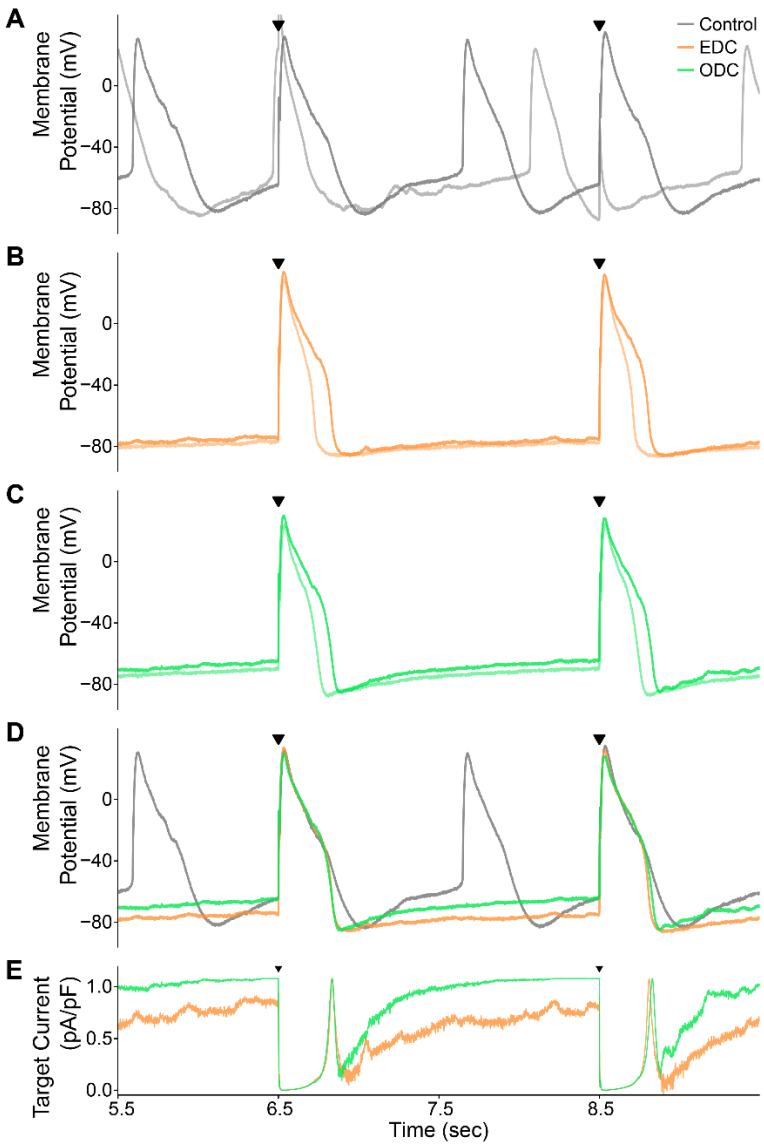

Figure 2.6: Example demonstrating the results of control, EDC and ODC after E-4031 addition

Example cell (cell 13, Figure 2.7) showing the effects of adding Itarget while paced at 0.5 Hz. The gray (A, D), orange (B, D, E) and green (C-E) traces represent the control without any current addition, adding I_{target} with EDC and adding I_{target} with ODC, respectively. (A-C) The darker traces represent the stimulated APs after E-4031 addition, while the light-colored traces represent the stimulated APs prior to E-4031 addition. (D) Overlays of AP traces from the three conditions after E-4031 addition. (E) Calculated target currents for EDC and ODC. Black triangles indicate when a stimulus current was delivered and provides a reference to which of the 10 paced APs in Appendix A9 are displayed. The time axis corresponds to the time within the full recording shown in Appendix A9.

The effect of E-4031 with EDC and ODC across all cells is depicted in Figure 2.7. In all cells, EDC and ODC were able to inhibit spontaneous activity seen in the absence of dynamic-clamp, allowing for an accurate measurement of AP characteristics. E-4031 increased the APD_{90} under control, EDC and ODC conditions, as expected (Figure 2.7A). Addition of simulated I_{K1} via both dynamic clamp platforms shortened the APD90 compared to the control, as expected with increased repolarizing current. ODC also shortened the APD_{90} to the same magnitude as EDC in individual cells and on average across all cells (Figure 2.7A, E). Cell 13 under the control condition yielded too much spontaneous activity after drug addition so that pacing did not override the intrinsic activity to yield stimulated action potentials. Similar to previous results without E-4031, the effect of ODC and EDC on pre-stimulation potential, fraction of repolarization time and triangulation compared to the control are similar (Figure 2.7B-D). The average of characteristics across all cells confirm the overall AP morphology (APD_{90}, fraction of repolarization, and triangulation) is nearly identical between EDC and ODC (Figure 2.7H). Of note, with E-4031, the control (without dynamic clamp) cells exhibited more dramatic drug-induced effects in terms of APD prolongation and larger triangulation compared to EDC and ODC, which likely indicates that in lack of sufficient I_{K1}, the hiPSC-CMs may be overly sensitive to classic hERG channel blockers. The agreement between the optical dynamic clamp and electrode dynamic clamp in the presence of E-4031 illustrates how ArchT can be used in place of an electrode in the context of drug screening.

Figure 2.7: Summary of the effect of adding IK1 via EDC or ODC after E-4031 addition on AP morphology paced at 0.5 Hz

The APD90 (A), pre-stimulation potential (C), fraction of repolarization (E) and triangulation (G) were measured without any current addition (grey), and with the addition of I_{target} via EDC (orange) or ODC (green) in individual cells (A) The empty markers represent the APD90 prior to drug addition and the dark circles represent the APD_{90} after E-4031 addition. Average of all cells and standard error mean (SEM) of the APD_{90} after drug addition (B), pre-stimulation potential (D), fraction of repolarization (F) and triangulation (H) by pacing frequency;

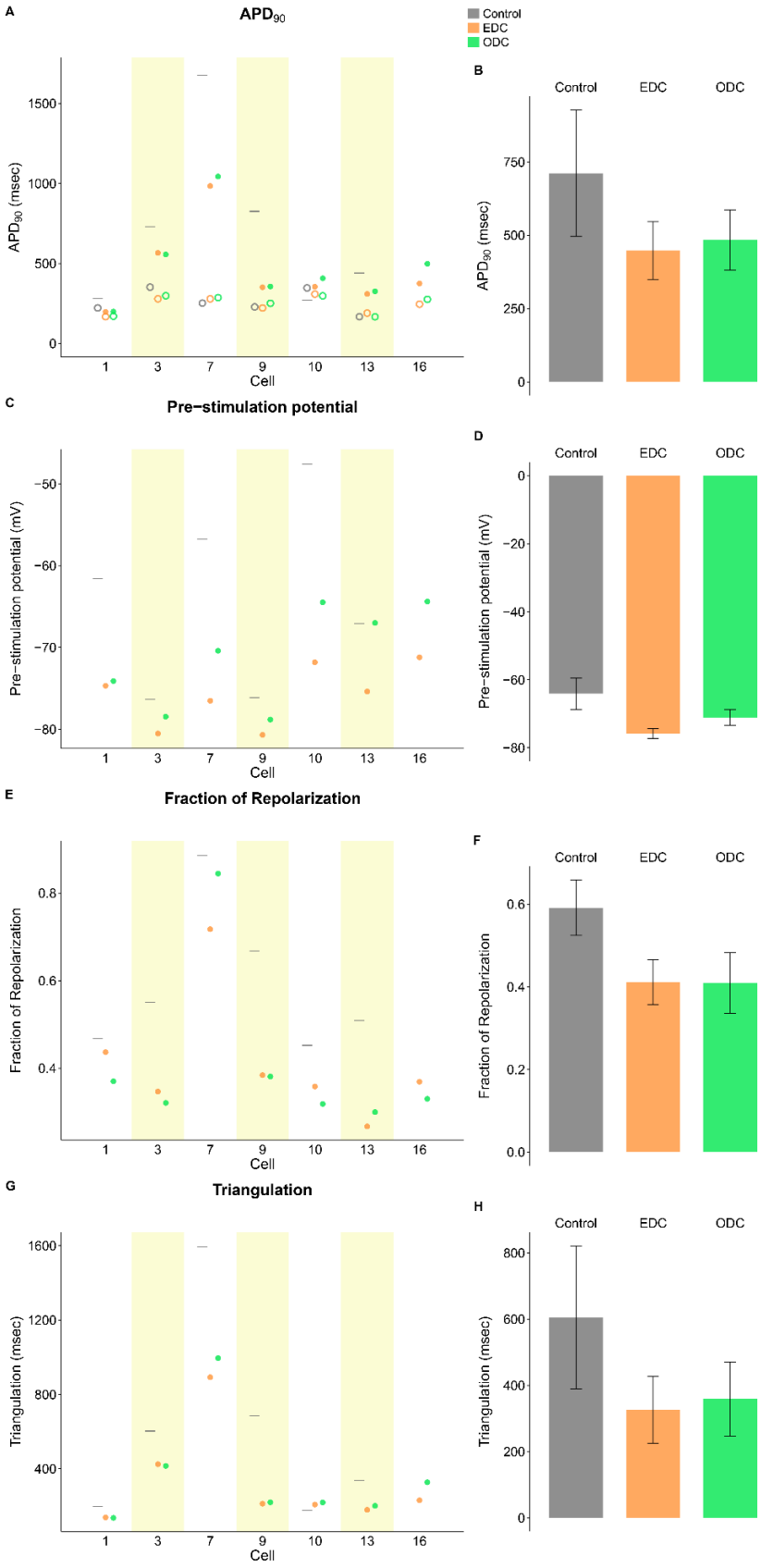
A
APD90
Control
EDC
ODC
APD90 (msec)
Cell
B
Control
EDC
ODC
APD90 (msec)
C
Pre−stimulation potential
Pre−stimulation potential (mV)
Cell
D
Control
EDC
ODC
Pre−stimulation potential (mV)
E
Fraction of Repolarization
Fraction of Repolarization
Cell
F
Control
EDC
ODC
Fraction of Repolarization
G
Triangulation
Triangulation (msec)
Cell
H
Control
EDC
ODC
Triangulation (msec)

2.4 Discussion

2.4.1 Optical Dynamic Clamp performance and limitations

Dynamic clamp is a technique that enables versatile and thorough probing of electrophysiology. However, its use for drug screening is limited because its standard implementation is low throughput. An optically-controlled version would enable more high throughput applications. Here, we have conducted proof-of-concept experiments, in which ArchT was controlled optically, injecting the I_{K1} target current and altering AP morphology similarly to electrode-based dynamic clamp. Our findings demonstrate: 1) the feasibility of using optogenetics to generate a dynamically controlled target current and 2) the ODC platform has the potential to be used for drug screening in place of EDC.

One shortcoming of ODC with respect to EDC was the decreased ability of ODC to maintain a hyperpolarized membrane potential between APs in some cells. The resulting differences in pre-stimulation potential could conceivably cause secondary changes in AP features. However, this possibility was ruled out, as there was no correlation between the difference in pre-stimulation potential between EDC and ODC on the differences of fraction of repolarization and triangulation (Appendix A4). One explanation for the inability of ArchT to maintain a hyperpolarized membrane potential as well as EDC does is the relatively low maximum current that a light-driven ion pump can generate.

Indeed, ArchT pushes one H^+ ion per photon, which is much less efficient than the operation of a light-sensitive ion channel. Furthermore, the ArchT current seemed to decay during the voltage-dependence part of the calibration protocol (Figure 2.2C). During the intervals between APs, such ArchT current decay could depolarize the membrane. We tested this hypothesis by quantifying the correlation between the cell-specific current decay and the difference between the pre-stimulation potentials between EDC and ODC (Appendix A5). No such correlation was found, suggesting that it is unlikely that the current decay is responsible for the lack of V_m maintenance.

Another potential limitation of ODC is that because ArchT is a proton pump, there may be a pH effect. Archaerhodopsins themselves are known to be pH sensitive, so a local change in pH could affect the ability of ArchT to generate a consistent current [145]–[147]. Local changes in pH could affect neighboring ion channels directly or indirectly by affecting the membrane and altering the overall electrophysiological properties of the cell [147]–[150]. The observation that ODC inhibited spontaneous activity more effectively than EDC (Appendix A3) may be evidence of this effect on other ion channels either by directly affecting the structure of the proximal channels or indirectly by altering the surrounding membrane properties. The increased inhibition of spontaneous activity with ODC can serve as an advantage over EDC since AP morphology can be measured without any distortion from underlying spontaneous events.

In some cells, we observed a voltage undershoot following the AP (Figure 2.4, Appendix A4) [7], [87], [151]–[153], [56], [67], [154], [155], [62], [156], [157]. The magnitude of this undershoot varied across cells. EDC was better able to inhibit this undershoot by injecting a depolarizing current (Appendix A4); not surprisingly, the hyperpolarizing opsin was not helpful in correcting this feature. The cause and consequences of this undershoot are not fully understood but can account for the differences between the ODC and EDC and explain why in some cases, the AP morphology with ODC looks more like the control than EDC (Appendix A7). The increased hyperpolarization seen in control and ODC conditions may have consequences for the subsequent AP by altering the activation state of other ion channels. Extension of the ODC method to incorporate a depolarizing opsin would allow bi-directional voltage control, and thereby compensate for the undershoot, similar to EDC. Indeed, this would allow the optical dynamic clamp to mimic any electrical current and thereby be fully versatile like EDC. Finally, there are limitations to our empirical approach to modeling ArchT as an on/off light switch in Eq. 2.1. Taking into account the ArchT's intermediate states of different conductance [126], [158], and developing more mechanistic models, as done for ChR2 [134], may help improve similarity between EDC and ODC. This will allow for better control of light levels and more precise generation of the predicted current.

The maximal I_{target} of 1.08 pA/pF used in our study was determined based on the maximal current that could be consistently generated by ArchT in the voltage

range relevant to I_{K1}. The I_{target} generated during our dynamic clamp experiments typically did reach 1.08 pA/pF during final repolarization (e.g., Figure 2.3), and did reach maximum during rest (where the maximum is around 0.5 pA/pF due to decreased driving force). We expect that a larger I_{target} would allow hyperpolarization to below the -80 mV level as seen in previous studies of EDC [21], [109], [154].

Dynamic clamp is based on a real-time feedback look and because ArchT is not an instantaneous current, there is the potential that its kinetics are slow for the purposes of dynamic clamp. We investigated the effect of the time constant of activation and deactivation on dynamic clamp performance *in silico* (Appendix A11A). The *in silico* results suggest that there is tolerability of the ODC system to accommodate a time constant of less than 60 ms, before the resulting AP waveform deviates substantially from the control. We measured the time constant in our cells to be less than 15 ms and therefore within the range of tolerability as predicted by our *in silico* experiment (Appendix A11A).

We have yet to eliminate the need for an electrode by incorporating an optical method to measure the membrane potential. When making this platform fully optical, there are several anticipated challenges worth discussing. Currently available optical methods of measuring membrane potential are voltage-sensitive dyes and other opsins (e.g., QuasAr2, Arch(D95X), and CaViar) [159], [160]. These options do not measure the absolute membrane potential, which

is required in the present setup to calculate the target current. Hou et al. (2014) reported a method of using the temporal dynamics of microbial rhodopsin fluorescence to measure the absolute membrane potential, but it is not compatible with the mechanics of dynamic clamp [161]. The noise of fluorescent markers may cause the calculated I_{target} to fluctuate, possibly affecting the accuracy of the dynamic clamp. In addition, dynamic clamp relies on the real-time feedback of information, so a fully-optical dynamic clamp platform would require a stable and rapidly responsive voltage sensor. Realization of the fully-optical dynamic clamp dream will require development of optical tools that are conducive to dynamic clamp.

2.4.2 Using optical dynamic clamp for drug screening

The tedious nature of dynamic clamp restricts its use, but were it high throughput, it would open the possibility for its use during pre-clinical drug development. To increase throughput, an all-optical system would require an optical voltage readout, using, e.g., a voltage sensitive dye (VSD) or a genetically encoded voltage indicator (GEVI). The necessary requirements for compatibility in the ODC system would be defined by phototoxicity, brightness, responsiveness, and wavelength crosstalk. One of the biggest advantages of the ODC platform is that it is compatible with a variety of cell formats. In spatially-extended systems (e.g., large beating clusters and monolayers), the EDC platform is not applicable, while the ODC platform can be used to illuminate

the arrhythmogenic effects of drugs. There are also many engineering methods and platforms that aim to physically mimic *in vivo* developmental conditions (i.e., extracellular matrix composition and organization, and cyclical stretch) [162]–[165]. These more tissue-like formats capture "in-context" cell behavior, including electrotonic coupling and other chemical influences from neighboring cells, and therefore are preferred to single cells. Furthermore, all-optical methods enable high-precision space-time control in such multicellular systems, as illustrated recently in neurons [166] and in cardiac preparations [167]. This allows users to re-direct the control of electrical activity from the single-cell behavior to the emergent (wave) behavior [167], [168].

2.4.3 Versatility and flexibility of ODC

With the right optogenetic tools and mathematical models, the optical dynamic clamp platform could open up more physiologically relevant formats for basic science research and drug development. Halorhodopsins, such as *Natronomonas pharaonis* halorhodopsin (NpHR) and its derivatives could also be used in this platform as an alternative to ArchT to inject a hyperpolarizing current given its fast kinetics [169]. Neither of these generate particularly high current, considering that they are light-sensitive ion pumps. GtACR1 is a Cl^- current with large amplitude [136], [170] that is also fast and thus very promising; its utility in adult cardiomyocytes and physiological concentrations remains to be demonstrated. BLINK1 is the first potassium-selective optogenetic tool

available, but its kinetics are currently too slow for the near real-time feedback requirements of ODC [131]. There are also several depolarizing opsins available that can be used in conjunction with hyperpolarizing opsins, so that any inward or outward current can be represented in cardiomyocytes[169], [171], [172]. Optogenetic tools are being engineered to activate/deactivate faster, generate larger photocurrents, be permeable to specific ionic species or be activated by specific wavelengths. As these developments progress, users can choose which optogenetic tool best suits their needs in the ODC platform.

One known drawback of EDC is that an electrode can only electrically mimic a current but cannot account for endogenous secondary effects that affect electrophysiology, such as activation of exchangers, pumps, or Ca^{2+}-dependent processes, which typically result from the change in intracellular ionic concentration. In this regard, because optogenetic tools alter the membrane potential by changing the intracellular ionic composition, the ODC platform may be more suitable for dynamic clamp than using an electrode because optogenetics can generate a custom-tailored current with the intended ionic species itself, reflecting how endogenous currents are generated. As with the standard dynamic clamp method, ArchT mimicked the electrical behavior of I_{K1}. But as potassium-selective tools are made compatible with the dynamic clamp system, the ODC platform may recapitulate both the electrical effect of I_{K1} and its effects from altering the intracellular potassium concentration. With the expansion of the optogenetic toolbox, the ODC platform will more accurately

investigate true influence of an ionic current on electrophysiological behavior by generating the current with the relevant species.

Optogenetic tools are being creatively incorporated into automated high-throughput drug screening platforms [117], [159], [173]. Using optogenetic tools dynamically could also potentially expand on the use of automated multi-channel patch clamp systems to multicellular preparations. Such a hybrid system could continue to use a patch electrode to read the V_m but instead use optogenetic methods to inject a dynamic current into the multicellular format. The ODC method contributes a novel approach to probe electrical dynamics in iPSC-CMs and to better reveal how electrical activity is controlled. Here, a proof-of-principle ODC application was demonstrated with ArchT to generate I_{K1} as target current in iPSC-CMs to simulate a more adult-like electrical phenotype. As the ODC platform develops, it should be possible to simulate abnormal currents or simulate heterogeneous current expression in iPSC-CM monolayers. This would provide a more powerful approach that enables researchers to address hypotheses that could not be investigated previously.

CHAPTER THREE

USING THE OPTICAL DYNAMIC CLAMP FOR SCREENING ION CHANNEL MODULATORS

3.1 Introduction

3.1.1 Outline

Chapter 2 presented the proof-of-concept of using optogenetics in lieu of an electrode to inject a target current, with the application of creating an optically-controlled version of dynamic clamp. In this chapter, the ODC platform is applied to drug screening of ion channel modulators. This chapter aims to investigate to what extent ODC can replace EDC and respond similarly to ion channel modulators. By determining this in single cells, we will be able to determine the effectiveness of this method compared to the status quo before extending the platform to further applications and expanding the platform to a greater variety of formats. Chapter 3 also aims to demonstrate the possible benefit of adding I_{K1} for drug screening. Using electrode-based dynamic clamp, Bett et al. (2013) demonstrated that the anticipated AP prolonging effect of the calcium channel agonist bayK 8664 was only observable when injecting an I_{K1}-like current [154]. In addition to the potential ease of use of the ODC platform, the extension to physiologically relevant formats that better resemble tissue-level properties may make the ODC platform more selective and sensitive than other electrophysiology-based platforms for predicting toxic or beneficial effect of

drugs in patients. As the results in this chapter will show, while our experiments demonstrate that the ODC platform can detect the anticipated effects of the ion channel modulators on AP characteristics, it also reveals some limitations in how effectively the current implementation of ODC can mimic EDC for drug screening. In addition, we were unable to demonstrate the benefit of using dynamic clamp to add I_{K1} with BayK 8664.

In this chapter, the following drugs were selected: BayK 8664, verapamil, and terfenadine. iPSC-CMs, without dynamic clamp, reflect the effect of verapamil and terfenadine through changes in AP characteristics that are driven by the activation of the ion channels that the drugs target. Because iPSC-CMs are able to respond predictably to these well-characterized ion channel modulators [174], [175], the condition without dynamic clamp serves as a good control in our experiments to ensure that the drug is active and the cells are responding appropriately to the drug based on the effect on AP characteristics. The EDC platform will demonstrate the effect of our target current on the results of the drug screen and will be used as a comparison of how ODC should ideally perform. iPSC-CMs with addition of I_{K1} via EDC has been demonstrated to be able to detect the anticipated AP prolongation and shortening in response to 1 μM BayK 8664 and 30 μM nifedipine (a calcium channel antagonist), respectively [90], [109].

3.1.2 **Ion channel modulators**

BayK 8664 is a positive ionotrope that has been shown to increase APD by binding to L-type calcium channels and decreasing the activation time and shifting the voltage-dependence more negative [176], [177]. By affecting channel opening time and left-shifting the voltage dependence, there is a greater peak Ca^{2+} current at more negative membrane potentials, causing a net effect of an earlier, and greater I_{CaL} current, and a more prolonged Ca^{2+} release from the sarcoplasmic reticulum (SR) during an AP [177], [178]. This means that BayK 8664 would prolong the APD_{90} by increasing the duration of the plateau phase, by increasing the probability of calcium channel opening from the shifted voltage-dependence, and decreasing the time of calcium channel activation. BayK 8664 has been shown to increase APD_{90} under standard electrode-based dynamic clamp conditions, so it is expected that ODC will yield the same effects [90], [109].

Terfenadine is a H1-receptor antagonist and was marketed as an antihistamine. However, terfenadine was shown to be arrhythmogenic, after it was approved by the FDA and distributed to patients. It was discovered in post-market research that its mechanism of toxicity was through hERG channel antagonism and terfenadine was withdrawn from the market for cardiotoxicity [32], [179]–[182]. Terfenadine is thought to bind within the central cavity of hERG and form crucial pi-pi stacking interactions, increasing its affinity to the channel [183].

Terfenadine was one of the first drugs that led to the discovery that I_{Kr} inhibition is a potential mechanism behind drug-induced cardiac arrhythmia. Now, measuring I_{Kr} inhibition is an important focus during drug development to help predict drug-induced cardiac toxicity. In response to terfenadine, the APD_{90} will also be prolonged and the time of repolarization will be increased, since I_{Kr} is an important repolarizing current [174].

Verapamil is a clinically-approved drug to treat high blood pressure, severe angina and arrhythmias [184]–[186]. Verapamil binds to L-type calcium channels in a voltage- and use-dependent manner, thereby blocking calcium channels when open or inactivated at depolarized potentials [184], [187]. Verapamil also has a similar affinity to hERG channels as it does to calcium channels, and its binding to the channel is also state-dependent [188]. Interestingly, it is clinically safe in patients, despite also being a hERG channel blocker [185], [186], [189], [190]. The antagonistic effect of verapamil on calcium channels counteracts the prolongation of the action potential caused by hERG antagonism [191]. With the finding that drugs that inhibit I_{Kr} also tend to induce cardiac toxicity, drug developers are discouraged from pursuing the development of drugs that decrease I_{Kr} or have hERG affinity. Verapamil is a great example of a drug that would probably not be pursued for drug development today, but would be a missed opportunity for a safe and beneficial drug. In response to verapamil, the earlier phase of the AP (i.e., APD_{30}) is shortened because of its effect on calcium channels, and averaging across

cells, APD_{90} does not change in a dose-dependent manner, although when looking at individual cells, both APD_{90} shortening and prolongation can be observed in cardiomyocytes of several species [174], [192]–[194].

How iPSC-CMs under I_{K1} addition with EDC would respond to terfenadine and verapamil has not been investigated in the literature. iPSC-CMs may overestimate the effect of drugs that affect I_{Kr}, since iPSC-CMs have decreased levels of the other native repolarizing currents, I_{K1} and I_{Ks}. Perhaps with the addition of I_{K1}, it could reduce this hypersensitivity to I_{Kr} inhibition. It will therefore be important to see the effects on AP characteristics of terfenadine and verapamil under dynamic clamp conditions compared to the control because of the addition of another repolarizing current.

3.2 Materials and Methods

3.2.1 Experimental protocol and analysis

Preparation of ArchT-expressing iPSC-CMs, the electrophysiological protocol and the EDC and ODC platform protocols are described in the Materials and Methods section in Chapter 2. The analysis of AP characteristics was also calculated as described in the Materials and Methods section in Chapter 2. All cells and trials were included in the analysis, unlike in Chapter 2 where trials were not included in the analysis if they contained more than one spontaneous

event under EDC or ODC conditions. All cells had to be included here because spontaneous events occurred in some section of each protocol due to the shorter pacing frequency and longer protocol. APs were analyzed only if evoked by a stimulus (i.e., spontaneously occurring APs were not included in the analysis).

3.2.2 Drug Screening Protocol

After obtaining a whole-cell perforated patch, cells were paced at 0.5 Hz and APs were measured under control (no dynamic clamp), EDC, and ODC conditions, in no particular order, to establish a baseline. Three concentrations per drug were tested, from lowest to highest. After establishing the baseline AP by pacing the cells at 0.5 Hz under the three conditions without any drug present, the cells were perfused with an extracellular solution containing the drug for 5 minutes, and then the cells were paced again at 0.5 Hz and the APs were recorded. This was repeated with higher drug concentrations and APs were again measured under control, EDC, and ODC conditions, in no particular order. This protocol is illustrated in Figure 3.1. The drug concentrations used for BayK 8664 were 0 nM, 50 nM, 500 nM, and 5 μM. These concentrations were chosen to measure a dose-response effect, and 1 μM has been used with BayK 8664 in iPSC-CMs to show that APD_{90} prolongation can be seen under I_{K1} addition via dynamic clamp [102], [154]. Terfenadine was used at 0 nM, 50 nM, 200 nM, and 500 nM. Verapamil was tested at 0 nM, 30 nM, 300 nM, and 3 μM.

The concentrations for terfenadine and verapamil used similar dose-response concentrations used in the literature [174]. For the remainder of the manuscript, “Drug None” refers to 0 nM of drug used, “Drug Low” refers to the smallest drug concentration used, “Drug Med” refers to the medium drug concentration used and “Drug High” refers to the highest drug concentration used.

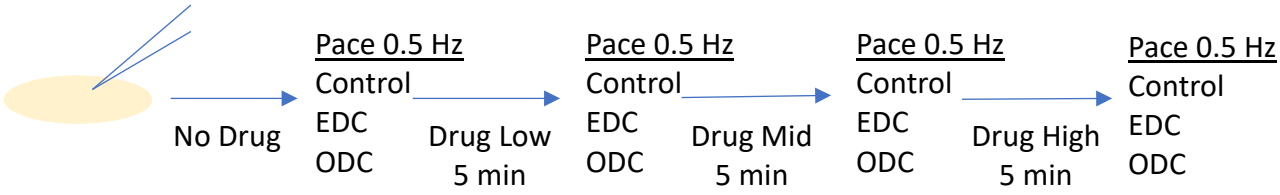

Figure 3.1: Illustration of the drug screening protocol
After obtaining a perforated patch on an iPSC-CM (left panel), the cell was perfused with various concentrations of drugs sequentially and paced at 0.5 Hz under the three conditions listed in no particular order.

3.3 Results

3.3.1 Representative examples of cell response from dose response experiment under control, EDC and ODC conditions

We analyzed the results from the drug screening experiments to determine how the ODC platform compared to the EDC platform, and if the platforms were still able to detect the anticipated changes on AP characteristics. The following figures illustrate an example of a cell that has undergone the drug screening protocol at the various concentrations of BayK 8664 (Figure 3.2), terfenadine

(Figure 3.3), or verapamil (Figure 3.4). The particular cells in Figures 3.2-3.4 were chosen because they demonstrate how the tested cells typically respond during the drug screening protocol. Under control conditions, there is a greater amount of spontaneous activity that is inhibited with both EDC and ODC conditions, reducing the effect of AP rate dependence on subsequent AP characteristics. Similar to the effect seen in Figure 2.4, the membrane potential between APs are not always as well maintained in ODC as in EDC, and this is also reflected in I_{target} (Figure 3.2A, 3.3 A-D). Looking at the resulting APs produced from the EDC and ODC platforms, the APs and I_{target} under EDC and ODC conditions generally overlap well during the AP, indicating that the ODC condition can produce similar results to EDC. In addition, ODC is able to reflect similar effects of the drug on AP morphology under EDC conditions, such as APD_{90} prolongation with increasing BayK 8664 and terfenadine. Overall response to drugs under the EDC and ODC platforms will be further discussed in the next section.

There are several cases where ODC does not overlap well with EDC during the AP (Figure 3.2A, 3.3A, 3.3D, and 3.4D). Similar to the results in Chapter 2, ArchT is unable to induce a negative current, unlike an electrode, so EDC is able to correct for the undershoot whereas ODC is unable to do so (Figure 3.3). The limitations of the ODC platform that could cause the mismatch of APs under ODC and EDC were described in Chapter 2 (Section 2.4.1) and are discussed further below (Sections 3.4.2 and 3.4.3).

In the results of Bett et al. (2013) the iPSC-CMs depolarized in the control in the presence of 1 μM BayK 8664 such that APs could not be stimulated and APs with a prolonged APD_{90} could only be successfully measured with dynamic clamp addition of I_{K1}. However, this was not the case with BayK 8664 administration in our experiments. The iPSC-CMs did not depolarize like the cells in Bett et al., and APs were still able to be stimulated. Unfortunately, because the AP-prolonging effect of BayK 8664 at Drug High was evident with and without dynamic clamp, we were unable to demonstrate the advantage of using dynamic clamp for drug screening.

Figure 3.2: Representative example of a cell under control, EDC and ODC conditions at different concentrations of BayK 8664
The top panel illustrates two stimulated APs from an example cell exposed to various drug concentrations: Drug None (A), Drug Low (B), Drug Med (C), Drug High (D). The black triangles indicate when a stimulus current was delivered. The middle panels show the calculated I_{target} (I_{K1}). The bottom panels show the calculated light intensity used to generate the target current.

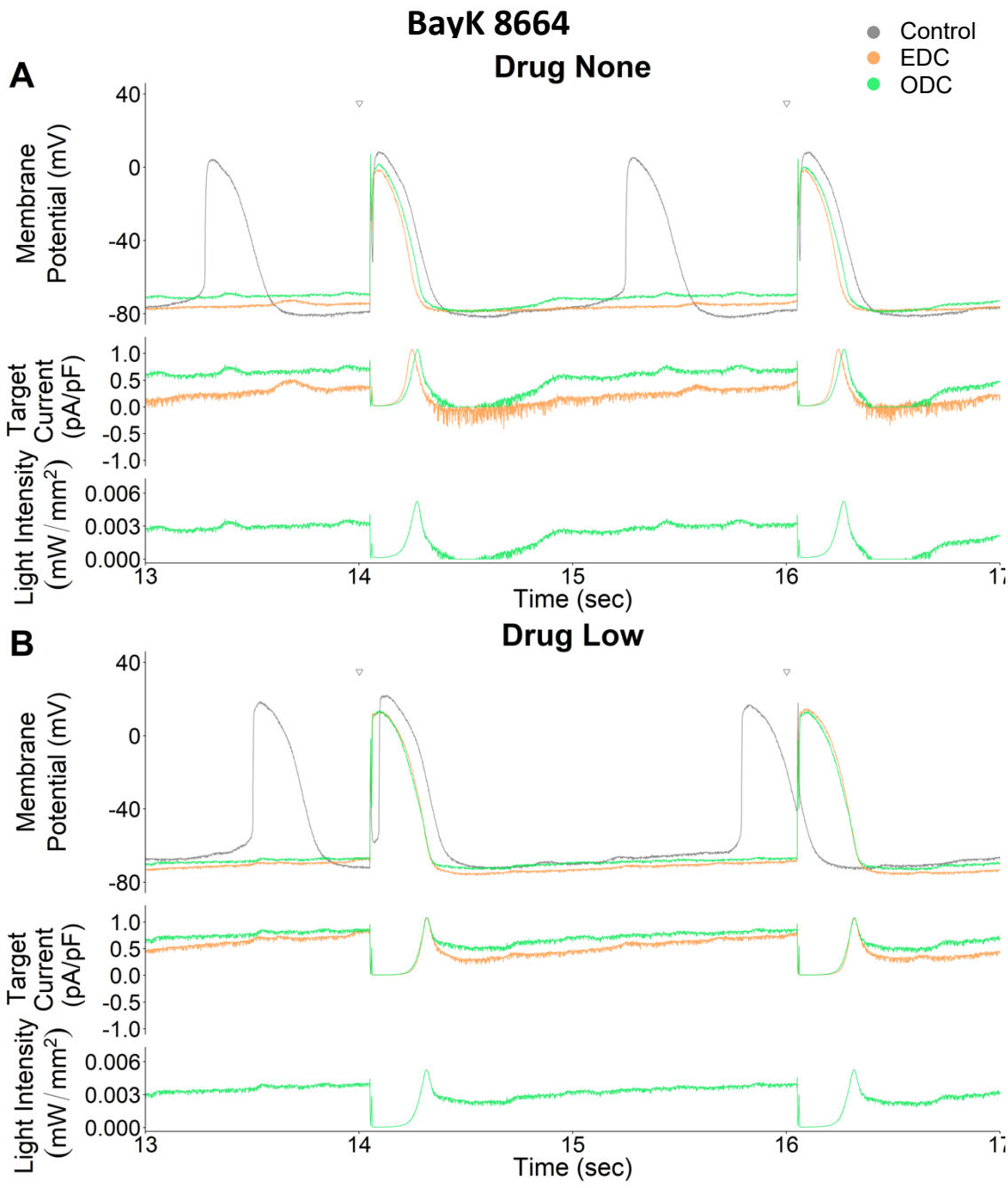
BayK 8664
Control
EDC
ODC
A
Drug None
Membrane Potential (mV)
40
0
-40
-80
Target Current (pA/pF)
1.0
0.5
0.0
-0.5
-1.0
Light Intensity (mW/mm²)
0.006
0.003
0.000
13
14
15
16
17
Time (sec)
B
Drug Low
Membrane Potential (mV)
40
0
-40
-80
Target Current (pA/pF)
1.0
0.5
0.0
-0.5
-1.0
Light Intensity (mW/mm²)
0.006
0.003
0.000
13
14
15
16
17
Time (sec)

Figure 3.2 (Continued)

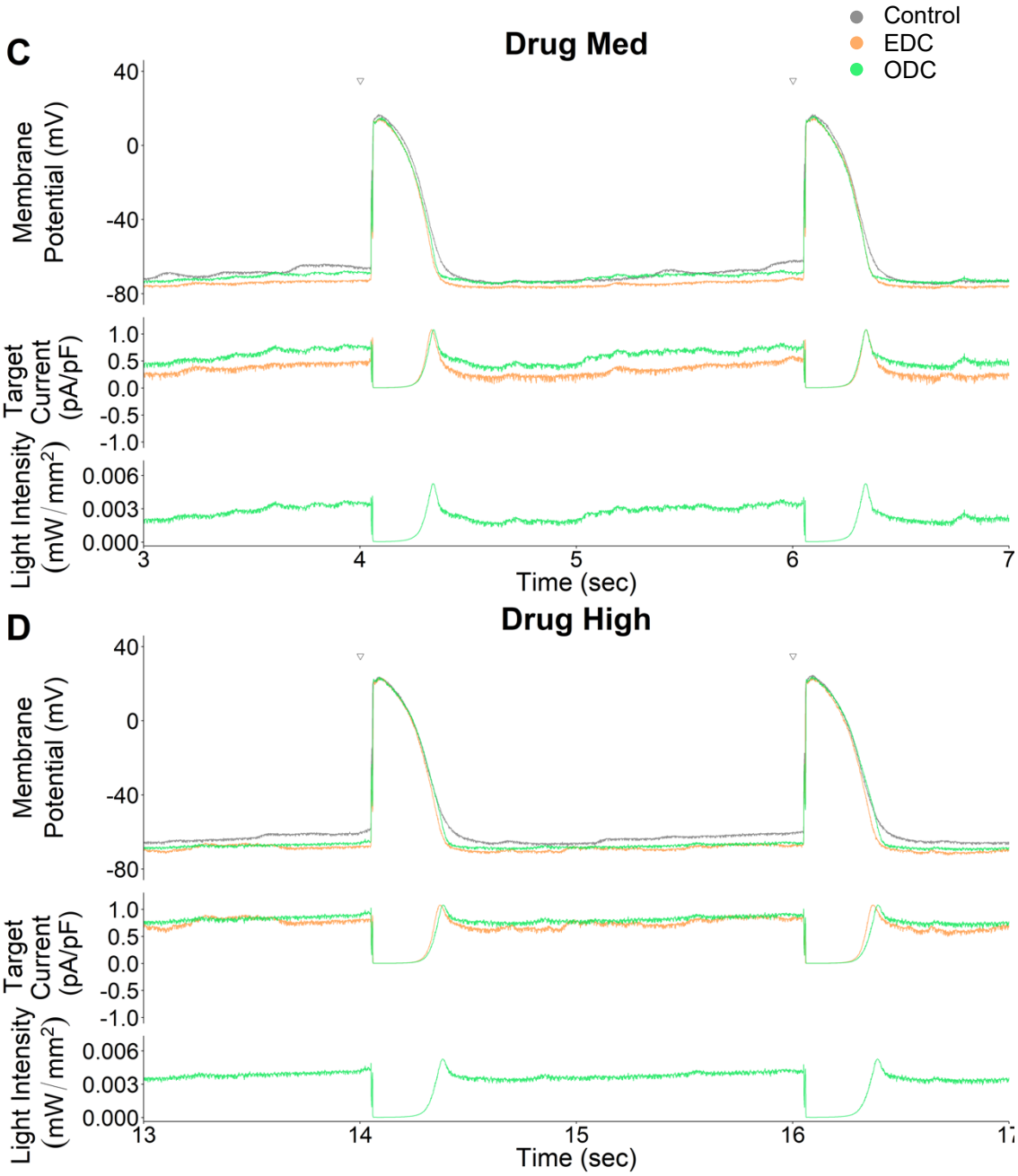

Figure 3.3: Representative example of a cell under control, EDC and ODC conditions at different concentrations of terfenadine
Figure is organized in the same manner as Figure 3.2.

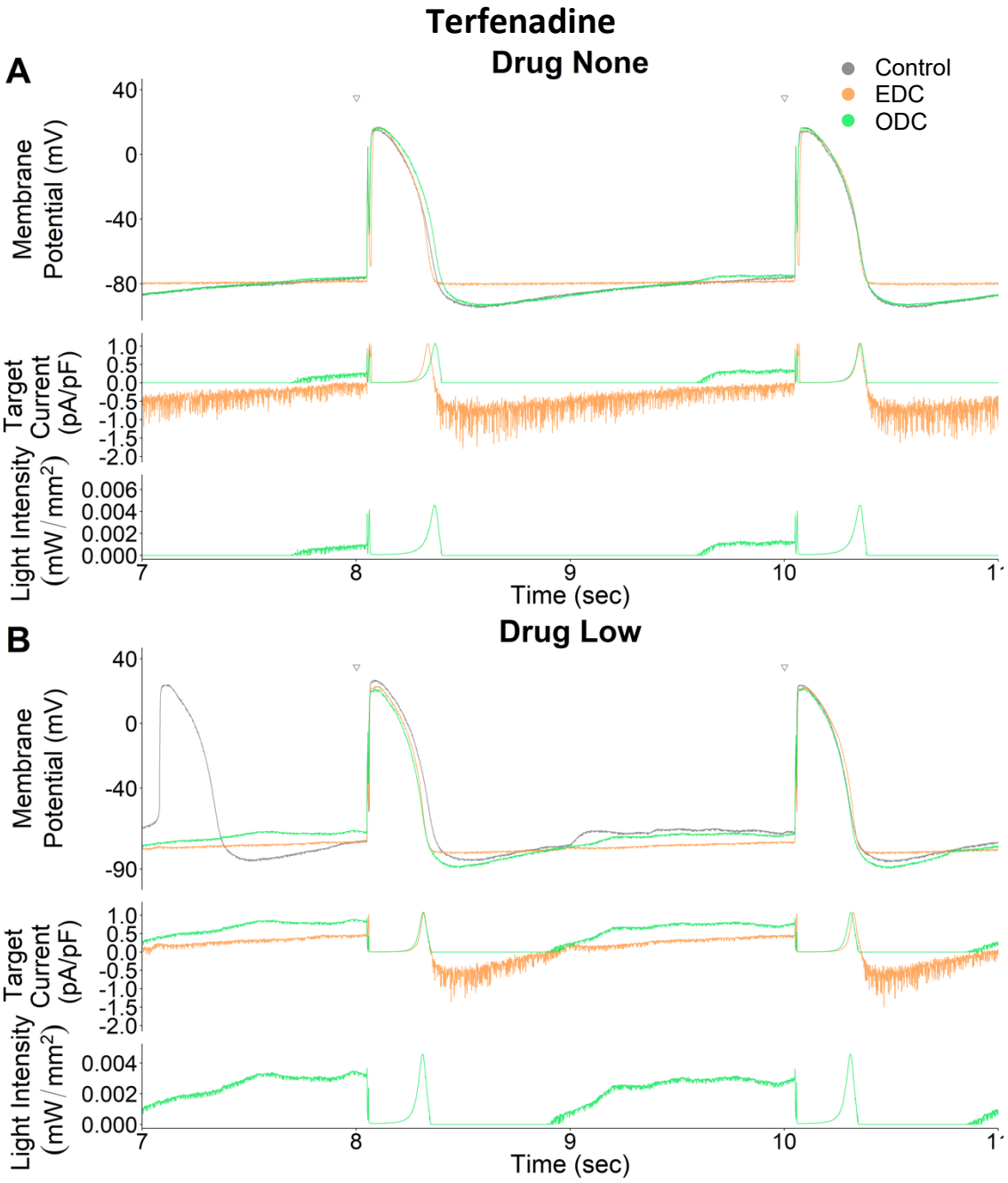
Terfenadine
A
Drug None
Control
EDC
ODC
Membrane Potential (mV)
40
0
-40
-80
Target Current (pA/pF)
1.0
0.5
0.0
-0.5
-1.0
-1.5
-2.0
Light Intensity (mW/mm²)
0.006
0.004
0.002
0.000
7
8
9
10
Time (sec)
B
Drug Low
Membrane Potential (mV)
40
0
-40
-90
Target Current (pA/pF)
1.0
0.5
0.0
-0.5
-1.0
-1.5
-2.0
Light Intensity (mW/mm²)
0.004
0.002
0.000
7
8
9
10
Time (sec)

Figure 3.3 (Continued)

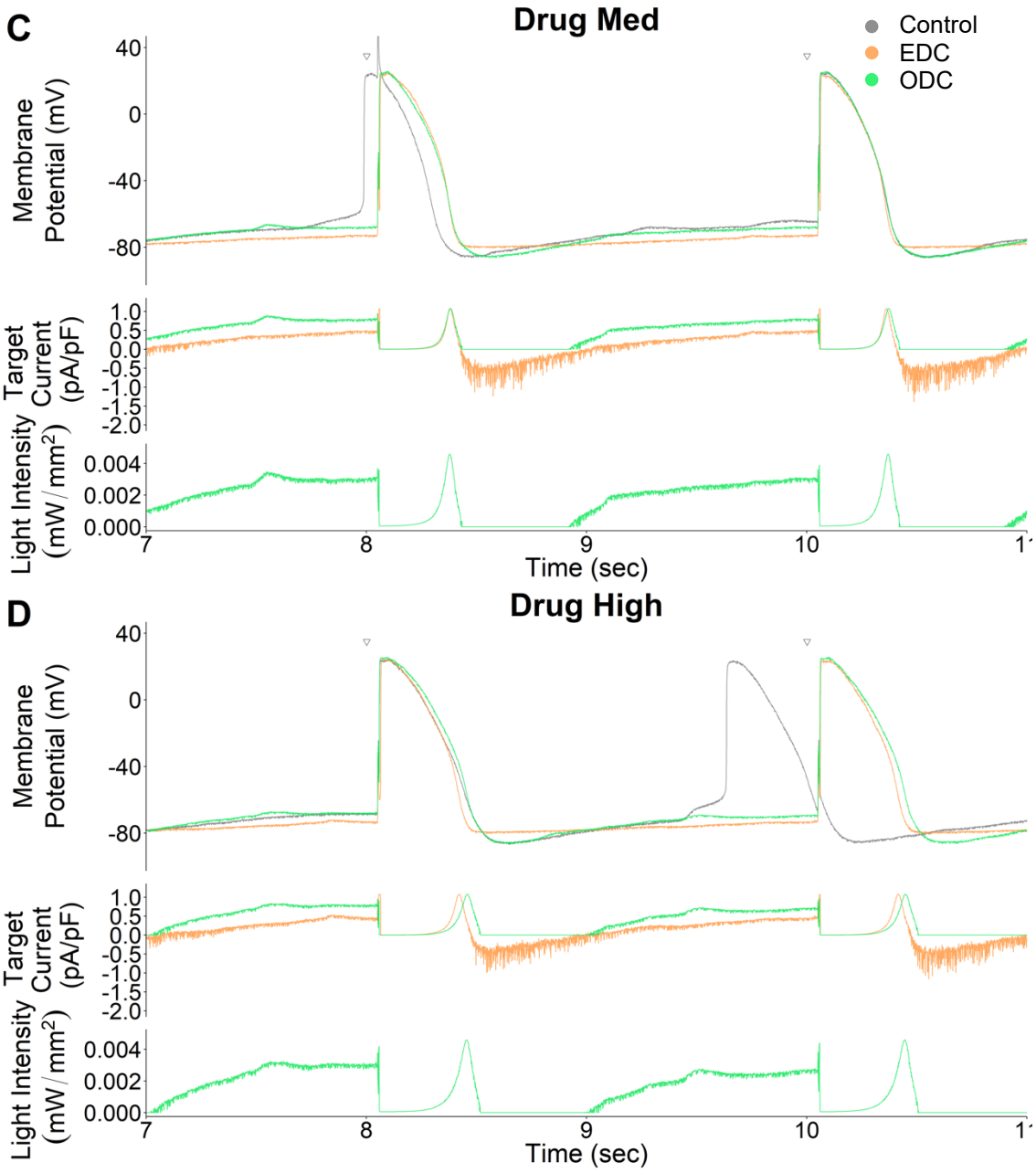

Figure 3.4: Representative example of a cell under control, EDC and ODC conditions at different concentrations of verapamil
Figure is organized in the same manner as Figure 3.2.

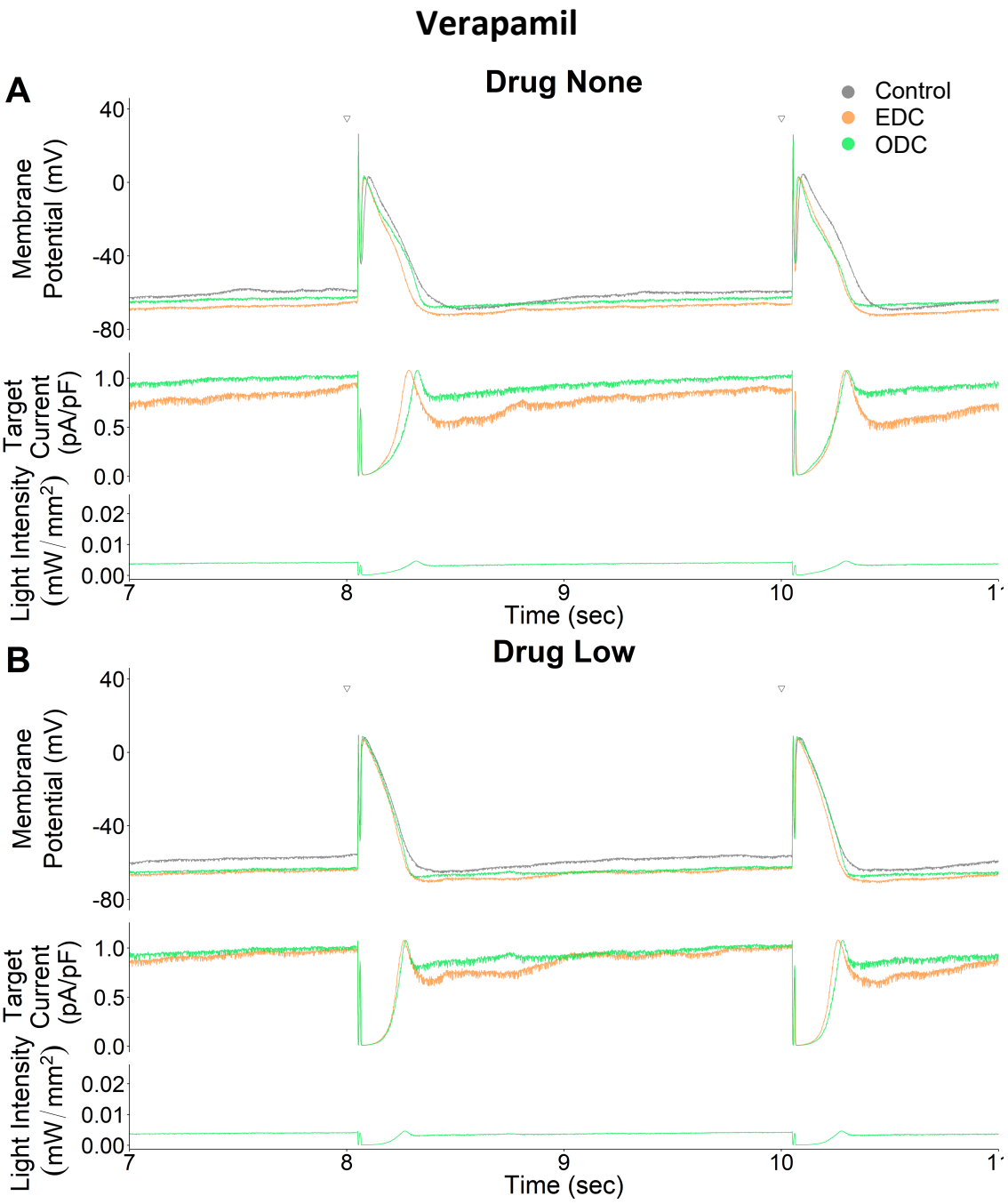
Verapamil
A
Drug None
Control
EDC
ODC
Membrane Potential (mV)
40
0
-40
-80
Target Current (pA/pF)
1.0
0.5
0.0
Light Intensity (mW/mm²)
0.02
0.01
0.00
7
8
9
10
Time (sec)
B
Drug Low
Membrane Potential (mV)
40
0
-40
-80
Target Current (pA/pF)
1.0
0.5
0.0
Light Intensity (mW/mm²)
0.02
0.01
0.00
7
8
9
10
Time (sec)

Figure 3.4 (Continued)

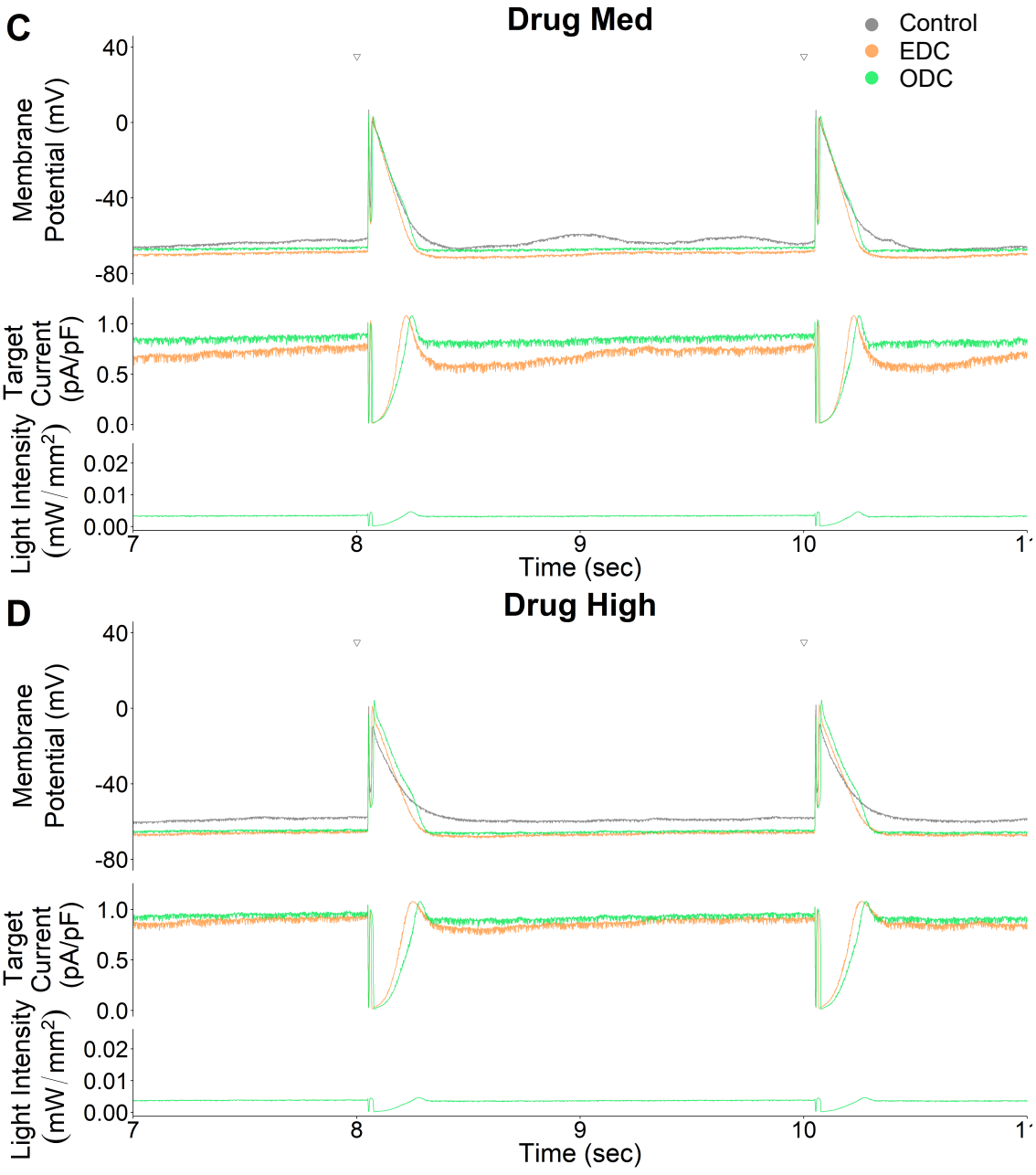

3.3.2 ODC platform can detect changes in AP characteristics in response to ion channel modulators

To determine the feasibility of the ODC platform for drug screening, we need to confirm if the ODC platform can detect the effects of ion channel modulators on AP characteristics. The control condition verifies that the drug is active and the cell is responding as predicted. The EDC determines if under dynamic clamp conditions, the effect of the drugs on AP morphology is detectable with the addition of I_{target} and is used to predict the effects the ODC platform should yield. Table 3.1 lists the average percent change of AP characteristics and SEMs of each drug tested and at each concentration.

3.3.2.1 BayK 8664

With increasing concentration of BayK 8664, we would expect APD_{30} and APD_{90} to increase because of its effect on I_{CaL}. Figure 3.5 illustrates the percent change in APD_{90}, APD_{30}, fraction of repolarization and triangulation, compared to the results within the same condition with Drug None, in response to treatment with BayK 8664 at different concentrations. An increase in APD_{90} is expectedly observed in the control, ODC and EDC conditions, but the increase in APD_{90} is statistically significant only at the highest concentration under control and ODC. The initial decrease of APD_{90}, mainly seen in ODC, is not expected but not statistically significant. The reasons for this remain unknown. The control, EDC

and ODC demonstrate an average increase in APD_{30} but this is not statistically significant and there is a great variability of responses. There is one outlier in the ODC APD_{30} measurement, which could give the illusion that the outlier is responsible for the increased average APD_{30} with ODC. The average percent change in APD_{30} under ODC without the outlier is as follows: Drug Low, -1.8; Drug Med, 12.2%; Drug High, 23.3%. Even without the outlier, there is an increase in percent change of APD_{30}. The decrease in average triangulation and fraction of repolarization is reflected by the increase in APD_{30} but not APD_{90}, and is not statistically significant. The activity of BayK 8664 used in these experiments had previously been confirmed with calcium imaging experiments with Fluo 4-AM with guinea pig cardiomyocytes (data not shown). The results of the drug-screening experiments were not due to inactivity of BayK 8664.

3.3.2.2 Terfenadine

Terfenadine, like BayK 8664, is expected to prolong the APD_{90} because of its effect on I_{Kr}. Because the drug is inhibiting a major repolarizing current, it is also expected that the fraction of repolarization and triangulation will both increase. Figure 3.6 displays the percent change of AP characteristics at different concentrations of terfenadine under control, EDC and ODC conditions. There is an unexpected but not statistically significant decrease in APD_{90} at Drug Low, followed by a dose-dependent increase in APD_{90} at Drug Med and High (only statistically significant at Drug Med in Control, and Drug High in all three

conditions). APD_{30} interestingly shortened at all drug concentrations in all three conditions, but less drastically in ODC. The decrease in APD_{30} was statistically significant in Control and EDC at Drug Low. The reason for this is unknown, but the effect could cause the initial decrease in APD_{90}. Perhaps greater I_{Kr} inhibition at higher drug concentrations was able to overcome this unknown effect and prolong APD_{90}. All three conditions expectedly yielded a significant increase in fraction of repolarization and triangulation in a dose-dependent manner after the initial decrease in APD_{90}. This demonstrates that the ODC platform is sensitive to I_{Kr} inhibition, which is crucial for future drug screening applications given its significance in predicting drug-induced cardiovascular toxicity.

3.3.2.3 Verapamil

Finally, unlike the other two drugs, verapamil affects two different ionic currents. With Ca^{2+} channel antagonism, APD_{90} and APD_{30} would shorten, and triangulation would increase. I_{Kr} inhibition would typically prolong APD_{90} and fraction of repolarization. Previous literature has demonstrated that as a net effect of both Ca^{2+} channel antagonism and I_{Kr} inhibition, APD_{90} does not typically change on average, but when looking at individual cells, a variety of effects on APD_{90} can be measured [174]. This is because individual cells with a net effect of shortening, prolonging, or not changing the APD_{90} may result from the varying contribution of I_{CaL} and I_{Kr} on the level of the individual cell to APD.

But when averaged across all cells, APD_{90} does not get prolonged in a dose-dependent manner despite inhibiting hERG channels, which is presumably why verapamil is safe for patients.

In the results of the verapamil screen (Figure 3.7), shortening of the APD_{30} in a dose-dependent manner can be observed in control, EDC and ODC conditions. Averaging across all cells, the APD_{90} initially shortens at lower drug concentrations and then increases back to baseline (Drug None). This observation is consistent to the opposing effects of I_{Kr} and I_{CaL} inhibition and consistent with what is seen in literature [93], [195]. APD_{30} decreases in a dose-dependent manner, presumably resulting from the I_{CaL} inhibition. Fraction of repolarization and triangulation all increase in a dose-dependent manner, as expected, under all three platform conditions [174]. The changes in fraction of repolarization and triangulation suggests inhibition of I_{Kr}. This demonstrates that the ODC platform can also reflect the overall effect of drugs that have multiple targets on AP characteristics.

In summary, the ODC platform is able to measure the expected changes in AP characteristics in response to various well-characterized ion channel modulators. This suggests the potential reliability of the ODC platform in drug screening applications.

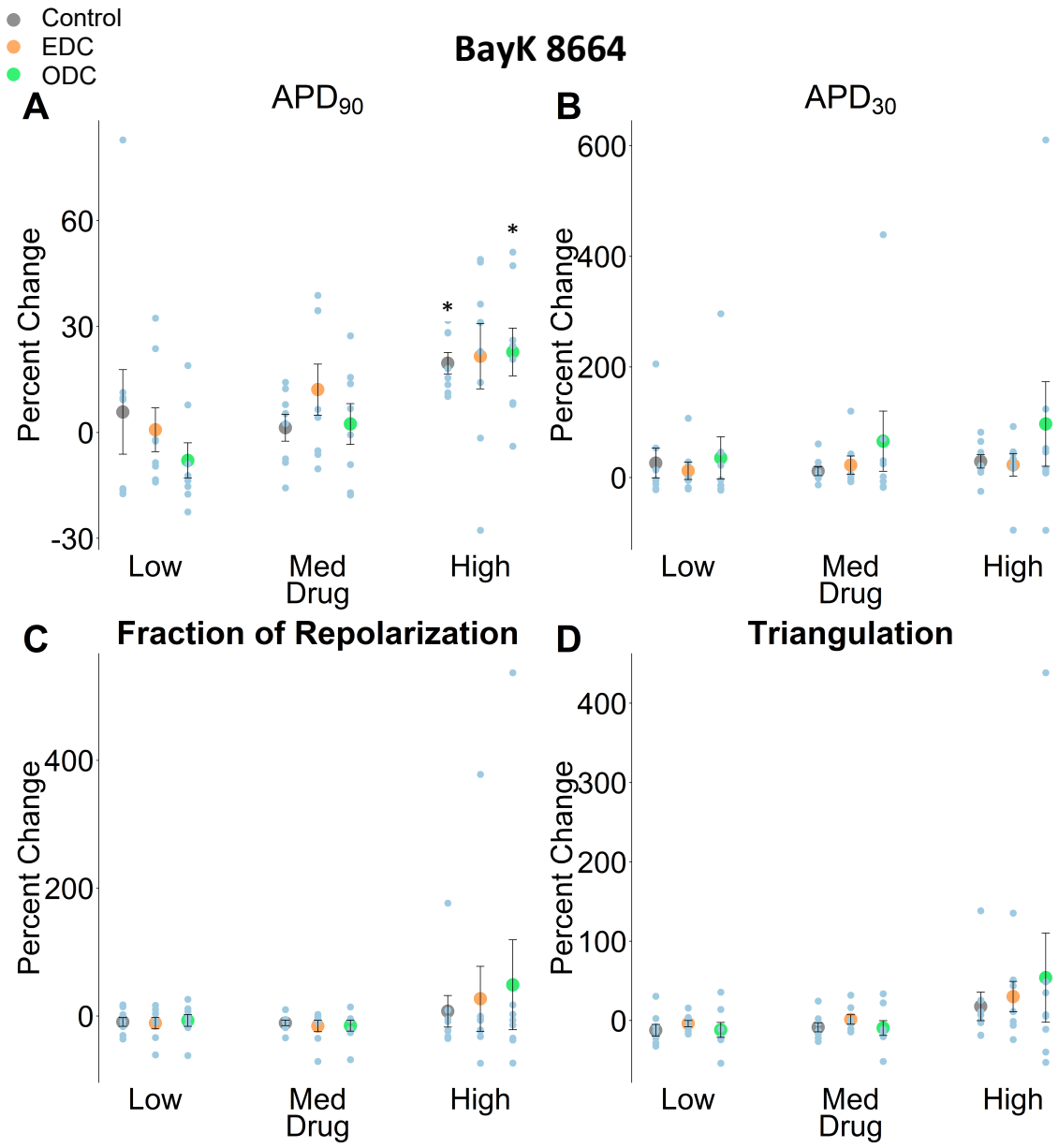

Figure 3.5: Effect of BayK 8664 at different concentrations on AP characteristics under Control, EDC and ODC conditions
Average and SEM percent change of several AP characteristics: APD_{90} (A), APD_{30} (B), Fraction of Repolarization (C) and Triangulation (D) at different drug concentrations. The gray, orange, and green points represent the results under control conditions, with EDC, and with ODC, respectively. The blue points represent individual cells.

n = 8

* $p < 0.05$ compared to Drug None of the same condition (Control, EDC or ODC)

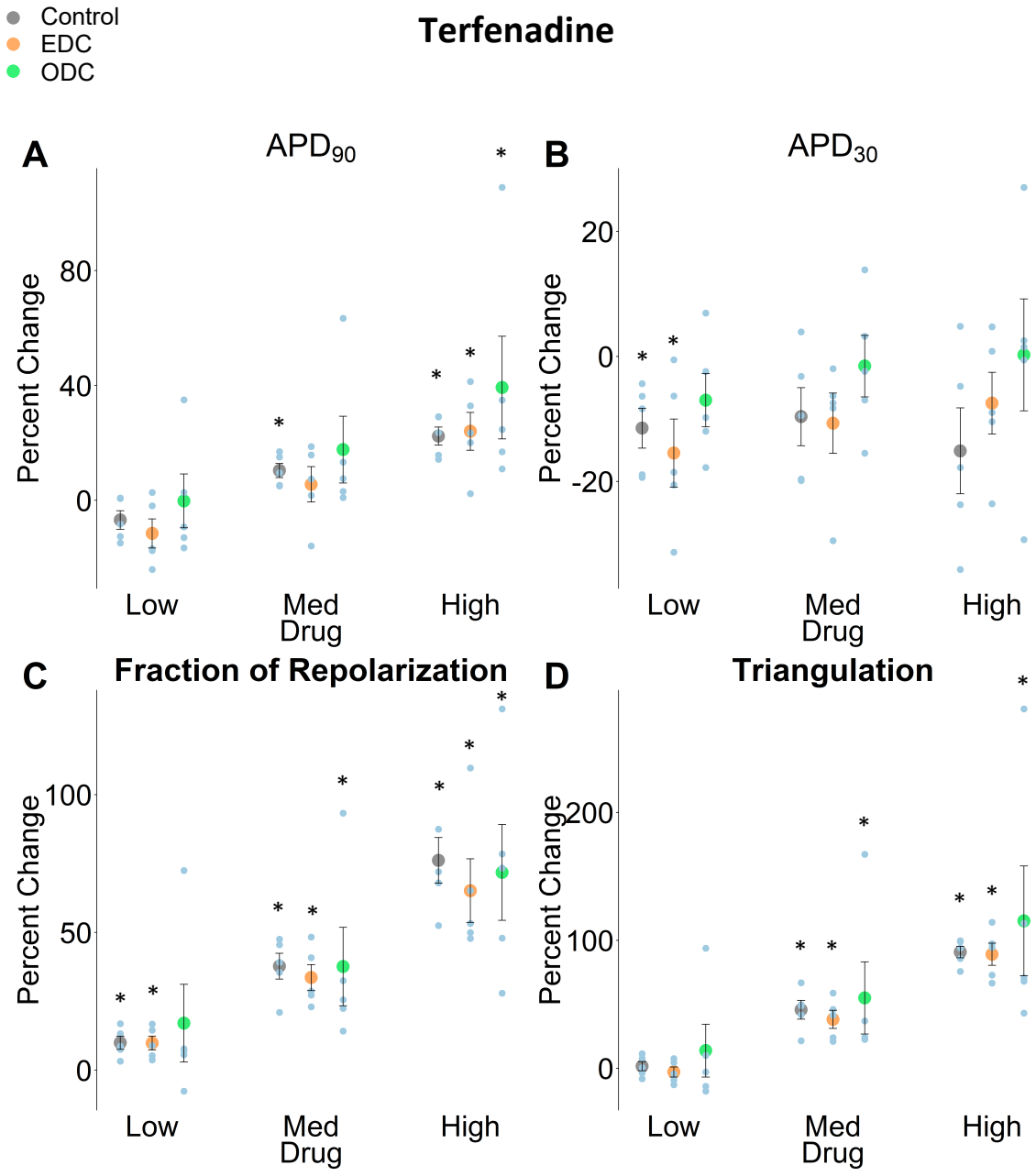

Figure 3.6: Effect of terfenadine at different concentrations on AP characteristics under Control, EDC and ODC conditions
Figure is organized in the same manner as Figure 3.4.

n = 5

* $p < 0.05$ compared to Drug None of the same condition (Control, EDC or ODC)

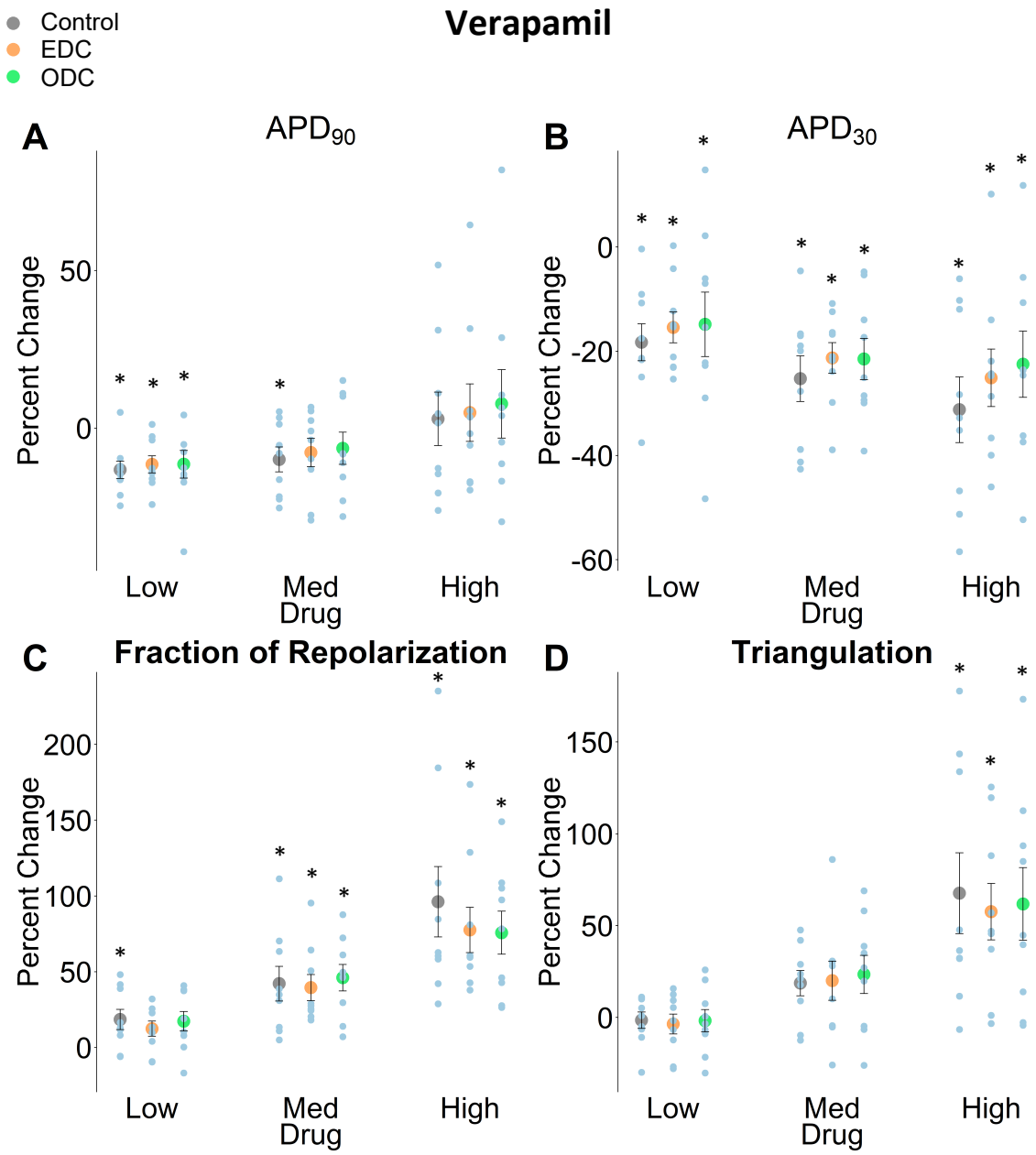

Figure 3.7: Effect of verapamil at different concentrations on AP characteristics under Control, EDC and ODC conditions
Figure is organized in the same manner as Figure 3.4.

n = 9

* $p < 0.05$ compared to Drug None of the same condition (Control, EDC or ODC)

Table 3.1: Average percent change relative to Drug None and SEM values of AP characteristics during drug screening protocol

APD_{90}

		Control		EDC		ODC	
		Average	SEM	Average	SEM	Average	SEM
BayK 8664	Low	5.8	12.0	0.8	6.2	-7.9	5.0
	Med	1.3	3.8	12.1	7.3	2.4	5.8
	High	19.6	3.0	21.6	9.3	22.8	6.8
Terfenadine	Low	-6.9	3.3	-11.5	5.1	-0.2	9.4
	Med	10.4	2.5	5.6	6.2	17.7	11.6
	High	22.3	3.2	24.0	6.6	39.3	17.9
Verapamil	Low	-13.2	2.8	-11.5	2.7	-11.5	4.4
	Med	-9.9	4.0	-7.7	4.5	-6.4	5.1
	High	2.9	8.5	4.9	9.1	7.7	10.9

APD_{30}

		Control		EDC		ODC	
		Average	SEM	Average	SEM	Average	SEM
BayK 8664	Low	26.2	27.0	12.2	15.9	35.4	38.2
	Med	11.5	8.1	22.5	16.4	65.5	54.4
	High	29.0	12.1	22.9	20.4	96.7	76.5
Terfenadine	Low	-11.5	3.2	-15.5	5.4	-7.0	4.3
	Med	-9.6	4.6	-10.7	4.8	-1.6	4.9
	High	-15.1	6.9	-7.5	4.9	0.2	8.9
Verapamil	Low	-18.3	3.6	-15.4	3.0	-14.8	6.2
	Med	-25.3	4.4	-21.3	2.9	-21.5	3.9
	High	-31.2	6.3	-25.1	5.5	-22.5	6.3

Fraction of Repolarization

		Control		EDC		ODC	
		Average	SEM	Average	SEM	Average	SEM
BayK 8664	Low	-9.3	6.9	-11.4	8.9	-7.1	9.3
	Med	-10.9	4.4	-15.7	8.9	-15.2	8.7
	High	7.3	24.7	26.8	50.8	48.8	70.4
Terfenadine	Low	9.9	2.4	9.8	2.5	17.1	14.1
	Med	37.7	4.7	33.6	4.7	37.6	14.2
	High	76.1	8.3	65.1	11.5	71.7	17.4
Verapamil	Low	18.4	6.7	12.4	5.0	17.4	6.4
	Med	42.1	11.4	39.5	8.6	46.0	8.7
	High	96.2	23.2	77.5	15.0	75.7	14.2

Triangulation

		Control		EDC		ODC	
		Average	SEM	Average	SEM	Average	SEM
BayK 8664	Low	-12.3	7.4	-3.8	3.9	-11.8	9.5
	Med	-8.5	5.8	1.3	6.0	-9.4	9.4
	High	17.7	18.0	30.2	19.0	54.0	56.2
Terfenadine	Low	1.6	3.6	-2.9	3.9	13.8	20.6
	Med	45.8	7.3	38.3	7.0	55.1	28.2
	High	90.9	4.5	89.2	8.6	115.3	42.9
Verapamil	Low	-1.5	4.4	-3.6	5.4	-1.8	6.1
	Med	18.7	6.9	20.0	10.7	23.4	10.4
	High	67.6	22.0	57.5	15.3	61.8	19.8

3.3.3 Comparing the effect of EDC and ODC on AP characteristics during drug screening

After demonstrating that the ODC platform can detect the expected drug-induced changes in AP characteristics, the accuracy of the ODC platform to yield similar results to the EDC platform must be investigated. Based on the results in Chapter 2, it is expected that APD_{90} would be shortened, and the fraction of repolarization and triangulation would also decrease when dynamic clamp is applied compared to the control without dynamic clamp. Ideally, it is also expected that ODC yield the same results to EDC, but based on the results in Chapter 2, ODC may not change AP characteristics by the same magnitude as EDC. Nonetheless, it should yield a similar positive or negative effect as EDC. Differences in the results between the ODC and EDC could be due to limitations to using ArchT or inaccuracies of the ArchT model used to calculate the light intensity. These were elaborated upon in the Discussion section of Chapter 2. Table 3.2 lists all the averages of AP characteristics and SEMs of each drug tested and at each concentration.

Figure 3.8 displays the average and standard error of the mean (SEM) of AP characteristics in control, EDC and ODC at different drug concentrations with bayK 8664 administration. EDC is able to produce the expected results on APD as stated above in most cases. EDC did not yield an expected decrease fraction of repolarization and only a modest decrease in triangulation was achieved. The

APD_{90} and APD_{30} of APs resulting from the ODC platform is similar to EDC in most cases (except APD_{90} at Drug None and Drug High). Looking at fraction of repolarization and triangulation, the results from ODC were not similar to EDC. ODC was more similar to the results from control, and sometimes were different from both control and EDC. The potential reasons as to why ODC did not perform as well as EDC are further discussed in the Discussion section.

In the presence of terfenadine, the EDC platform shortened the APD_{90}, and decreased fraction of repolarization and triangulation, as expected at different drug concentrations (Figure 3.9). ODC had a similar effect on these parameters as EDC, but not to the same magnitude as EDC did. This suggests that although ODC does affect AP characteristics as expected with dynamic clamp addition of I_{target}, it does not behave identically to an electrode.

In Figure 3.10, results from the drug screen with verapamil shows that EDC decreased APD_{90}, fraction of repolarization and triangulation, as expected with dynamic clamp. But as was the case with terfenadine application, ODC has a similar effect as EDC on AP characteristics, but it did not have the same magnitude of an effect as EDC. This supports the idea that the ODC platform is able to affect AP characteristics, but it does not behave identically to EDC.

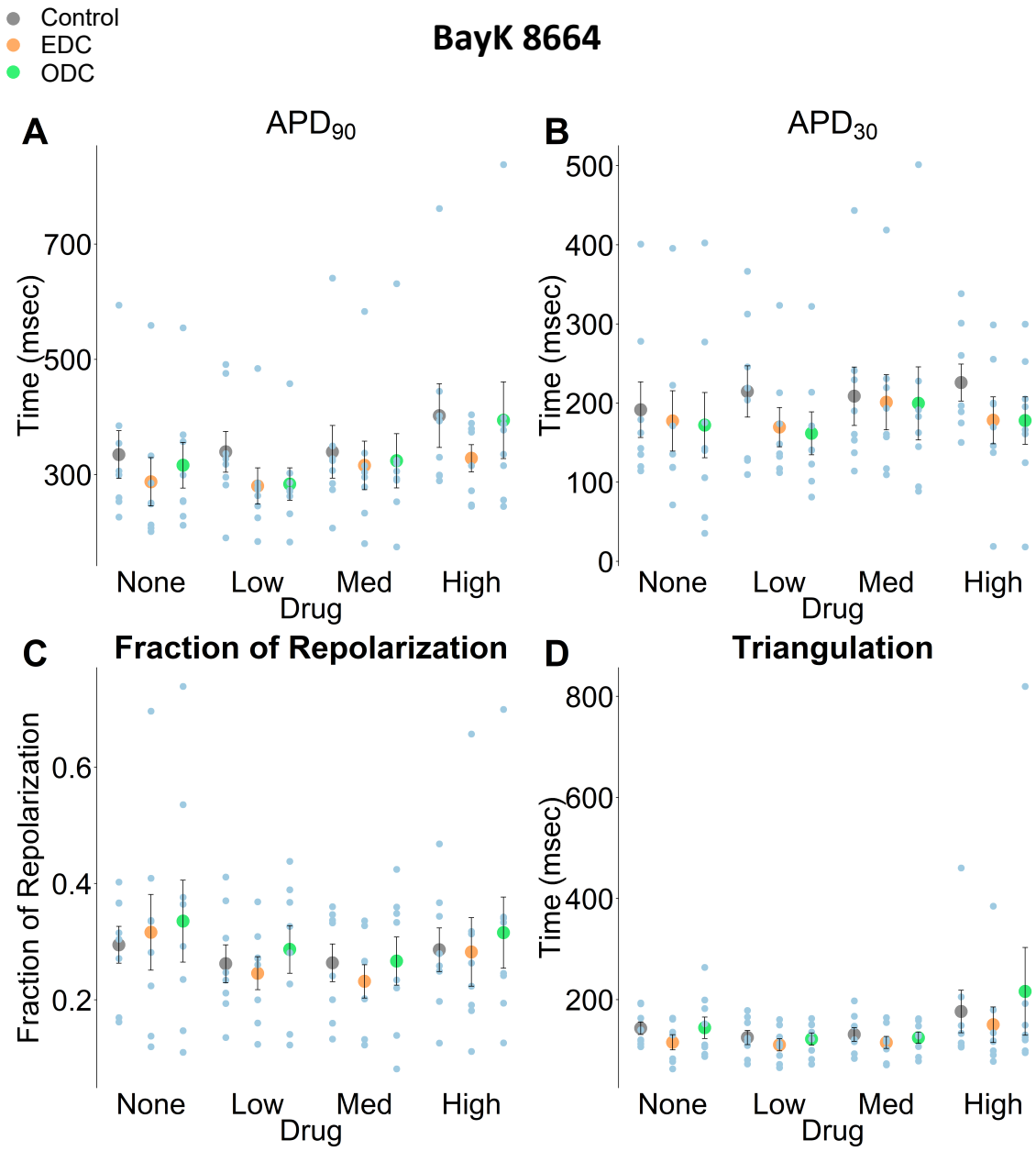

Figure 3.8: Comparing the average effect of bayK 8664 on AP characteristics between Control, EDC and ODC

Average and SEM of several AP characteristics: APD_{90} (A), APD_{30} (B), Fraction of Repolarization (C) and Triangulation (D) at different drug concentrations. The gray, orange, and green points represent the results under control conditions, with EDC, and with ODC, respectively. The blue points represent individual cells.

n = 8

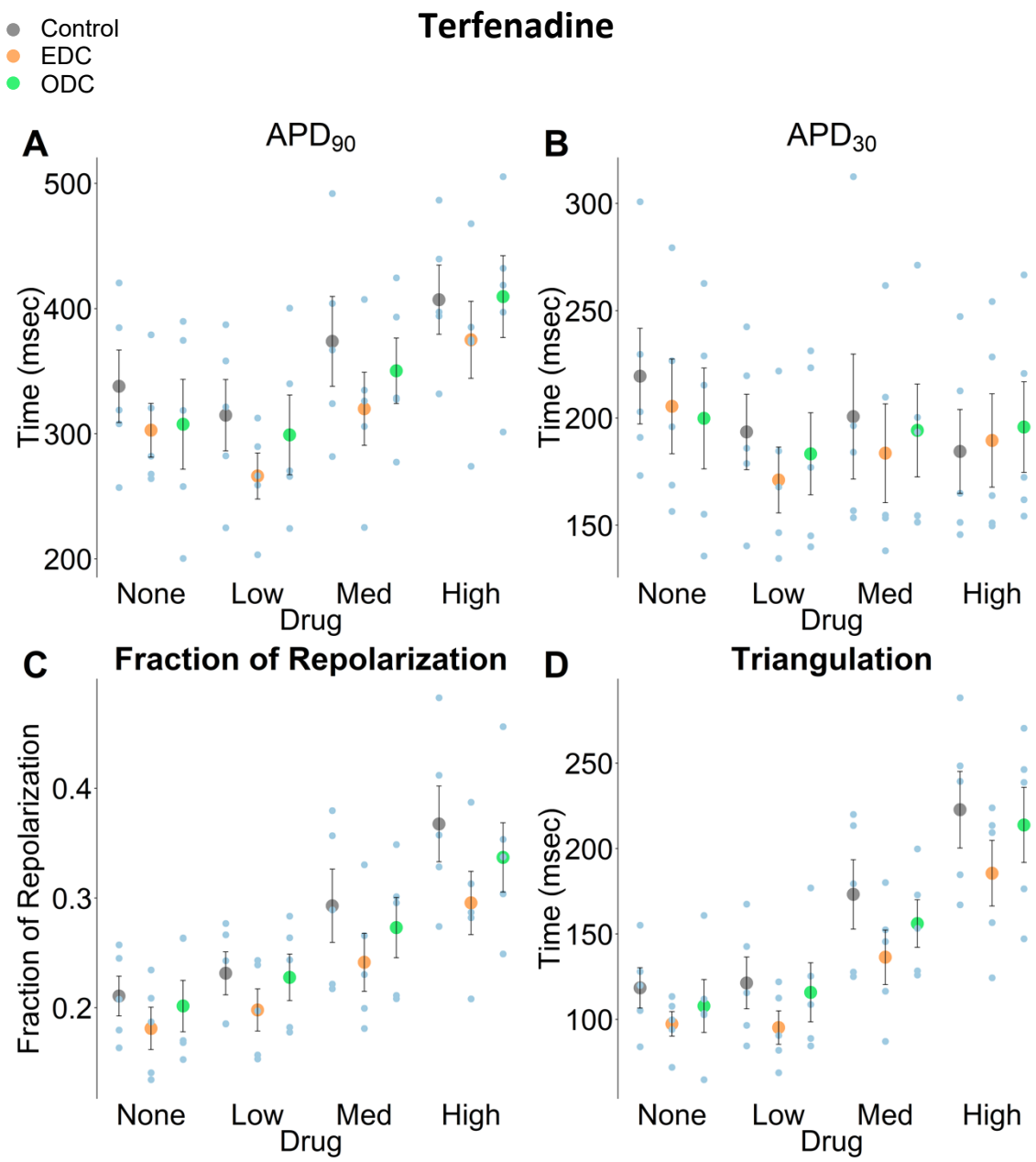

Figure 3.9: Comparing the average effect of terfenadine on AP characteristics between Control, EDC and ODC
Figure is organized in the same manner as Figure 3.8.

n = 5

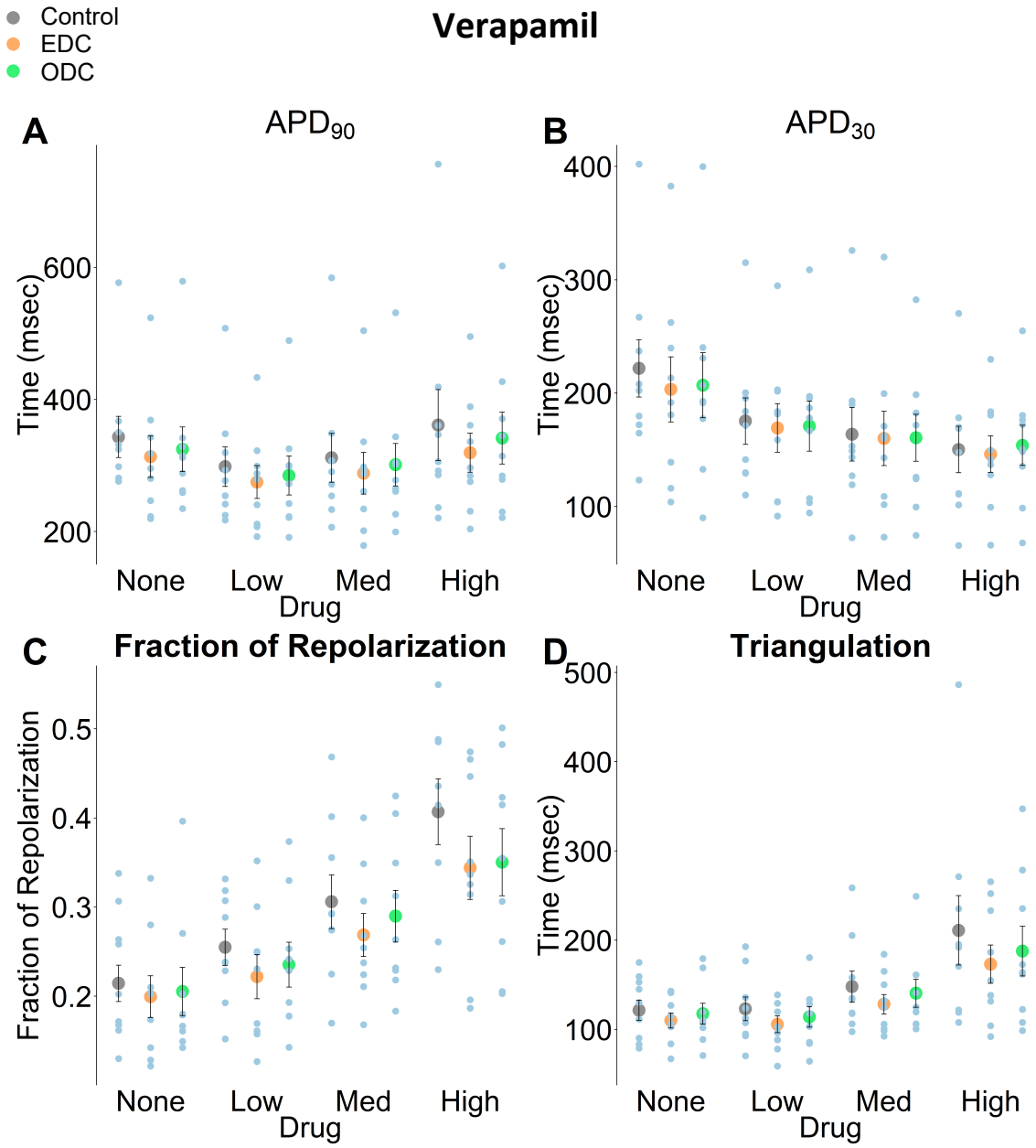

Figure 3.10: Comparing the average effect of verapamil on AP characteristics between Control, EDC and ODC
Figure is organized in the same manner as Figure 3.8.

n = 9

Table 3.2: Average and SEM values of AP characteristics during drug screening protocol

APD_{90} (msec)

		Control		EDC		ODC	
		Average	SEM	Average	SEM	Average	SEM
BayK 8664	None	334.9	41.4	287.7	41.8	316.4	39.6
	Low	339.5	35.3	280.2	31.4	283.6	28.1
	Med	339.5	45.7	316.1	42.0	324.1	47.1
	High	402.3	55.2	328.4	23.5	394.2	66.6
Terfenadine	None	337.9	29.0	302.7	21.6	307.6	35.9
	Low	314.8	28.5	266.2	18.3	299.1	31.9
	Med	373.8	35.9	319.9	29.2	350.2	26.1
	High	407.1	27.6	375.1	30.8	409.6	32.7
Verapamil	None	343.3	31.2	313.3	31.4	324.5	33.9
	Low	298.3	29.9	274.9	24.9	284.9	29.5
	Med	311.6	37.0	288.2	31.7	301.1	32.1
	High	361.3	53.9	319.3	29.5	341.6	39.3

APD_{30} (msec)

		Control		EDC		ODC	
		Average	SEM	Average	SEM	Average	SEM
BayK 8664	None	191.6	35.1	177.4	38.1	172.2	41.3
	Low	214.7	32.5	169.7	24.8	161.8	27.1
	Med	208.7	36.9	201.0	34.7	199.7	46.2
	High	225.9	23.5	178.2	29.7	178.0	29.9
Terfenadine	None	219.5	22.3	205.4	22.1	199.8	23.5
	Low	193.5	17.6	171.1	15.4	183.3	19.1
	Med	200.6	29.1	183.5	23.0	194.2	21.7
	High	184.4	19.6	189.5	21.7	195.7	21.1
Verapamil	None	221.8	25.3	203.4	28.7	207.0	28.7
	Low	175.3	20.5	169.3	21.4	170.9	22.1
	Med	163.7	23.6	160.0	23.9	160.6	20.7
	High	150.3	20.5	146.2	16.1	153.9	17.7

Fraction of Repolarization

		Control		EDC		ODC	
		Average	SEM	Average	SEM	Average	SEM
BayK 8664	None	0.29	0.03	0.32	0.07	0.34	0.07
	Low	0.26	0.03	0.25	0.03	0.29	0.04
	Med	0.26	0.03	0.23	0.03	0.27	0.04
	High	0.29	0.04	0.28	0.06	0.32	0.06
Terfenadine	None	0.21	0.02	0.18	0.02	0.20	0.02
	Low	0.23	0.02	0.20	0.02	0.23	0.02
	Med	0.29	0.03	0.24	0.03	0.27	0.03
	High	0.37	0.03	0.30	0.03	0.34	0.03
Verapamil	None	0.21	0.02	0.20	0.02	0.21	0.03
	Low	0.25	0.02	0.22	0.02	0.24	0.03
	Med	0.31	0.03	0.27	0.02	0.29	0.03
	High	0.41	0.04	0.34	0.04	0.35	0.04

Triangulation (msec)

		Control		EDC		ODC	
		Average	SEM	Average	SEM	Average	SEM
BayK 8664	None	143.3	12.5	115.5	15.0	144.2	21.3
	Low	124.9	13.9	110.5	12.2	121.8	12.0
	Med	130.8	13.4	115.1	11.9	124.4	11.1
	High	176.4	42.1	150.2	35.3	216.3	86.9
Terfenadine	None	118.4	11.8	97.3	7.2	107.8	15.5
	Low	121.3	15.2	95.1	9.8	115.8	17.3
	Med	173.1	20.3	136.3	15.9	156.1	13.9
	High	222.7	22.4	185.6	19.2	213.8	22.0
Verapamil	None	121.5	11.4	109.9	8.3	117.6	11.8
	Low	123.0	13.3	105.6	9.4	114.0	11.5
	Med	147.9	17.5	128.2	10.8	140.5	15.7
	High	211.0	38.9	173.1	21.5	187.7	27.9

Pre-Stimulation Potential (mV)

		Control		EDC		ODC	
		Average	SEM	Average	SEM	Average	SEM
BayK 8664	None	-69.9	2.8	-70.3	1.7	-67.6	2.5
	Low	-67.2	2.1	-68.8	1.8	-65.7	1.7
	Med	-67.0	2.7	-70.3	2.2	-67.4	2.8
	High	-68.7	3.2	-69.2	2.0	-67.4	1.8
Terfenadine	None	-74.0	2.4	-73.3	1.4	-73.0	2.1
	Low	-70.6	2.4	-69.6	2.2	-68.9	2.3
	Med	-66.6	2.2	-69.7	1.3	-67.3	2.2
	High	-63.1	2.2	-69.0	1.7	-64.6	1.4
Verapamil	None	-70.5	3.0	-71.7	2.3	-71.9	1.9
	Low	-66.9	2.5	-70.5	1.6	-69.4	2.1
	Med	-65.7	1.6	-69.2	1.4	-66.9	1.8
	High	-62.2	2.2	-69.5	1.3	-67.9	1.2

3.4 Discussion

3.4.1 ODC platform reveals effects of ion channel modulation on AP characteristics but does not replicate EDC results

The ODC platform can yield overlapping results from the EDC platform, but not consistently (Figures 3.2-3.4). The dose-response experiments screening BayK 8664 demonstrated a significant APD_{90} prolongation only at the highest drug concentration. (Figures 3.5, Table 3.1). The dose-response experiments with terfenadine yielded a dose-dependent increase in APD90, fraction of repolarization and triangulation (Figure 3.6, Table 3.1). In addition, there was no difference in sensitivity to the drug when I_{K1} was simulated with dynamic clamp conditions. Dose-response experiments with verapamil demonstrated APD_{30} shortening, increase in triangulation and increase in fraction of repolarization in a dose-dependent manner (Figure 3.7, Table 3.1). APD_{90} did not change in a dose-dependent manner, as anticipated.

ODC generally had a similar effect (e.g., increasing or decreasing) on AP characteristics as EDC, but did not have the same magnitude of an effect on AP characteristics as the EDC platform (Figures 3.8-3.10). In addition, even though the ODC platform results sometimes overlaps with the EDC results, this may not happen throughout the entire protocol with a specific cell (Figures 3.5-3.7). This reveals a concern and implies that something is hindering the ODC

platform performance. There are a number of potential causes. First, as previously mentioned in Chapter 2, the ArchT model used to calculate the light intensity could be limited and so we are not generating the target current that we are predicting with our model. Second, there may be downstream consequences of using opsins, which would prevent ODC from exactly mimicking an electrode. This is further elaborated in in Section 3.4.3.

3.4.2 Limitation in analysis of AP characteristics

Calcium-handling abnormalities of iPSC-CMs could be another potential reason that obscures the success of the BayK 8664 drug screen. As briefly described in Section 1.4, iPSC-CMs have abnormal spontaneous calcium release, which underlies spontaneous activity, and they also lack T-tubules. The lack of T-tubules prevents the co-localization of membrane calcium channels and ryanodine receptors (RyR), thus preventing the coordinated intracellular calcium release typical of adult ventricular cardiac myocytes [76]. The subcellular spontaneous calcium release underlying spontaneous activity signifies the lack of coordination between voltage and calcium release and the immature calcium handling properties. One potential mechanism of how spontaneous calcium release leads to a spontaneous event is that the SR activates the sodium calcium exchanger (NCX) until the threshold is reached and an AP is initiated [80]. The lack of coordination between I_{CaL} and RyR could blunt the response to BayK 8664. A 20% increase in APD_{90} was observed in our experiments, but a

prolongation of about 30% and 200% was seen with 1 μM Bay K8664 in other papers that used dynamic clamp to mimic I_{K1} [102], [154]. This is indicative of inter-lab differences of iPSC-CMs, which will be addressed again later in this section. Perhaps in our experiments, I_{CaL} agonism caused by BayK 8664 at lower concentrations is less coordinated with RyR activation and unable to trigger as much calcium-induced calcium release (CICR) and thus APD_{90} is not significantly prolonged until higher concentrations.

We speculate that in the iPSC-CMs used in the experiments presented in Chapter 3, I_{CaL} does not greatly contribute to APD_{90} because strong repolarizing currents are present, perhaps I_{K1}. In the experiments conducted, the pre-stimulation potential (Table 3.2) did not change between different concentrations of BayK 8664 in any of the three conditions. In contrast, 1 μM BayK 8664 greatly depolarized the MDP [154]. In the automated patch clamp experiments injecting a different formulation of I_{K1} in iPSC-CMs conducted by Goversen et al., a greater maximum conductance was used, pushing the resting membrane potential to -94 mV. Perhaps this was able to better suppress spontaneous calcium release and thus spontaneous activity compared to our experiments; the potential influence of spontaneous activity will be discussed later on in this section. I_{K1} addition via dynamic clamp may be necessary for pushing iPSC-CM electrical maturity but not sufficient when there are other important components missing. I_{K1} expression suppresses spontaneous activity by making iPSC-CMs less prone to reaching a threshold, but it is dysregulated

calcium release that triggers spontaneous APs [80], [196]. Cyclical spontaneous calcium release can push calcium channels into a refractory period and decrease the time for the SR to refill its Ca^{2+} stores, such that the resulting calcium transient is shorter in duration and amplitude [197]. The dysregulation of the iPSC-CM calcium system and its consequences on the ability of iPSC-CM to reflect adult cardiomyocyte behavior needs to be further investigated. After these experiments were performed, unfortunately a literature search with a slightly different spellings of BayK 8664 (Bay K8664 and Bay K 8664) revealed that iPSC-CMs in different labs were able to expectedly prolong APD_{90} with 1 μM BayK 8664 [198], [199]. To make matters more confusing, there are also other labs that used BayK 8664 and concluded that BayK 8664 did not see an increase the calcium current in iPSC-CMs [200], [201]. In hindsight, BayK 8664 was not the best drug to test with the purpose of demonstrating an advantage of dynamic clamp. Given the variability of responses of iPSC-CMs to BayK 8664 in different labs, this would not be an ideal drug candidate to demonstrate the benefits of dynamic clamp and to test the ability of iPSC-CMs under the ODC platform to respond to ion channel modulators. In addition, perhaps the concentrations chosen for the dose-response experiments should be increased.

The results of Chapter 2 were interpreted from trials and cells that did not contain more than one spontaneous event under EDC or ODC. The cells used in Chapter 3 were spontaneously active, which when combined with the slower pacing frequency of 0.5 Hz, makes it difficult to outpace the intrinsic rate of

spontaneous activity (Figures 3.2 and 3.3), whereas in Chapter 2, faster pacing frequencies prevented the occurrence of spontaneous events. Cardiomyocyte APs are affected by the rate of AP firing, both stimulated and spontaneous. The presence of spontaneous events is problematic because these sporadic events affect the AP morphology of the subsequent event, thereby skewing the measured AP characteristics. The proximity of a spontaneous event prior to a stimulated AP can stunt the amount of ionic channel activation because they may not have recovered from the spontaneous event. The closer the prior event, the less recovery time there is for voltage-gated channels, thus affecting the AP characteristics of the subsequent event (i.e., smaller APD, shorter APA) [202], [203]. In other words, the morphology and quantitative features such as APD of a stimulated AP without a proximal prior spontaneous event would be different from those of a stimulated AP with a proximal prior spontaneous event. This is typically observed in native cardiomyocytes and is known as restitution. Because of this, it is not fully accurate to compare EDC and ODC when there are spontaneous events present. Unfortunately, we are unable to analyze trials without any spontaneous events because all trials had spontaneous events during some portion of the protocol. Figure 3.11 displays the average rate of spontaneous activity of different drugs, at different concentrations and in different conditions. The average rate of spontaneous activity generally exceeds the pacing frequency, making it inevitable to analyze cells with spontaneous activity. As previously seen in Chapter 2 and again seen in Chapter 3, dynamic clamp tends to suppress the rate of spontaneous activity, demonstrating an

advantage of dynamic clamp (Figures 2.4, 2.6, 3.2-3.4, 3.11, Appendix A3). The rate and timing of spontaneous activity prior to a stimulated AP in EDC and ODC is not identical across cells, between conditions, or across drug concentrations. This prevents a clean comparison between the EDC and ODC results and across drug concentrations. This is a limitation in the analysis, which can be overcome with non-spontaneously active iPSC-CMs. Unfortunately, given the current nature of iPSC-CM derivation, spontaneously active iPSC-CMs are selected for patching because the researcher is confident that the cell was successfully differentiated into a cardiomyocyte, albeit an immature one.

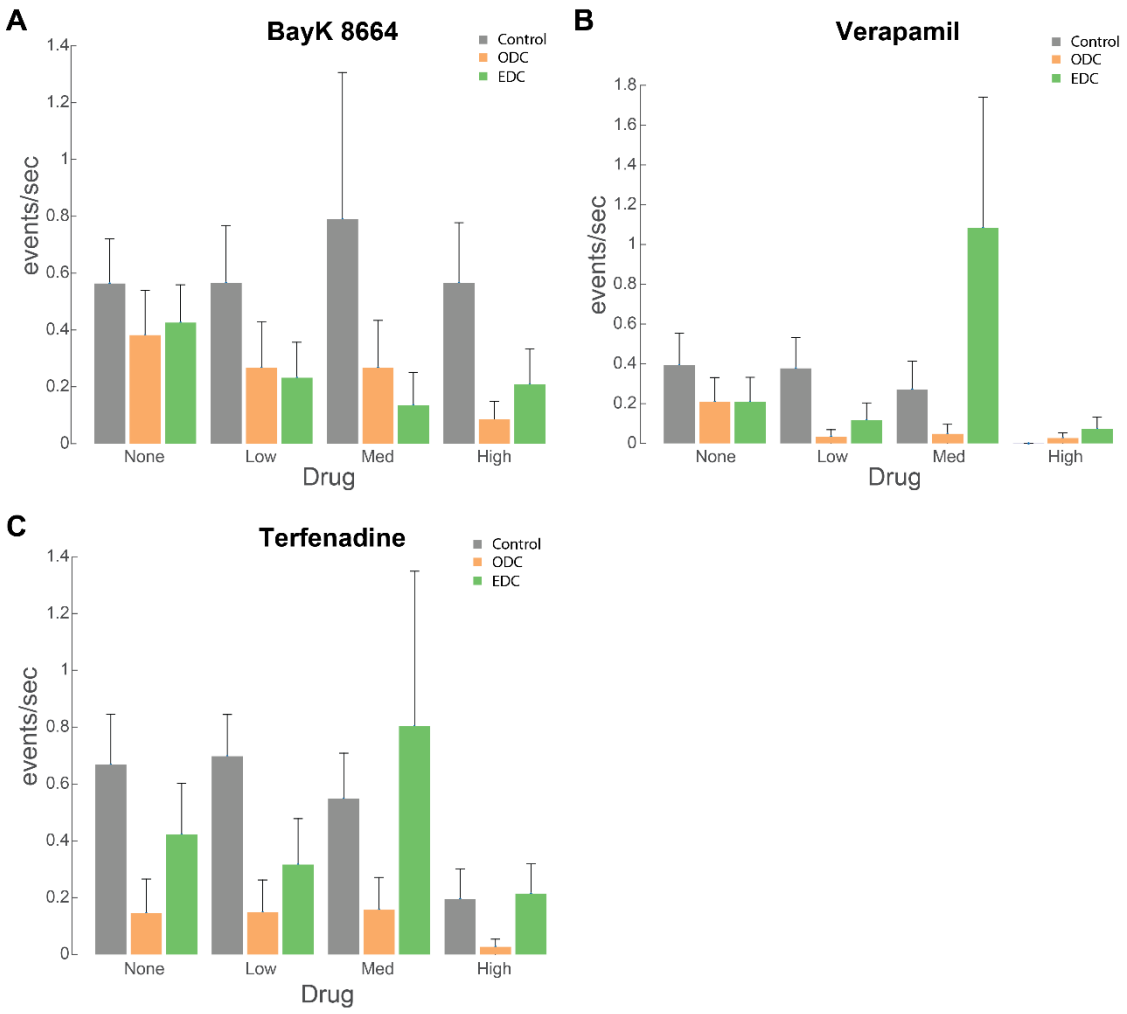

Figure 3.11: Average rate of spontaneous activity under Control, EDC and ODC conditions at different drug concentrations of BayK 8664, terfenadine and verapamil

Average and SEM of rate of spontaneous events under control, EDC and ODC conditions with (A) BayK 8664, (B) terfenadine and (C) verapamil at different drug concentrations. The gray, orange, and green bars represent the results under control conditions, with EDC, and with ODC, respectively.

3.4.3 The ODC platform in more mature and relevant formats

There is a myriad of abnormalities in iPSC-CMs that can decrease its relevance to adult cardiomyocytes. It is difficult to pinpoint what is the highest priority to address but it will be revealed as differentiation techniques that mimic cardiac development are discovered. A disadvantage of the current ODC implementation is that it requires single cells. Not only is the relevance of single cells limited, but also single cells have less markers of maturity than monolayers [165], [204]. The ODC platform has the potential to be used in monolayers, unlike EDC. This format would incorporate electrical coupling properties into the *in vitro* model, and the iPSC-CMs would be inherently more mature. In addition, the ODC platform does not need to use a monolayer exclusively composed of iPSC-CMs but can also include other cardiac cell types (i.e., cardiac fibroblasts, endothelial cells) and further promote maturity by mimicking cardiac development [205], [206]. The ODC platform would mimic a current of interest and allows for spatial resolution, opening a door to expand experimental possibilities to enable the power of dynamic clamp in many different types of cardiac tissue-like preparations.

3.4.4 Conclusion

This chapter first aimed to demonstrate the feasibility of the ODC system to be used for drug screening. The failure of ODC to replicate EDC results is not ideal,

but as described above, may not be due to the inability of optogenetics to precisely inject a target current. The success of ODC to demonstrate some of the effects of ion channel modulators suggests it may still be useful for drug screening, but with limitations. The possibilities of the ODC platform (e.g., using dynamic clamp in monolayers, using dynamic clamp in co-cultures, generating currents driven by a specific ionic species) may outweigh the drawbacks (decreased precision of injecting a target current). The second aim of the chapter was to demonstrate an advantage of dynamic clamp addition of I_{K1}, but unfortunately, no benefit to using dynamic clamp to add I_{K1} was demonstrated. Surprisingly the cells were able to detect Ca^{2+} agonism without dynamic clamp, contrary to the results in another lab [154]. This highlights the problem of inter-lab or iPSC source and batch variability [207]. Another reason could be that supplementing the lack of I_{K1} is not as important to produce an adult electrophysiological phenotype in iPSC-CMs. Genetic expression of I_{K1} alone does not solve the problem of electrical immaturity [196]. As mentioned in Section 3.4.2, abnormal calcium dynamics also underlies abnormal behavior. Other abnormalities, i.e., ultrastructural, protein expression, etc. mentioned in Section 1.4 also have global consequences that could limit the extent iPSC-CMs can behave like an adult cardiomyocyte. Further development is needed before ODC can be confidently used in lieu of an electrode-based system, but the current ODC platform is an important first step that provides a proof-of-concept of using optogenetics in a fully optically-controlled dynamic clamp system for drug screening.

CHAPTER FOUR

CONCLUSIONS AND FUTURE DIRECTIONS

4.1 Summary

4.1.1 Optogenetics as a tool to inject a dynamically-changing target current

Optogenetic tools have been previously used to statically stimulate electrical activity using depolarizing opsins or inhibit electrical activity using hyperpolarizing opsins. This has been fruitful to dissect neurological pathways by stimulating or inhibiting specific regions of the brain [149], [150], [208]–[214]. In cardiology, the idea of using optogenetics as a replacement for a pacemaker has been proposed [143], [171], [172], [215]–[217]. Optogenetics were also used to inhibit specific regions in the zebrafish heart to identify the pacemaker cells or which cells to stimulate that elicited a desired response (i.e., tachycardia, bradycardia, atrioventricular blocks, and cardiac arrest) [215]. Optogenetics and iPSC-CMs are also being combined in the hopes of developing all-optical electrophysiology that can current clamp, voltage clamp, and measure calcium transients [117], [133]–[137], [170], [208]. In this thesis, we aim to demonstrate a proof-of-concept where we can precisely control opsins to produce a dynamically-changing current of interest based on real-time feedback from voltage input for drug screening applications.

4.1.1.1 Gaining control of ArchT to generate a dynamic current

Of the hyperpolarizing tools available, we chose ArchT because of its fast kinetics, which is necessary for the real-time requirements of dynamic clamp. As discussed in Chapter 2.4.1., an opsin whose activation and deactivation kinetics are less than 60 msec would not compromise the real-time feedback loop (Appendix A11) [89]. There are currently more enhanced versions of ArchT (e.g. eArchT) that can generate a larger photocurrent if the user wanted to generate a larger current that exceeds the limit of 1.08 pA/pF that was imposed in the experiments conducted. Even though the ODC platform was developed using ArchT, it would be feasible to use many optogenetic proteins, as long as there is a mathematical model available to calculate the light intensity needed to activate the opsin and generate a target current. This flexibility is important, as more opsins are being developed to be faster, more specific for certain ions, and produce a larger photocurrent.

To control our selected opsin to generate a specified current, we would first need to understand how ArchT behaves, describe it in a mathematical model, and then use the mathematical model to predict the conditions needed to generate the specified current. The model developed for ArchT (Eq. 2.1) was built to predict what current would be produced, given the V_m and the light intensity, not based on the structural mechanism of ArchT activation.

To investigate the light-intensity dependence, the iPSC-CMs were voltage clamped at various holding potentials (mV): -100, -60, -20 and 20 (Figure 4.1). At each holding potential, the cells were then “light clamped”, meaning they were illuminated at various LED outputs, with 5V being the maximum (Figure 4.1A). The amount of current produced at different light intensities was measured. Figure 4.1B illustrates the normalized results from individual cells. This shows the heterogeneity of the light-dependence behavior of ArchT in different cells and the need for a cell-specific ArchT model to precisely calculate the light intensity needed. Figure 4.1C illustrates the average and SEM of the normalized current produced at a different LED outputs across all cells. The equation, $b_1\left(1 - e^{-b_2 \cdot E_e}\right)$, can be used to describe the light-intensity dependence relationship. To address the heterogeneity of the light-dependence behavior, the parameters of the light-dependence equation, b_1 and b_2, can be determined for each cell with the calibration protocol and thus the light-dependence component of the ArchT equation can be tailored to the individual cell (Figure 2.2). Figure 4.1D plots the average light-dependence at different holding potentials. This ensures that despite the voltage sensitivity of ArchT, the light-dependence relationship remains consistent across different holding potentials. These experiments informed us on how to build the light-intensity dependence of the ArchT model (Eq. 2.1).

The voltage dependence of ArchT was also investigated with voltage clamp and light clamp experiments, by illuminating the cells with the same light intensity at

different holding potentials (Figure 4.2A). Figure 4.2B displays the normalized ArchT current produced at different holding potentials in individual cells. The results also demonstrate a great heterogeneity of voltage dependence between cells. This further bolsters the need for a cell-specific ArchT model (Figure 4.2B). A linear model would be apt to describe the voltage dependence of ArchT and the parameters can be measured in a specific cell using the calibration protocol (Figure 4.2C). The voltage-dependence term of the ArchT mathematical model behaves like a scaling factor to the light-intensity dependence.

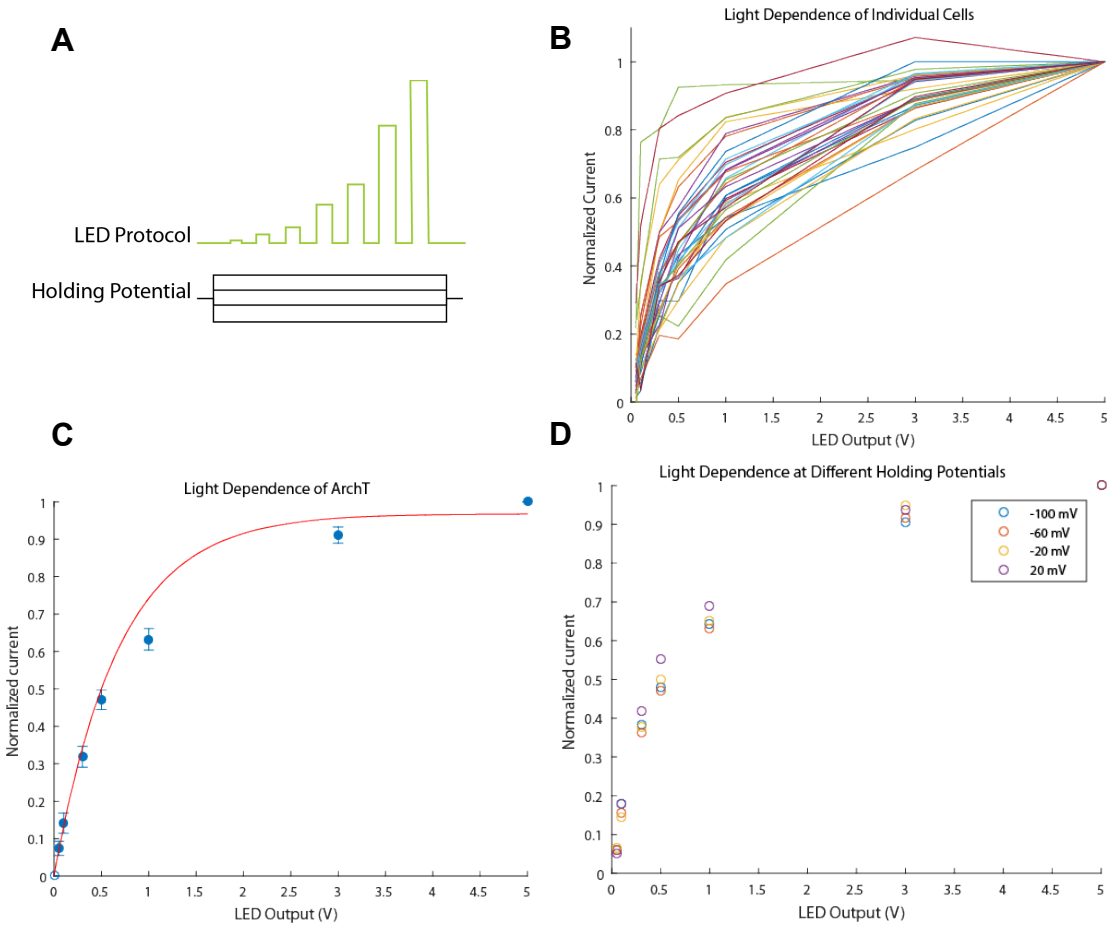

Figure 4.1: Investigating light-intensity dependence of ArchT
The cells were illuminated for 1 second with 1 second light off in between. The cells were held at -100 mV, then the light clamp protocol would illuminate the cells at 0.05 V, 0.1 V, 0.3 V, 0.5 V, 1 V, 3 V, 5 V LED output, which translates to 0.005, 0.01, 0.03, 0.05, 0.1, 0.3, 0.5 mW/mm^2 light intensities (A).
The normalized traces of the results from the protocol in (A) in individual cells are displayed (B).
(C) illustrates the average and the SEM. The red line demonstrates the power equation used to fit the light-intensity dependence of ArchT.
The normalized light-dependence relationship at different holding potentials were averaged (D).

n = 26

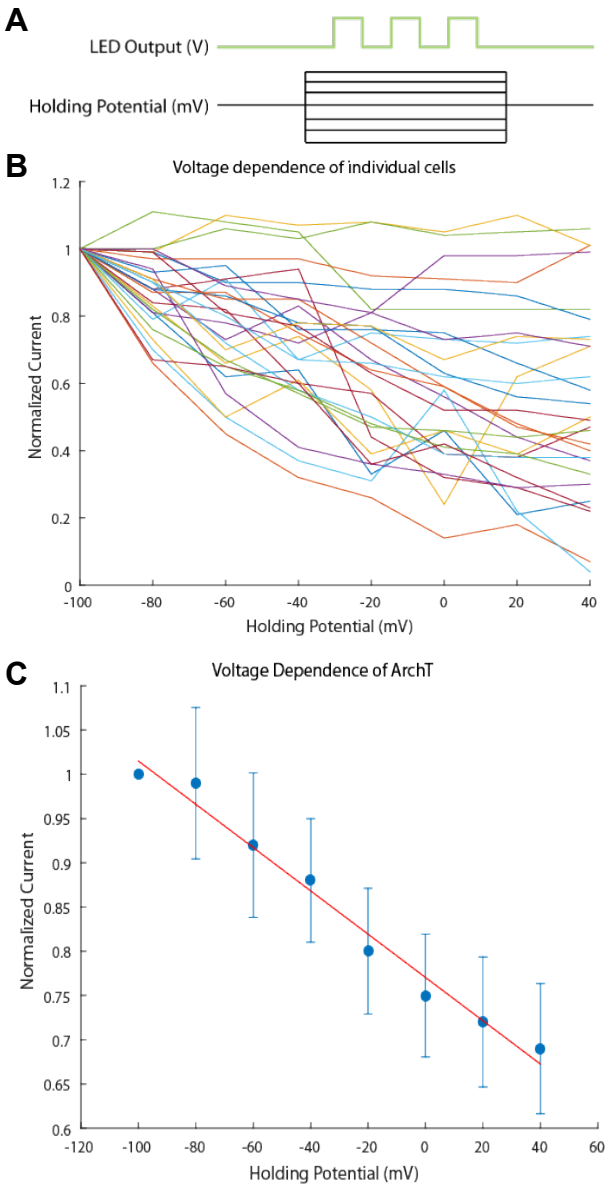

Figure 4.2 Investigating voltage dependence of ArchT
The cell was illuminated at 5V LED output (0.5 mW/mm^2) for 1 second three times with 1 second of light off in between each light pulse while being held at -100 mV, -80 mV, -60 mV, -40 mV, -20 mV, 0 mV, 20 mV, and 40 mV (A). The normalized traces displaying the results of the protocol of individual cells are displayed (B). The average and SEM of the traces are displayed and the red line displays the linear model used to describe the average voltage dependence (C).

n = 26

4.1.1.2 Using ArchT to generate a dynamic current

Chapter 2 presents how to obtain a cell-specific ArchT model using a calibration protocol and use it to dynamically generate a target current in iPSC-CMS in a real-time feedback loop. This was demonstrated by mimicking I_{K1} in iPSC-CMs and comparing the results to using an electrode. I_{K1} was chosen because iPSC-CMs have reduced I_{K1} and addition of I_{K1} improved electrophysiological maturity [22], [87], [102], [107], [154], [196]. Chapter 2 revealed that ArchT could be dynamically controlled to generate a target current. Looking at individual cells, there were cells where the ODC platform mimicked the EDC platform nearly identically, but there were also some cases where ODC affected AP characteristics similarly to EDC but not to the same magnitude. The reason for this discrepancy remains unknown. Possible reasons, as previously discussed in Section 2.4.1, include the type of opsin chosen has unknown downstream consequences, or the ArchT model needs to be improved for more accuracy.

After demonstrating a proof-of-concept of controlling opsins to dynamically generate a target current, we wanted to test how the platform responds to I_{Kr} inhibition by administering E-4031 to demonstrate its applicability for preclinical drug development. With E-4031 administration, the APD_{90} was prolonged, as expected, in control, EDC and ODC conditions compared to the same condition without drug. Both EDC and ODC shortened the APD_{90} compared to the control

and the stimulated APs between ODC and EDC had similar AP characteristics. This demonstrates that the ODC platform is also able to detect similar effects as the standard EDC method when challenged with I_{Kr} inhibition, which is currently used during drug development as an important factor to predict potential cardiovascular toxicity in patients.

4.1.2 Using the ODC platform for drug screening

In the context of drug discovery, optogenetics have been used to automate high-throughput assays. Replacing traditional patch clamp methods with optogenetics to make these useful techniques more accessible and high-throughput is of great interest for drug-discovery purposes. Currently, methods to simultaneously stimulate and image multiple cells to optically current clamp, and methods to hold the membrane potential to optically voltage clamp are being developed [117], [129], [143], [144], [218]. There are also different platforms being developed or adapted to incorporate LEDs that enables the use of optogenetics in a high-throughput manner, through automated imaging and/or stimulating multiple wells simultaneously [117], [120], [159], [173], [219].

Chapter 3 aims to investigate how the ODC platform performs in the presence of ion-channel modulators. Terfenadine, verapamil, and BayK 8664 were tested. Similar to the results in Chapter 2, the ODC platform performed identically to

EDC in some cases and did not mimic EDC in some cells. The iPSC-CMs under control, EDC and ODC conditions responded as anticipated to terfenadine and verapamil in Chapter 3, demonstrating some potential for the ODC platform to be used for drug screening. The use of BayK 8664 in the experiments executed in Chapter 3 was meant to demonstrate a benefit to using the dynamic clamp platform, since the effects should only be observed with addition of I_{K1} via dynamic clamp. However, results with BayK 8664 were more inconclusive and the expected result was only observed at the highest drug concentration. iPSC-CMs also have varying responses to BayK 8664 across labs [154], [199]–[201], [220], [221]. Both dynamic clamp platforms were unable to demonstrate a benefit over the control when challenged with BayK 8664. Reasons for this were discussed in Section 3.4.2. Bett et al. (2013) had demonstrated that the effects of BayK 8664 were detectable only under dynamic clamp conditions [154]. Unfortunately, the benefit of I_{K1} addition was not reproduced in this work because the effect of BayK 8664 was detected without I_{K1} addition. The iPSC-CMs used in Chapters 2 and 3 were more hyperpolarized than the iPSC-CMs in Bett et al. (2013) and did not depolarize significantly in the presence of BayK 8664, so APs could still be successfully stimulated and the effects of BayK 8664 could be detected under control conditions. Given how iPSC-CMs in our experiments and from other published work cannot consistently recapitulate the effect of how native cardiomyocytes respond to BayK 8664 suggests that our results may be due to the immaturity of iPSC-CMs, rather than a reflection of true biological significance related to adult cardiomyocytes.

4.1.3 Limitations

4.1.3.1 Inconsistent iPSC-CMs limit reproducibility

The consistency of iPSC-CMs is important for reproducibility and therefore drawing meaningful conclusions. It is difficult to determine if experimental results using iPSC-CMs are due to the properties of the lot of cells, or are due to a biological property consistent across all iPSC-CM lines and native human cardiomyocytes. This variability affects ion-channel expression and response to ion-channel modulators [207], [222]. For this reason, it may be good practice to use iPSC-CMs from multiple sources, e.g., from different companies, patients, or labs in any study. The consequence of this is that more trials on different lines would need to be performed, making automated and high-throughput assays more critical.

The issue of variability between different iPSC-CM lots/sources was notable in this work, as the cells used for the work described in Chapter 2 were phenotypically different from the cells used for the work described in Chapter 3. Since the cells were purchased from a company and the company aims to produce the best quality iPSC-CM, the differentiation and maturation protocols have also evolved over time and we were unable to keep a consistent lot, nor were different lots derived with the same protocol. The cells from Chapter 3 were purchased about a year after the cells from Chapter 2. In addition, the

differentiation protocol is not public, nor is the composition of the media, both of which can have a significant effect on iPSC-CM behavior [9], [223]. Comparing the characteristics of the cells from Chapter 2 and Chapter 3, the pre-stimulation potential of the cells in Chapter 2 are more depolarized (-64.6 ± 4.4 mV versus -71.1 ± 1.7 mV) and the APD_{90} of the cells in Chapter 2 are shorter (254.1 ± 30.1 msec versus 338.7 ± 20.0 msec) (Table 3.2 and Appendix A13). Figure 4.3 also illustrates spontaneous events from the cells from Chapter 2 (Figure 4.3A, n = 12) and Chapter 3 (Figure 4.3B, n = 14). The spontaneous events of Chapter 3 are also more hyperpolarized, the upstroke velocity is noticeably faster and the morphology is less rounded than the spontaneous events from the iPSC-CMs used in Chapter 2. Figure 4.3C quantifies the average and SEM of AP characteristics. The impact of adding I_{K1} is dampened in the more hyperpolarized iPSC-CMs of Chapter 3. The electrophysiological differences observed between the cells used in Chapter 2 and 3 makes it difficult to compare the results of the two chapters because those differences suggest that these cells are phenotypically different. Improved consistency of iPSC-CMs would make the *in vitro* model more robust for drug-screening applications. It is unreliable to draw reproducible scientific conclusions about adult cardiomyocyte behavior if it is obscured by the inherent variability of the *in vitro* model or if the result can only be produced with specific iPSC-CM lines.

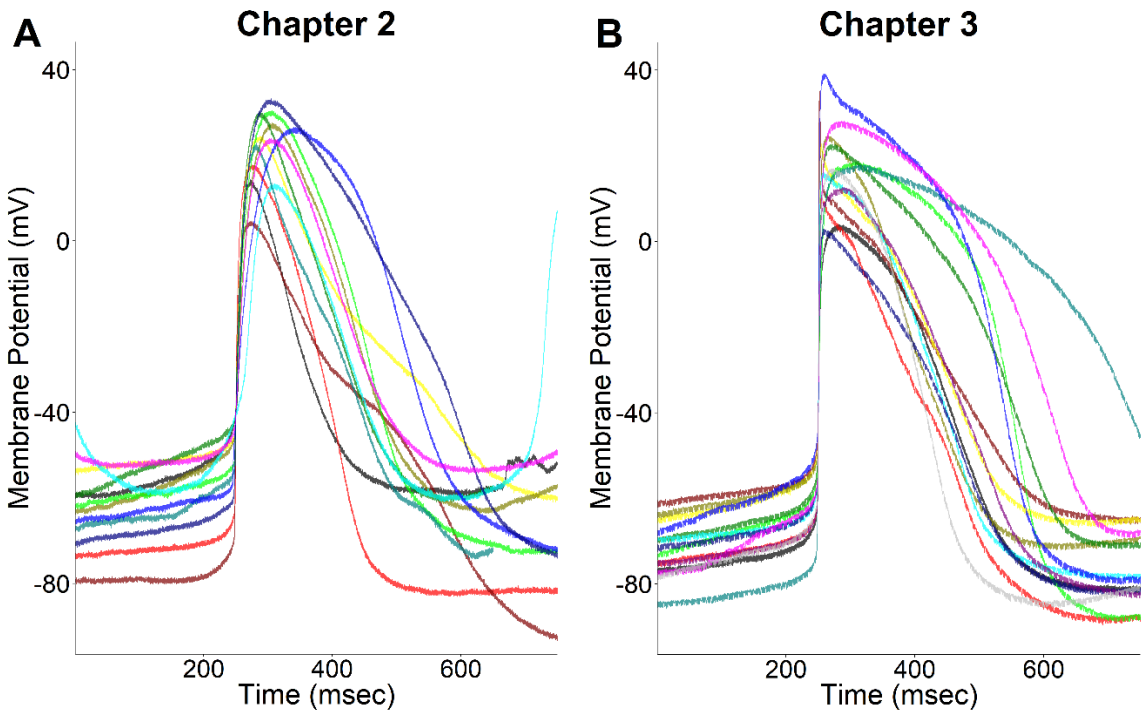

C

	Chapter 2	Chapter 3
Pre-Stimulation Potential (mV)	-61.5 ± 2.4	-69 ± 1.8
APD_{90} (msec)	364.0 ± 50.7	305.7 ± 21.8
Triangulation (msec)	107.8 ± 35.9	46.14 ± 5.7
Fraction of Repolarization	0.41 ± 0.05	0.31 ± 0.03

Figure 4.3: Spontaneous events in cells from Chapter 2 and Chapter 3
Example spontaneous event from 12 different cells from Chapter 2 experiments (A). Example spontaneous event from 14 different cells from Chapter 3 experiments (B). (C) Average ± SEM of AP characteristics.

4.1.3.2 Spontaneous activity affects AP analysis

If spontaneous events occur prior to the stimulated event, it can alter the measured AP characteristics of the analyzed stimulated AP. The presence of spontaneous activity makes it difficult to truly compare between conditions. In Chapter 2, cells were omitted from the analysis of AP characteristics if they contained more than one spontaneous event under EDC or ODC. In Chapter 3, we were unable to apply the same selection criteria as in Chapter 2 because all trials had spontaneous events during some portion of the protocol so the trials used for analysis were affected by the presence of spontaneous activity.

Calcium is an important co-factor for many enzymes, including kinases that are responsible for the phosphorylation of ion channels. The inappropriate spontaneous release of calcium underlying spontaneous action potentials may affect the baseline state of the cell and yield results that are a consequence of the immature calcium handling properties. If the rate of spontaneous activity is also different between cells, then the degree of the effect of spontaneous calcium release may increase the heterogeneity of responses between cells. Another possibility is that the consistent spontaneous release of calcium can activate pumps and exchangers (e.g., Na^{+}-Ca^{2+} exchanger) and affect the intracellular ionic composition. The caveat of choosing non-spontaneously active cells for experiments is that it is difficult to determine if the chosen cell was successfully differentiated into a cardiomyocyte. The spontaneously active

cells provide reassurance that the chosen cell had differentiated into a cardiomyocyte, even though it is an immature one.

4.1.3.3 Immaturity of iPSC-CM is not as simple as supplementing the missing I_{K1}

Much attention given to I_{K1} as a marker for immaturity, because it is not expressed in fetal cardiomyocytes and because of its role to establish the resting membrane potential and in repolarization during an action potential. Reintroduction of I_{K1} has been shown to improve AP characteristic markers to more resemble adult cardiomyocytes. But it is important to remember that reduced I_{K1} expression is not a cause of immaturity but a symptom of it. The delicate interconnectedness between protein transcription, expression, activation limits the use of iPSC-CMs as a model. To give an idea of the complexity, with respect to I_{K1}, iPSC-CMs have reduced expression of *KCNJ2*, the gene that encodes for I_{K1} [198]. In native adult cardiomyocytes, Kir2.1 interacts with $Na_V1.5$ (channel that contributes to I_{Na}) in a complex along with other proteins (not all have been identified) and reciprocally regulate expression and function [224]. I_{K1} expression has also been associated with high intracellular calcium and calmodulin kinase II activity [225], [226]. Parts of this mechanism is regulated by lipids, including phosphoinositide 4, 5-biphosphate and cholesterol [227], [228]. Also, I_{K1} is regulated by protein kinases A, B and C signaling [229]–[231]. Because of the interplay between I_{K1} and a myriad of

different components, it is unknown if reduced I_{K1} is a symptom of a more important issue, or itself is an important contributor to the abnormal phenotype of I_{K1}. It is difficult to determine what is important to "fix" in iPSC-CMs to yield a suitable *in vitro* cardiomyocyte model. Nevertheless, we started with I_{K1} because of its decreased expression in iPSC-CMs and its important contribution to the AP morphology.

Given the myriad of differences between adult cardiomyocytes and iPSC-CMs, careful consideration needs to be taken to how iPSC-CMs are being used as a model. For example, when looking at calcium-dependent or -related processes, it would be important to note that there is spontaneous calcium release, the I_{CaL} and CICR is not as well coordinated, there are less mitochondria, which also contributes to Ca^{2+} uptake and release, and the lack of T-tubules decreases the coordination of Ca^{2+} channel activation throughout the entire cell. I_{K1} is important to adult cardiomyocyte electrophysiology, but injecting I_{K1} alone may not be enough to fully make iPSC-CM electrophysiology equivalent to that of an adult. Achieving maturity in iPSC-CMs will be valuable, even if dynamic clamp is still needed to "correct" some aspects of the electrophysiology.

4.1.3.4 Selection bias of experiments

As previously noted, there is a selection bias towards spontaneously active cells. Another issue, especially in Chapter 3, is that because the protocol is very

long, this selects for cells that can survive being patched for extended periods of time. In addition, there may have been cells that expired during the protocol because it may have a higher reliance on the current that is being affected by the ion-channel modulator. It is difficult to determine why some cells were unable to undergo the full protocol (unless it was from a technical issue), but the long and arduous protocol also introduces a selection bias of the types of iPSC-CMs.

4.2 Future Directions

4.2.1 Fully-optical dynamic clamp

To realize the ideal fully-optical high-throughput ODC platform, the membrane potential must also be measured through optical means, making the need for an electrode obsolete. As discussed in Chapter 2 (Section 2.4.3), optogenetics could be used to generate a current composed of the ionic species of interest to preserve intracellular contents and to be able to observe downstream consequences of activation of the ionic current of interest. Even though there are many potential advantages to the ODC platform, an optical voltage reporter is needed to make this platform practically implementable for research. There are several options for choosing an optical readout of membrane potential: genetically-encoded voltage indicators (GEVI), and voltage sensitive dyes (VSD). However, there are several obstacles to realizing the fully-optical form

of ODC. On a practical level, RTXI, the software used to execute the experiments described in this thesis, is currently not developed to obtain optical information from a camera for real time feedback during experiments, such that we are unable to execute the closed-loop system between the LED and the optical measurement of V_m, which is necessary for dynamic clamp. Once this is achieved, the potential of the fully ODC system can enable more flexible formats.

4.2.1.1 Optical tools to read membrane potential

The ideal optical tool (i.e., GEVI, and VSD) would provide the absolute membrane potential, respond to changes in membrane potential quickly, and provide high temporal resolution. However, fluorescent indicators yield noisy data, which would affect the calculation of I_{target}. All the options available only report the relative membrane potential, where the current dynamic clamp setup requires absolute values to calculate the target current. One possible hypothetical way to overcome this is to create some sort of calibration or table-lookup protocol such that the relative fluorescent data could be converted into absolute values, but how this can be done, or if it is feasible, is unclear.

4.2.2 Enabling dynamic clamp in expanded cell formats

Because the ODC platform opsins can be expressed in and generate a current in multiple cells, the idea of expanding the cell formats had been eluded to throughout the thesis. The first step towards this is to establish the full ODC platform in single cells before transitioning to other formats. With the continued development and optimization of automated patch clamp systems, dynamic clamp can be run in a more high-throughput manner using single iPSC-CMs [102]. The advantage of the ODC method is that it enables dynamic clamp within clusters and monolayers. As discussed in Chapters 2 (Section 2.4.2), first, iPSC-CMs in more tissue-like preparations are more mature and relevant to arrhythmia compared to single cells. Second, the ODC platform would also be compatible with co-culturing. There are several cell types in the heart that directly impact cardiomyocyte function, including endothelial cells and cardiac fibroblasts. *In vivo*, signals from neighboring cells directly impact cardiomyocyte function and co-culturing has been shown to improve maturity and better reflect adult cardiomyocyte behavior. For example, more 3D vascularized tissues had a different doxorubicin toxicity response than 2D monolayers [205]. In addition co-culturing promoted maturity markers and improved response to chronotropic drugs [206], [232]. The application of ODC to these more tissue-like platforms can enable more electrophysiological investigations into the effects of perturbing different currents by various degrees or in specified locations. Dynamic clamp with traditional whole-cell patch clamp is limited to single cells,

which are useful when studying dynamics on a unit level, but in terms studying of cardiac arrhythmia which occurs on a multicellular level, it is difficult to extrapolate the behavior from a single cell unit to interconnected tissues. By expanding the use of dynamic clamp to multicellular platforms, ODC can enable further mechanistic studies to identify therapeutic targets or simulate different disease states to test the efficacy and safety of drug candidates.

4.3 Conclusion

This thesis presented how we dynamically activated ArchT to generate a specified I_{ArchT} current in iPSC-CMs. This takes the first proof-of-principle step towards the establishment of the optically-controlled dynamic clamp technique. This work serves as a proof-of-principle that demonstrates that fine-tuned control of optogenetic proteins can be gained for temporal activation.

In Chapter 2, we were able to implement this dynamic control of ArchT in iPSC-CMs to inject a target current that mimicked I_{K1}, demonstrating its potential to replace an electrode, with the goal of developing a fully-optical dynamic clamp platform. In Chapter 3, we aimed to demonstrate an advantage of dynamic clamp for drug screening and to demonstrate that the ArchT-based ODC platform would perform similarly to the electrode-based EDC platform during drug screening. Unfortunately, we were unable to demonstrate an advantage of using dynamic clamp, as the ODC platform yielded similar changes in AP

morphology as EDC, but did not consistently replicate the resulting APs of EDC. This is most likely due to the strong presence of spontaneous activity during the experiments, which obscured the interpretation of AP characteristics. The cells of Chapter 2 did not have this problem because the cells were phenotypically different than those of Chapter 3, most likely due to: (1) lot-to-lot variation, (2) the protocol was shorter, and (3) spontaneous activity was not as prominent during trials. Moving forward, patching cells without spontaneous activity would be ideal; however, this would require the presence of another marker to give the experimentalist the ability to select fully-differentiated cardiomyocytes (i.e., in lieu of the spontaneity criterion). In addition, the long protocol used in Chapter 3 also creates another selection bias of cells – i.e., those that are able to survive the protocol and being patched for that duration.

The fully-optical dynamic-clamp platform would replace the need for whole-cell patch clamp and thus increases the success rate of these drug-screening experiments. Because the fully-optical dynamic clamp platform would be free of the restrictions that are inherent to whole-cell patch clamp, the fully ODC platform could be applied to multi-cellular formats that are not exclusive to just cardiomyocytes. If the potential of the fully optogenetic dynamic clamp platform is reached, it could become a powerful research tool that pushes the frontiers of what can be achieved with dynamic clamp.

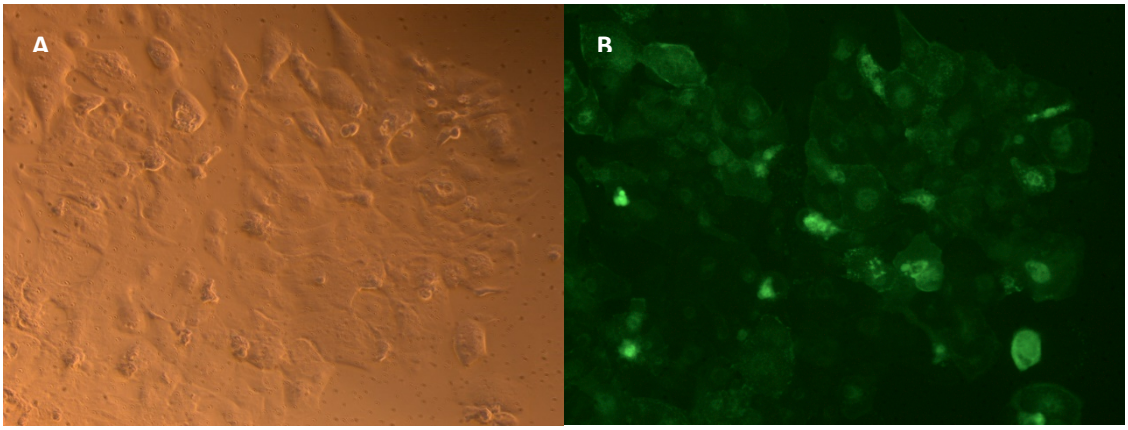

Appendix A1: Successful ArchT-eGFP expression in iPSC-CMs
Visualization of eGFP expression following the transfection protocol by Ambrosi and Entcheva (2014). (A) displays brightfield image of iPSC-CM beating clusters at 40x. (B) displays the corresponding image of eGFP fluorescence at 40x.

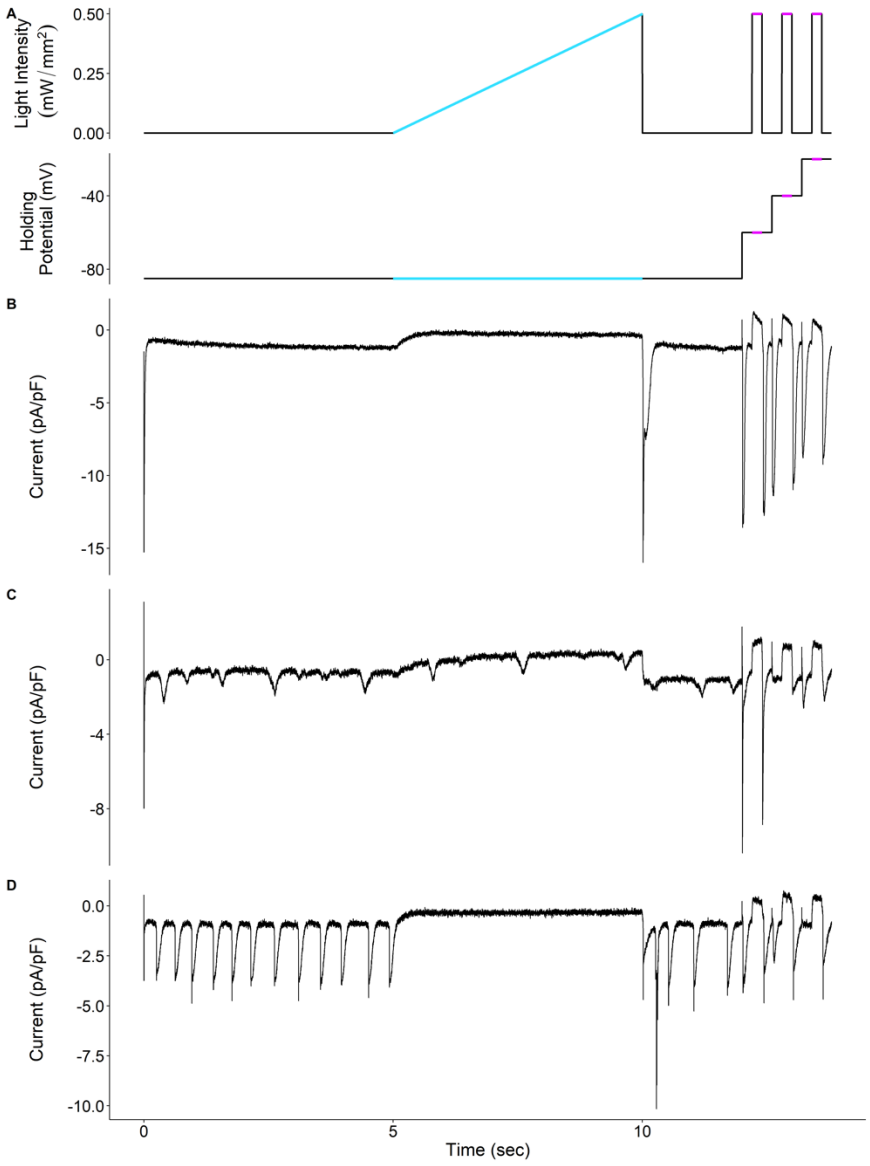

Appendix A2: Representative examples of calibration protocol outputs
The calibration protocol (A) can yield a variety of current outputs (B-D) that may be interrupted by repetitive large inward currents (C, D). These inward currents are associated with spontaneous contractions (C, D) which in some cases are suppressed with ArchT activation (D).

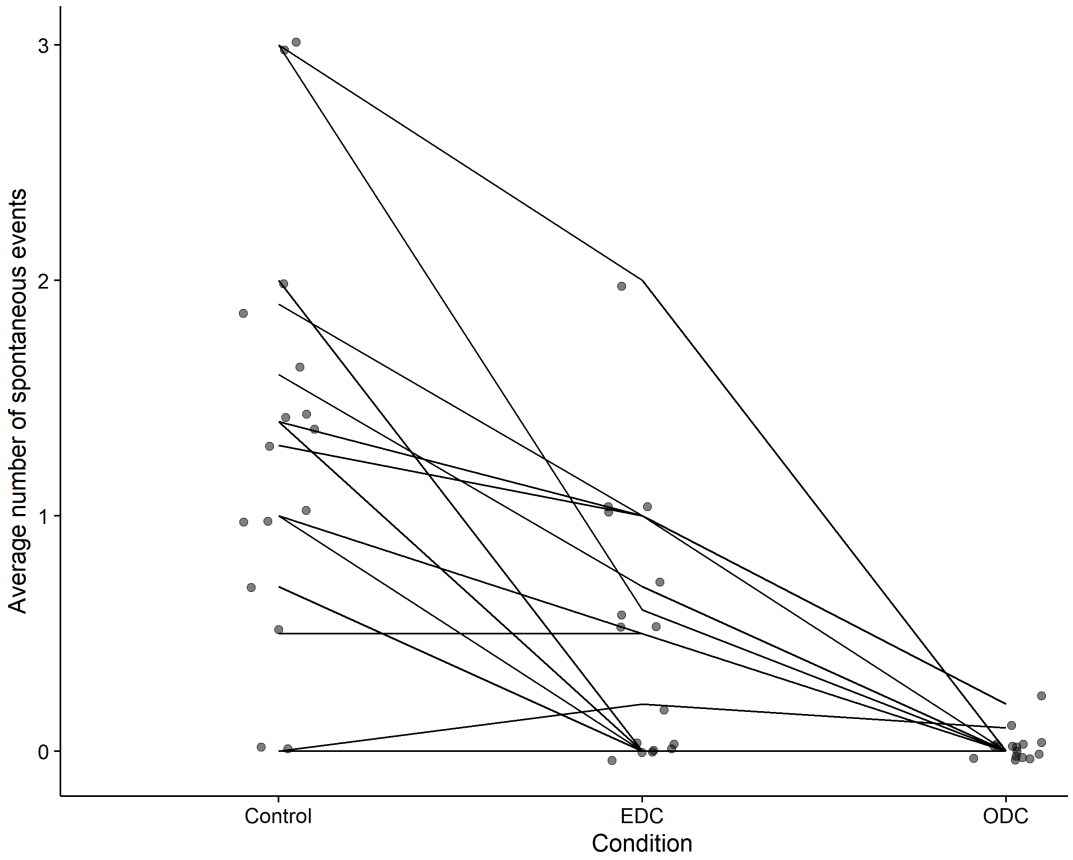

Appendix A3: Decrease in spontaneous activity with ODC.
Average number of spontaneous events occurring during sequence of 10 stimulated APs at 0.5 Hz pacing. Each point represents a different cell and the lines connect the results from the same cell.

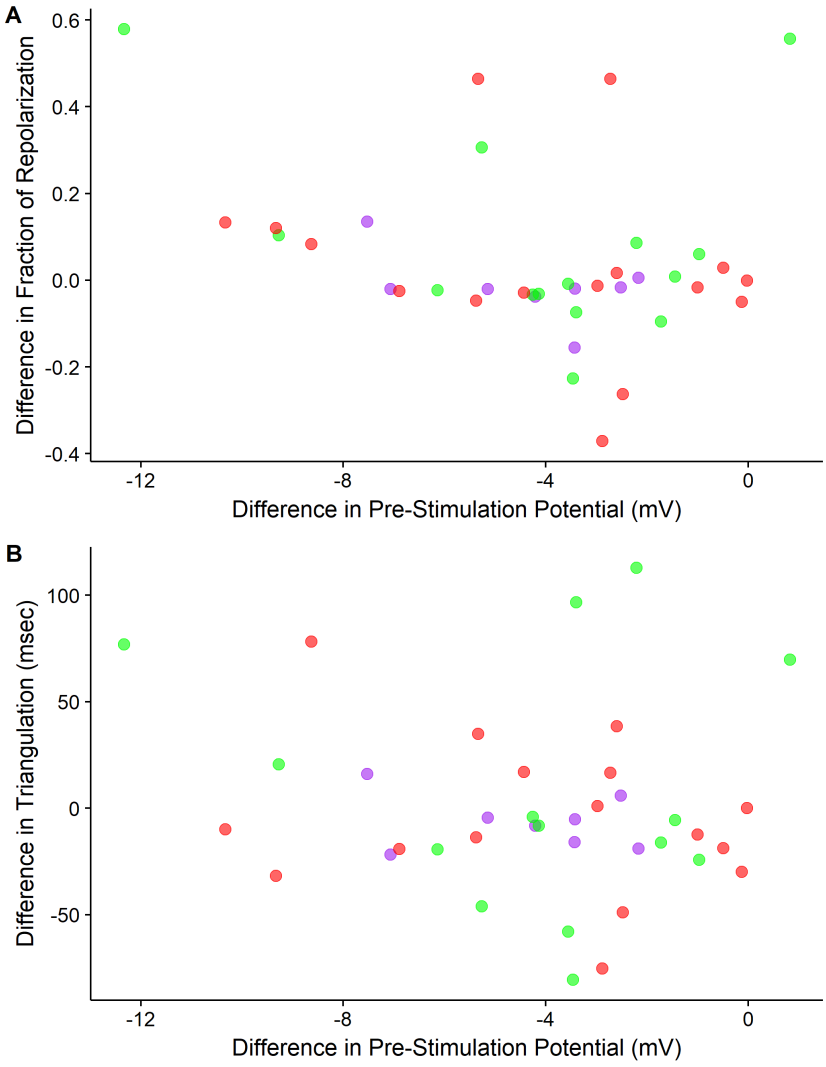

Appendix A4: Difference in pre-stimulation potential between EDC and ODC does not correlate with differences in AP morphology characteristics between EDC and ODC

(A) Difference in pre-stimulation potential on difference in fraction of repolarization time. Results at 0.5 Hz, 1 Hz and 2 Hz pacing are purple, green, and red, respectively.

(B) Difference in pre-stimulation potential on difference in triangulation. Results at 0.5 Hz, 1 Hz and 2 Hz pacing are purple, green, and red, respectively.

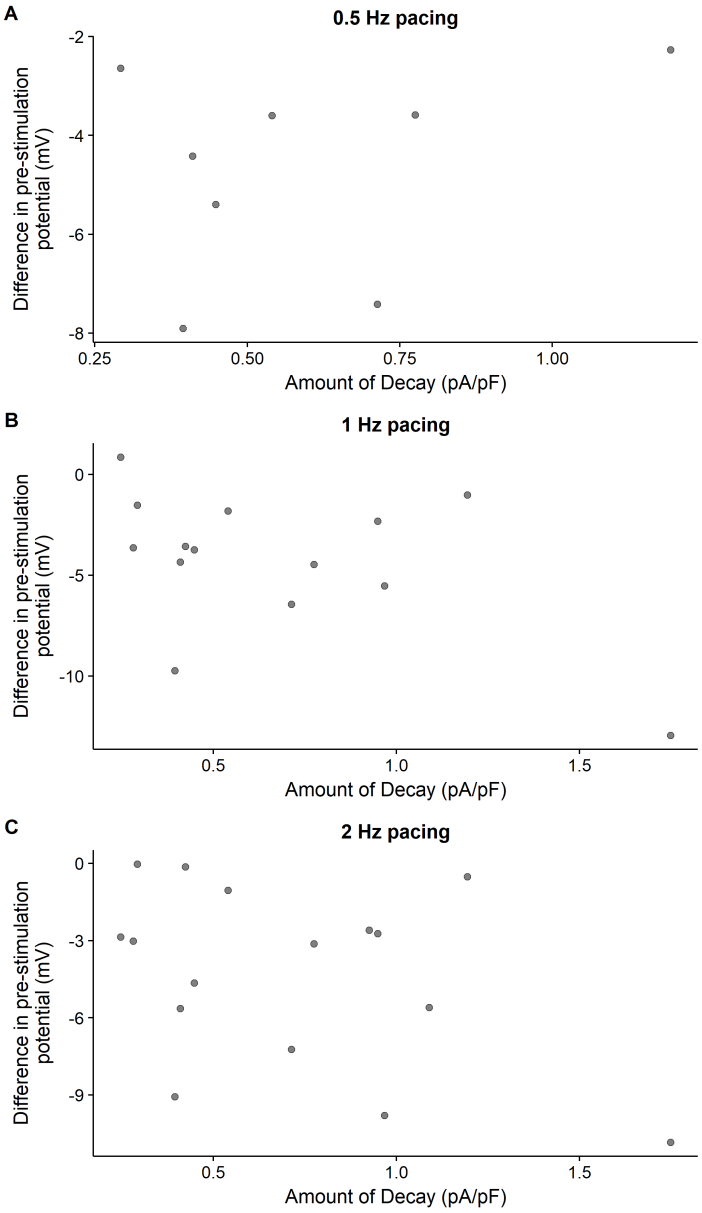

Appendix A5: Amount of current decay during constant-intensity light pulses does not correlate with the difference in pre-stimulation potential between EDC and ODC

The amount of current decay was measured as an average difference between the initial current and the final current during the three constant-intensity (0.5 mW/mm^2) light pulses during the calibration protocol. The amount of current decay was compared to the average difference in pre-stimulation potential (mV) between EDC and ODC at (A) 0.5 Hz, (B) 1 Hz, and (C) 2 Hz. Each point represents a different cell.

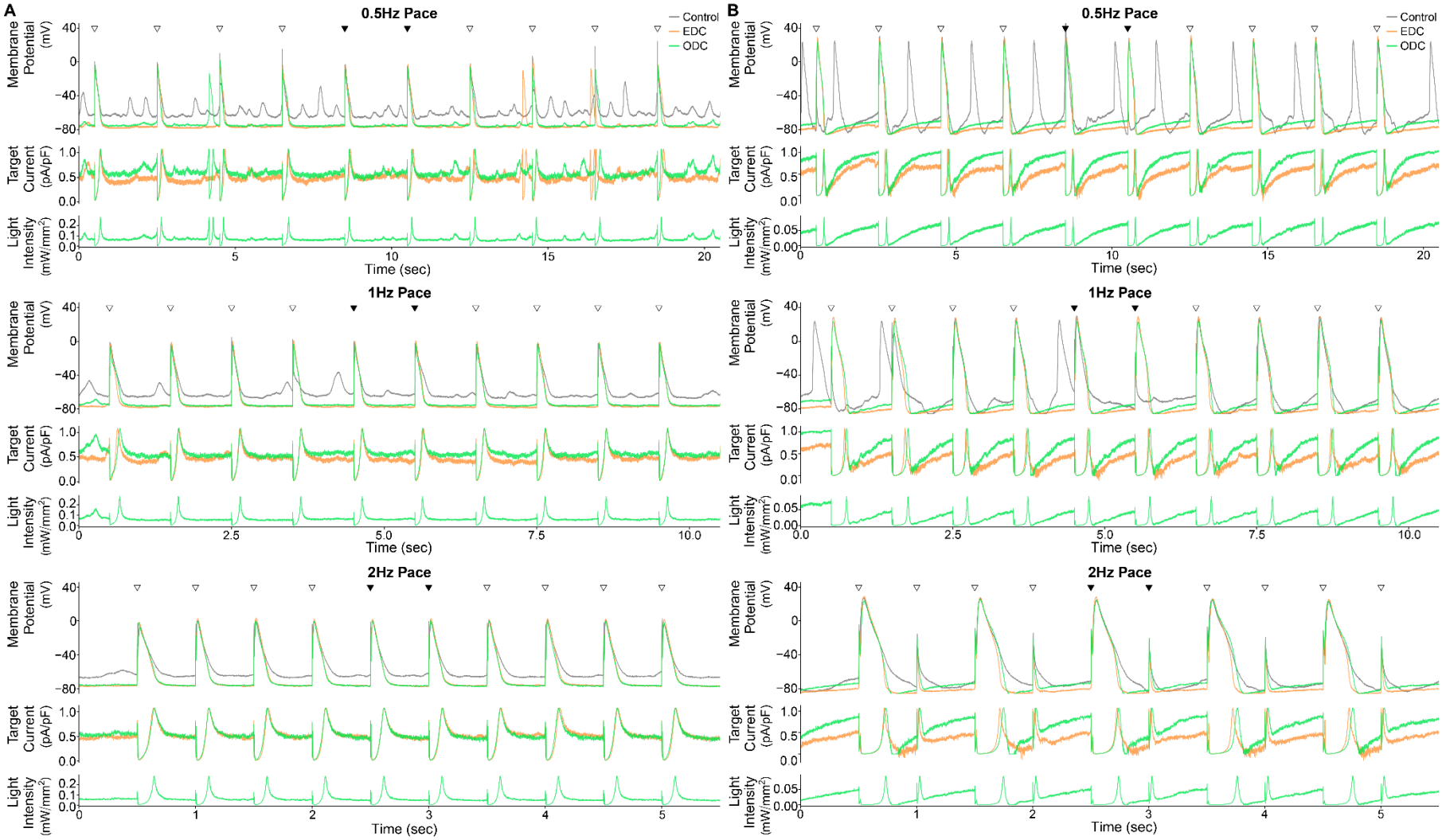
A
B
0.5Hz Pace
1Hz Pace
2Hz Pace
Control
EDC
ODC
Membrane Potential (mV)
Target Current (pA/pF)
Light Intensity (mW/mm²)
Time (sec)

Appendix A6: Entire trace of 10 paced APs demonstrating the results of the EDC and ODC platforms from example cells

Results from example cell 1 (A) and cell 10 (B) showing the effects of adding I_{K1} while paced 10 times at 3 different frequencies: 0.5 Hz (top), 1 Hz (middle), 2 Hz (bottom). The gray, orange and green traces represent the control without any current addition, adding I_{target} with EDC, and adding I_{target} with ODC, respectively. For each pacing rate, the top panel overlays the 10 paced AP traces over time under control and both dynamic-clamp conditions, and the black triangles indicate when a stimulus current was delivered. In the middle panel, the traces give the calculated target currents for EDC and ODC. The bottom panel shows the calculated light intensity used to generate the target current. The filled black triangles indicate when a stimulus current was delivered and provides a reference to which of the 10 paced APs in Figures 3 (A) and 4 (B) are displayed.

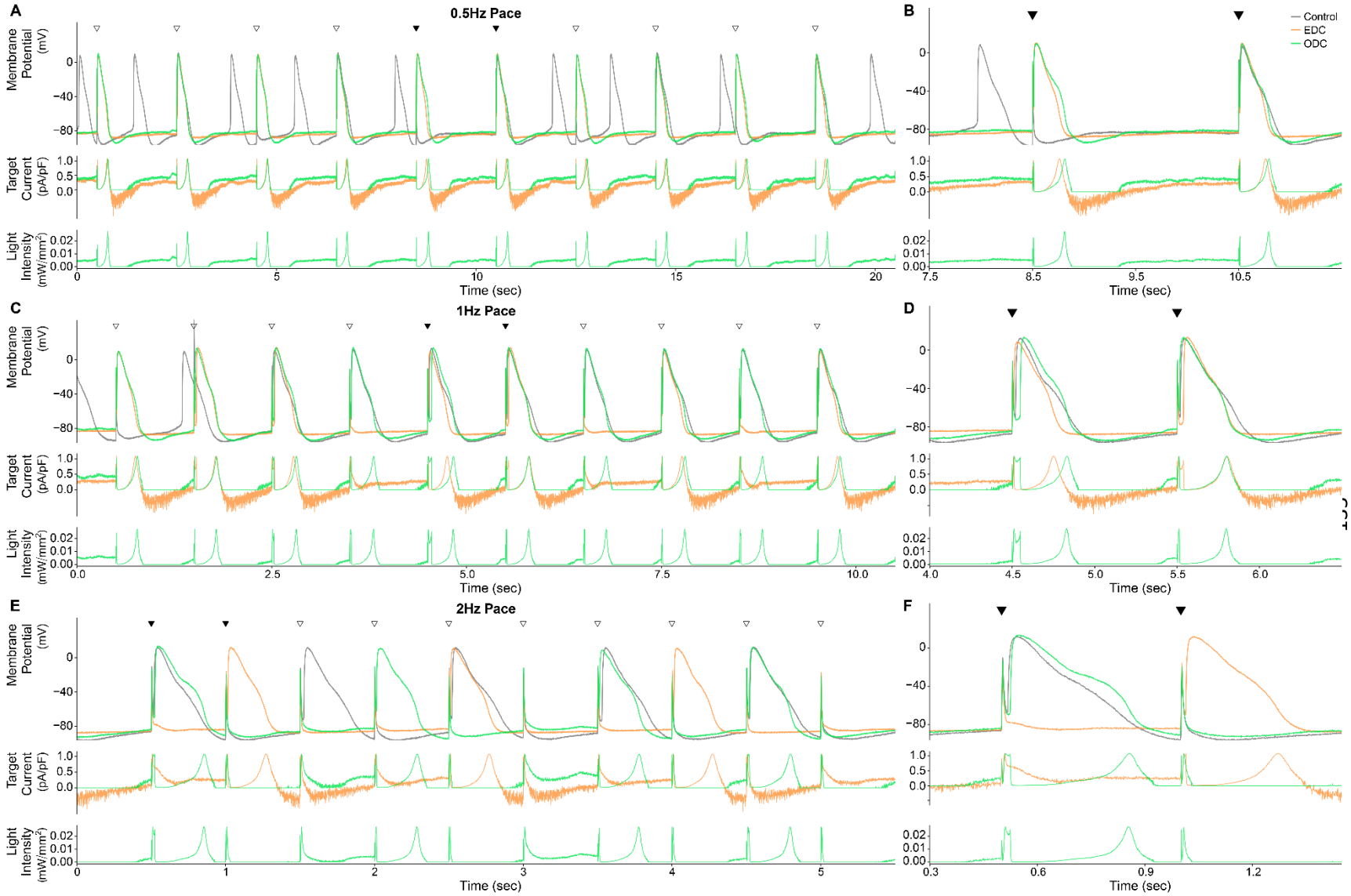
A
0.5Hz Pace
B
Control
EDC
ODC
C
1Hz Pace
D
E
2Hz Pace
F
Membrane Potential (mV)
Target Current (pA/pF)
Light Intensity (mW/mm²)
Time (sec)

Appendix A7: Representative example of a large undershoot after an AP and how EDC is able to compensate for the undershoot

Example cell (cell 3) showing the effects of adding I_{K1} while paced 10 times at 3 different frequencies: (A, B) 0.5 Hz, (C, D) 1 Hz, (E, F) 2 Hz. The gray, orange and green traces represent the control without any current addition, adding I_{target} with EDC, and adding I_{target} with ODC, respectively. The top panels overlay the 10 paced AP traces under control and both dynamic-clamp conditions, and the black triangles indicate when a stimulus current was delivered. In the middle panels, the traces give the calculated target currents for EDC and ODC. The bottom panels show the calculated light intensity used to generate the target current with ODC. The filled black triangles in the top panels (A, C, E) provide a reference for zoomed portions shown in B, D, and F, respectively.

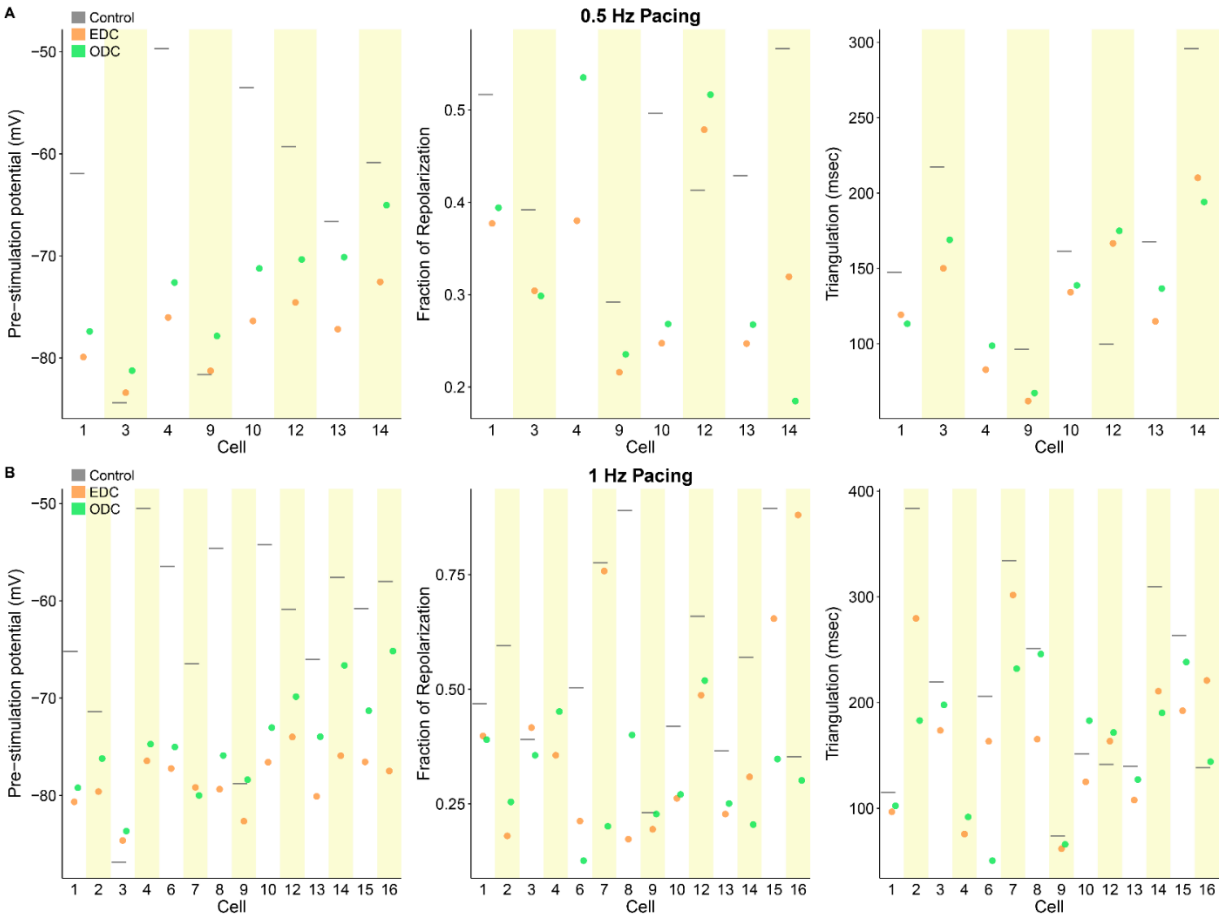

Appendix A8: Summary of the effects of EDC or ODC on AP morphology at different pacing frequencies

Pre-stimulation potential (left), fraction of repolarization (middle) and triangulation (right) of individual cells at 0.5 Hz (A) and 1 Hz (B) pacing in control (gray) and after adding an I_{K1} target current via EDC (orange) or ODC (green).

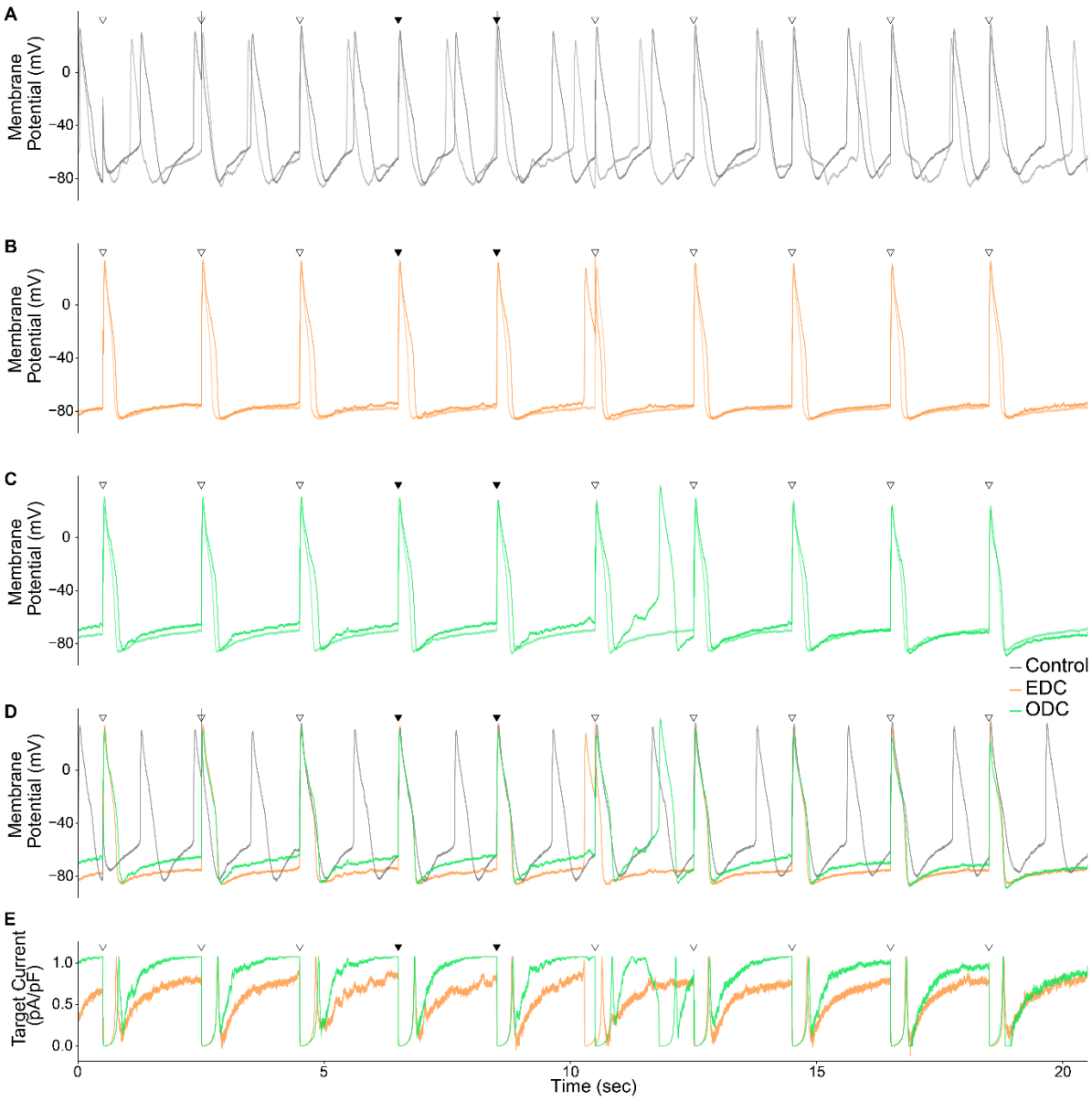

Appendix A9: Entire trace of 10 paced APs demonstrating the results of the EDC and ODC platforms from example cell with E-4031 addition
Results from example cell 13 showing the effects of adding I_{K1} while paced 10 times at 0.5 Hz. The figure is organized in the same manner as Appendix A6.

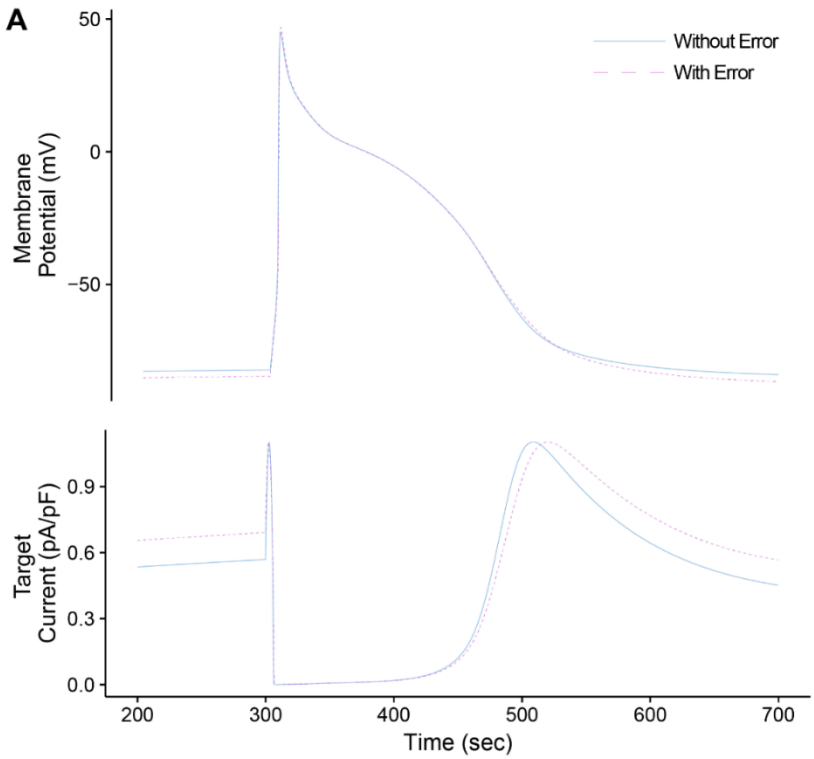

B

	Without Error	With Error
Pre−Stimulation Potential (mV)	−82.4	−84.7
APD_{90} (msec)	214.4	221.9

Appendix A10: *In silico* model prediction shows that the error between RTXI and the amplifier has limited impact on dynamic clamp experiments

To predict the effects on dynamic clamp performance of the 5% error between the membrane potential measured by the amplifier versus the membrane potential reported by RTXI, we used an *in silico* approach, simulating I_{K1} dynamic clamp injection into an iPSC-CM computational model (Paci et al., (2013)). We used the same equations for I_{K1} as in our experiments and clamped intracellular [Na^+] to mimic a patched cell. The dynamically clamped iPSC-CM model was run for 810 beats at a 1 Hz pacing rate with and without the amplifier calibration error and the last 10 APs were analyzed. (A) The top panel illustrates the last AP waveform with (dashed purple trace) and without (blue trace) the error. The bottom panel shows the corresponding target I_{K1}. The presence of the calibration error leads to an overestimation of this current during phase 4 of the AP, causing a small (about 2 mV) hyperpolarization of the resting membrane potential. (B) The resulting AP characteristics with and without the calibration error are very close, with about a 3% change in APD_{90}. Importantly, the predicted effect of the calibration error calculated here does not depend on how the dynamic clamp target current is added to the cell and is therefore expected to affect I_{target} calculated by the EDC and ODC systems equally.

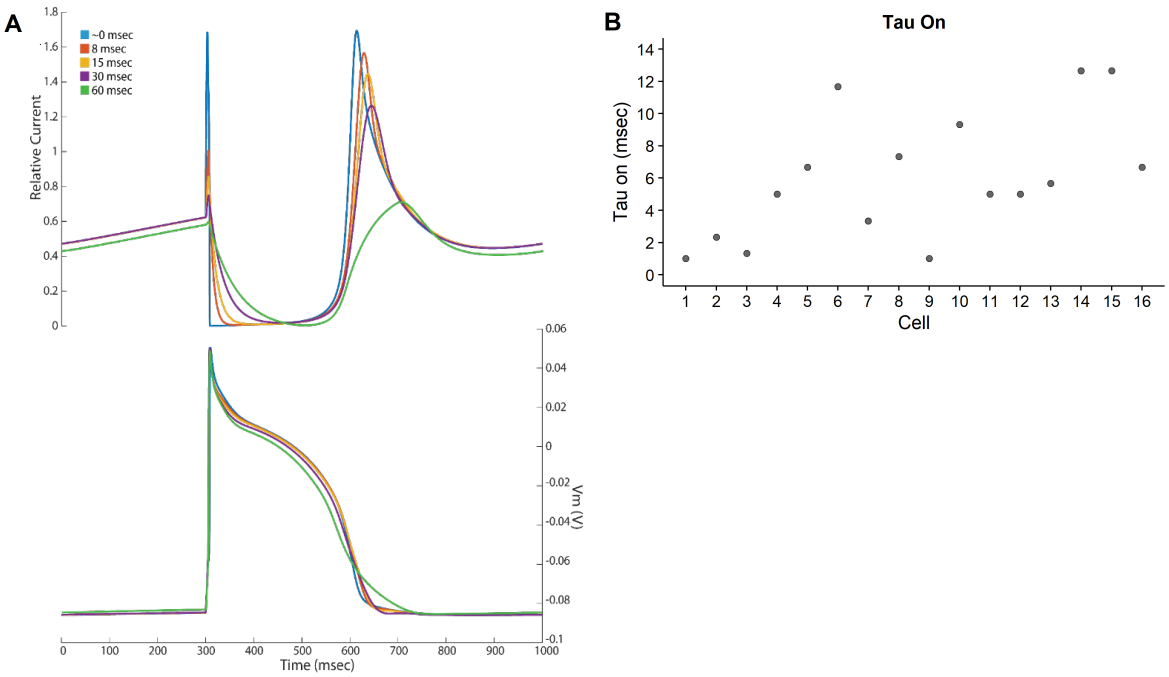

Appendix A11: *In silico* model predicting the effect of activation and deactivation kinetics on dynamic clamp performance and experimentally measured ArchT time constants

(A) To test that the kinetics of ArchT are not prohibitively slow for dynamic clamp, we simulated our ODC platform using the Paci et al. (2013) iPSC-CM model with an added ArchT model having a single time constant for activation and deactivation. We varied this time constant to see how large of a delay could be tolerated. The ArchT current generated with different time constants are displayed in the panel above and sthe resulting stimulated APs are in the panel below. (B) Experimentally measured time constants of activation of ArchT in each cell.

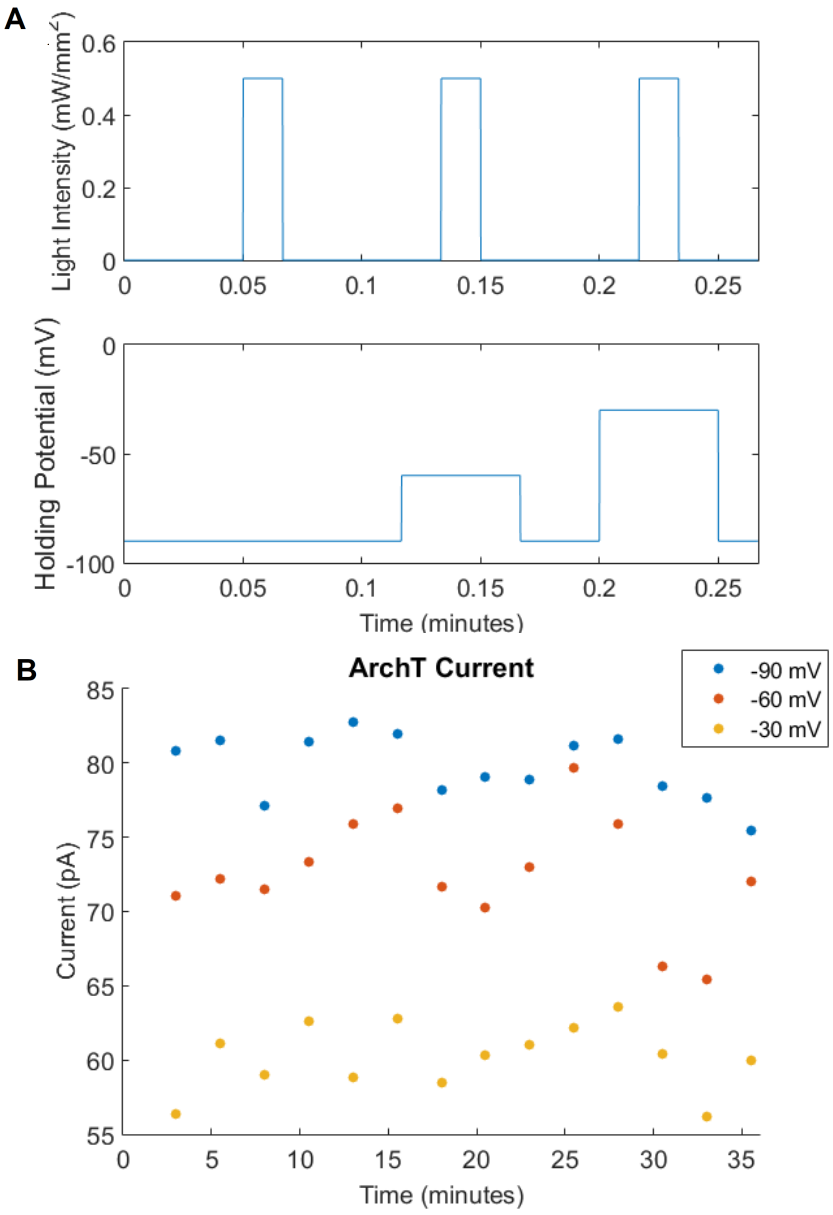

Appendix A12: Measuring stability of ArchT illumination during a voltage clamp and light clamp protocol

(A) The top panel shows the light clamp protocol and the bottom panel shows the voltage clamp protocol. This protocol was cycled through repeatedly to measure I_{ArchT} over time and at different holding potentials. (B) Results from a representative cell showing I_{ArchT} produced at different times of the protocol and at different holding potentials.

	PSP			Overshoot			APD_{90}		
	Control	EDC	ODC	Control	EDC	ODC	Control	EDC	ODC
2Hz	-64.9 ± 2.5	-78.3 ± 0.7	-74.2 ± 1.3	22.5 ± 2.9	21.5 ± 2.4	15.4 ± 2.3	265.3 ± 17.7	251.8 ± 17.5	267.0 ± 18.5
1 Hz	-63.2 ± 2.7	-78.6 ± 0.8	-74.5 ± 1.4	21.6 ± 3.4	21.1 ± 5.6	14.6 ± 2.5	269.9 ± 22.4	259.6 ± 20.7	261.7 ± 19.9
0.5 Hz	-64.6 ± 4.4	-77.7 ± 1.3	-73.2 ± 1.9	18.3 ± 4.9	14.8 ± 5.2	11.6 ± 3.8	254.1 ± 30.1	235.2 ± 24.9	241.0 ± 28.1
E4031	-64.1 ± 4.6	-75.8 ± 1.4	-71.1 ± 2.3	7.8 ± 7.3	16.7 ± 6.3	16.4 ± 5.3	711.6 ± 215.8	448.2 ± 98.3	483.6 ± 103.1

Appendix A13: AP morphology characteristics

The average and SEM of pre-stimulation potential (PSP) (mV), overshoot (mV), and APD_{90} (msec) without dynamic clamp, with EDC and with ODC. The characteristics after E-4031 addition are also listed.

BIBLIOGRAPHY

[1] H. Olson *et al.*, "Concordance of the Toxicity of Pharmaceuticals in Humans and in Animals," *Regul. Toxicol. Pharmacol.*, vol. 32, no. 1, pp. 56–67, Aug. 2000.

[2] H. Laverty *et al.*, "How can we improve our understanding of cardiovascular safety liabilities to develop safer medicines?," *Br. J. Pharmacol.*, vol. 163, no. 4, pp. 675–693, Jun. 2011.

[3] J. L. Stevens and T. K. Baker, "The future of drug safety testing: expanding the view and narrowing the focus," *Drug Discov. Today*, vol. 14, no. 3–4, pp. 162–167, Feb. 2009.

[4] S. Scott *et al.*, "Design, power, and interpretation of studies in the standard murine model of ALS," *Amyotroph. Lateral Scler. Off. Publ. World Fed. Neurol. Res. Group Mot. Neuron Dis.*, vol. 9, no. 1, pp. 4–15, 2008.

[5] I. W. Mak, N. Evaniew, and M. Ghert, "Lost in translation: animal models and clinical trials in cancer treatment," *Am. J. Transl. Res.*, vol. 6, no. 2, pp. 114–118, Jan. 2014.

[6] K. Takahashi *et al.*, "Induction of pluripotent stem cells from adult human fibroblasts by defined factors," *Cell*, vol. 131, no. 5, pp. 861–872, Nov. 2007.

[7] I. Itzhaki *et al.*, "Modelling the long QT syndrome with induced pluripotent stem cells," *Nature*, vol. 471, no. 7337, pp. 225–229, Mar. 2011.

[8] H.-P. Huang *et al.*, "Human Pompe disease-induced pluripotent stem cells for pathogenesis modeling, drug testing and disease marker identification," *Hum. Mol. Genet.*, vol. 20, no. 24, pp. 4851–4864, Dec. 2011.

[9] F. M. Drawnel *et al.*, "Disease Modeling and Phenotypic Drug Screening for Diabetic Cardiomyopathy using Human Induced Pluripotent Stem Cells," *Cell Rep.*, vol. 9, no. 3, pp. 810–820, Nov. 2014.

[10] A. Raya *et al.*, "Disease-corrected haematopoietic progenitors from Fanconi anaemia induced pluripotent stem cells," *Nature*, vol. 460, no. 7251, pp. 53–59, Jul. 2009.

[11] J. Zou, P. Mali, X. Huang, S. N. Dowey, and L. Cheng, "Site-specific gene correction of a point mutation in human iPS cells derived from an adult patient with sickle cell disease," *Blood*, vol. 118, no. 17, pp. 4599–4608, Oct. 2011.

[12] K. J. Brennand *et al.*, "Modelling schizophrenia using human induced pluripotent stem cells," *Nature*, vol. 473, no. 7346, pp. 221–225, May 2011.

[13] T. Yagi *et al.*, "Modeling familial Alzheimer's disease with induced pluripotent stem cells," *Hum. Mol. Genet.*, vol. 20, no. 23, pp. 4530–4539, Dec. 2011.

[14] M. A. Israel *et al.*, "Probing sporadic and familial Alzheimer's disease using induced pluripotent stem cells," *Nature*, vol. 482, no. 7384, pp. 216–220, Jan. 2012.

[15] T. Kondo *et al.*, "Modeling Alzheimer's disease with iPSCs reveals stress phenotypes associated with intracellular Aβ and differential drug responsiveness," *Cell Stem Cell*, vol. 12, no. 4, pp. 487–496, Apr. 2013.

[16] S. J. Chamberlain *et al.*, "Induced pluripotent stem cell models of the genomic imprinting disorders Angelman and Prader-Willi syndromes," *Proc. Natl. Acad. Sci. U. S. A.*, vol. 107, no. 41, pp. 17668–17673, Oct. 2010.

[17] S. M. Choi *et al.*, "Efficient drug screening and gene correction for treating liver disease using patient-specific stem cells," *Hepatol. Baltim. Md*, vol. 57, no. 6, pp. 2458–2468, Jun. 2013.

[18] Z. Ye *et al.*, "Human-induced pluripotent stem cells from blood cells of healthy donors and patients with acquired blood disorders," *Blood*, vol. 114, no. 27, pp. 5473–5480, Dec. 2009.
[19] J. Zou *et al.*, "Oxidase-deficient neutrophils from X-linked chronic granulomatous disease iPS cells: functional correction by zinc finger nuclease-mediated safe harbor targeting," *Blood*, vol. 117, no. 21, pp. 5561–5572, May 2011.
[20] G. C. L. Bett *et al.*, "Electronic 'Expression' of the Inward Rectifier in Cardiocytes Derived from Human Induced Pluripotent Stem Cells," *Heart Rhythm Off. J. Heart Rhythm Soc.*, vol. 10, no. 12, Dec. 2013.
[21] R. M. E. Meijer van Putten *et al.*, "Ion channelopathies in human induced pluripotent stem cell derived cardiomyocytes: a dynamic clamp study with virtual IK1," *Front. Physiol.*, vol. 6, Feb. 2015.
[22] A. O. Verkerk, C. C. Veerman, J. G. Zegers, I. Mengarelli, C. R. Bezzina, and R. Wilders, "Patch-Clamp Recording from Human Induced Pluripotent Stem Cell-Derived Cardiomyocytes: Improving Action Potential Characteristics through Dynamic Clamp," *Int. J. Mol. Sci.*, vol. 18, no. 9, Aug. 2017.
[23] K. E. Lasser, P. D. Allen, S. J. Woolhandler, D. U. Himmelstein, S. M. Wolfe, and D. H. Bor, "Timing of New Black Box Warnings and Withdrawals for Prescription Medications," *JAMA*, vol. 287, no. 17, pp. 2215–2220, May 2002.
[24] D. S. Echt *et al.*, "Mortality and Morbidity in Patients Receiving Encainide, Flecainide, or Placebo," *N. Engl. J. Med.*, vol. 324, no. 12, pp. 781–788, Mar. 1991.
[25] A. P. Hallstrom *et al.*, "Time to arrhythmic, ischemic, and heart failure events: Exploratory analyses to elucidate mechanisms of adverse drug effects in the Cardiac Arrhythmia Suppression Trial," *Am. Heart J.*, vol. 130, no. 1, pp. 71–79, Jul. 1995.
[26] W. S. Redfern *et al.*, "Relationships between preclinical cardiac electrophysiology, clinical QT interval prolongation and torsade de pointes for a broad range of drugs: evidence for a provisional safety margin in drug development," *Cardiovasc. Res.*, vol. 58, no. 1, pp. 32–45, Apr. 2003.
[27] D. Atkinson, A. Dunne, and M. Parker, "Torsades de pointes and self-terminating ventricular fibrillation in a prescription methadone user," *Anaesthesia*, vol. 62, no. 9, pp. 952–955, Sep. 2007.
[28] A. Selzer and H. W. Wray, "Quinidine Syncope: Paroxysmal Ventricular Fibrillation Occurring during Treatment of Chronic Atrial Arrhythmias," *Circulation*, vol. 30, no. 1, pp. 17–26, Jul. 1964.
[29] F. Dessertenne, "Ventricular tachycardia with 2 variable opposing foci (in French)," *Arch. Mal. Coeur Vaiss.*, vol. 59, pp. 263–72, Mar. 1966.
[30] H. Tie, B. D. Walker, S. M. Valenzuela, S. N. Breit, and T. J. Campbell, "The heart of psychotropic drug therapy," *The Lancet*, vol. 355, no. 9217, p. 1825, May 2000.
[31] M. Taglialatela *et al.*, "Molecular basis for the lack of HERG K+ channel block-related cardiotoxicity by the H1 receptor blocker cetirizine compared with other second-generation antihistamines," *Mol. Pharmacol.*, vol. 54, no. 1, pp. 113–121, Jul. 1998.
[32] H. Suessbrich, S. Waldegger, F. Lang, and A. E. Busch, "Blockade of HERG channels expressed in Xenopus oocytes by the histamine receptor antagonists terfenadine and astemizole," *FEBS Lett.*, vol. 385, no. 1–2, pp. 77–80, Apr. 1996.
[33] H. Suessbrich, R. Schönherr, S. H. Heinemann, B. Attali, F. Lang, and A. E. Busch, "The inhibitory effect of the antipsychotic drug haloperidol on HERG potassium channels

expressed in Xenopus oocytes," *Br. J. Pharmacol.*, vol. 120, no. 5, pp. 968–974, Mar. 1997.
[34] J. Kang, L. Wang, X. L. Chen, D. J. Triggle, and D. Rampe, "Interactions of a series of fluoroquinolone antibacterial drugs with the human cardiac K+ channel HERG," *Mol. Pharmacol.*, vol. 59, no. 1, pp. 122–126, Jan. 2001.
[35] I. Splawski *et al.*, "Spectrum of mutations in long-QT syndrome genes. KVLQT1, HERG, SCN5A, KCNE1, and KCNE2," *Circulation*, vol. 102, no. 10, pp. 1178–1185, Sep. 2000.
[36] F. De Ponti, E. Poluzzi, and N. Montanaro, "Organising evidence on QT prolongation and occurrence of Torsades de Pointes with non-antiarrhythmic drugs: a call for consensus," *Eur. J. Clin. Pharmacol.*, vol. 57, no. 3, pp. 185–209, Jun. 2001.
[37] S. Zhang, Z. Zhou, Q. Gong, J. C. Makielski, and C. T. January, "Mechanism of block and identification of the verapamil binding domain to HERG potassium channels," *Circ. Res.*, vol. 84, no. 9, pp. 989–998, May 1999.
[38] D. M. Krikler and P. V. Curry, "Torsade De Pointes, an atypical ventricular tachycardia.," *Br. Heart J.*, vol. 38, no. 2, pp. 117–120, Feb. 1976.
[39] Y. G. Yap and J. Camm, "Risk of torsades de pointes with non-cardiac drugs. Doctors need to be aware that many drugs can cause qt prolongation," *BMJ*, vol. 320, no. 7243, pp. 1158–1159, Apr. 2000.
[40] J. T. Barbey, J. C. Pezzullo, and S. L. Soignet, "Effect of Arsenic Trioxide on QT Interval in Patients With Advanced Malignancies," *J. Clin. Oncol.*, vol. 21, no. 19, pp. 3609–3615, Oct. 2003.
[41] L. Eckardt, G. Breithardt, and W. Haverkamp, "Electrophysiologic Characterization of the Antipsychotic Drug Sertindole in a Rabbit Heart Model of Torsade de Pointes: Low Torsadogenic Potential Despite QT Prolongation," *J. Pharmacol. Exp. Ther.*, vol. 300, no. 1, pp. 64–71, Jan. 2002.
[42] B. M. Swinkels, G. Hoedemaker, and R. van Stralen, "Self-terminating torsades de pointes in a patient with bradycardia-induced long-QT syndrome," *Neth. Heart J.*, vol. 14, no. 9, p. 314, Sep. 2006.
[43] S. Authier *et al.*, "Proarrhythmia liability assessment and the comprehensive in vitro Proarrhythmia Assay (CiPA): An industry survey on current practice," *J. Pharmacol. Toxicol. Methods*, vol. 86, pp. 34–43, Jul. 2017.
[44] H. L. Tan, "Electrophysiologic Mechanisms of the Long QT Interval Syndromes and Torsade de Pointes," *Ann. Intern. Med.*, vol. 122, no. 9, p. 701, May 1995.
[45] "CIPA |." .
[46] "The 2012 Nobel Prize in Physiology or Medicine - Press Release." [Online]. Available: https://www.nobelprize.org/nobel_prizes/medicine/laureates/2012/press.html. [Accessed: 24-Apr-2018].
[47] Q. Zhang *et al.*, "Direct differentiation of atrial and ventricular myocytes from human embryonic stem cells by alternating retinoid signals," *Cell Res.*, vol. 21, no. 4, pp. 579–587, Apr. 2011.
[48] W.-Z. Zhu, Y. Xie, K. W. Moyes, J. D. Gold, B. Askari, and M. A. Laflamme, "Neuregulin/ErbB Signaling Regulates Cardiac Subtype Specification in Differentiating Human Embryonic Stem CellsNovelty and Significance," *Circ. Res.*, vol. 107, no. 6, pp. 776–786, Sep. 2010.
[49] Z. Weng *et al.*, "A Simple, Cost-Effective but Highly Efficient System for Deriving Ventricular Cardiomyocytes from Human Pluripotent Stem Cells," *Stem Cells Dev.*, vol. 23, no. 14, pp. 1704–1716, Feb. 2014.

[50] Tanwar Vineeta *et al.*, "Gremlin 2 Promotes Differentiation of Embryonic Stem Cells to Atrial Fate by Activation of the JNK Signaling Pathway," *STEM CELLS*, vol. 32, no. 7, pp. 1774–1788, Jun. 2014.
[51] R. Josowitz *et al.*, "Identification and Purification of Human Induced Pluripotent Stem Cell-Derived Atrial-Like Cardiomyocytes Based on Sarcolipin Expression," *PLOS ONE*, vol. 9, no. 7, p. e101316, Jul. 2014.
[52] A. Bizy *et al.*, "Myosin light chain 2-based selection of human iPSC-derived early ventricular cardiac myocytes," *Stem Cell Res.*, vol. 11, no. 3, pp. 1335–1347, Nov. 2013.
[53] A. D. Witty *et al.*, "Generation of the epicardial lineage from human pluripotent stem cells," *Nat. Biotechnol.*, vol. 32, no. 10, pp. 1026–1035, Oct. 2014.
[54] D. Iyer *et al.*, "Robust derivation of epicardium and its differentiated smooth muscle cell progeny from human pluripotent stem cells," *Dev. Camb. Engl.*, vol. 142, no. 8, pp. 1528–1541, Apr. 2015.
[55] X. Lian *et al.*, "Efficient Differentiation of Human Pluripotent Stem Cells to Endothelial Progenitors via Small-Molecule Activation of WNT Signaling," *Stem Cell Rep.*, vol. 3, no. 5, pp. 804–816, Nov. 2014.
[56] A. Moretti *et al.*, "Patient-Specific Induced Pluripotent Stem-Cell Models for Long-QT Syndrome," *N. Engl. J. Med.*, vol. 363, no. 15, pp. 1397–1409, Oct. 2010.
[57] E. Matsa *et al.*, "Drug evaluation in cardiomyocytes derived from human induced pluripotent stem cells carrying a long QT syndrome type 2 mutation," *Eur. Heart J.*, vol. 32, no. 8, pp. 952–962, Apr. 2011.
[58] A. L. Lahti *et al.*, "Model for long QT syndrome type 2 using human iPS cells demonstrates arrhythmogenic characteristics in cell culture," *Dis. Model. Mech.*, vol. 5, no. 2, pp. 220–230, Mar. 2012.
[59] A. Fatima *et al.*, "The disease-specific phenotype in cardiomyocytes derived from induced pluripotent stem cells of two long QT syndrome type 3 patients," *PloS One*, vol. 8, no. 12, p. e83005, 2013.
[60] R. P. Davis *et al.*, "Cardiomyocytes derived from pluripotent stem cells recapitulate electrophysiological characteristics of an overlap syndrome of cardiac sodium channel disease," *Circulation*, vol. 125, no. 25, pp. 3079–3091, Jun. 2012.
[61] O. Caspi *et al.*, "Modeling of arrhythmogenic right ventricular cardiomyopathy with human induced pluripotent stem cells," *Circ. Cardiovasc. Genet.*, vol. 6, no. 6, pp. 557–568, Dec. 2013.
[62] D. Ma *et al.*, "Generation of patient-specific induced pluripotent stem cell-derived cardiomyocytes as a cellular model of arrhythmogenic right ventricular cardiomyopathy," *Eur. Heart J.*, vol. 34, no. 15, pp. 1122–1133, Apr. 2013.
[63] C. Kim *et al.*, "Studying arrhythmogenic right ventricular dysplasia with patient-specific iPSCs," *Nature*, vol. 494, no. 7435, pp. 105–110, Feb. 2013.
[64] X. Carvajal-Vergara *et al.*, "Patient-specific induced pluripotent stem-cell-derived models of LEOPARD syndrome," *Nature*, vol. 465, no. 7299, pp. 808–812, Jun. 2010.
[65] J.-M. Itier *et al.*, "Effective clearance of GL-3 in a human iPSC-derived cardiomyocyte model of Fabry disease," *J. Inherit. Metab. Dis.*, vol. 37, no. 6, pp. 1013–1022, Nov. 2014.
[66] G. Wang *et al.*, "Modeling the mitochondrial cardiomyopathy of Barth syndrome with induced pluripotent stem cell and heart-on-chip technologies," *Nat. Med.*, vol. 20, no. 6, pp. 616–623, Jun. 2014.

[67] N. Sun *et al.*, “Patient-Specific Induced Pluripotent Stem Cells as a Model for Familial Dilated Cardiomyopathy,” *Sci. Transl. Med.*, vol. 4, no. 130, pp. 130ra47-130ra47, Apr. 2012.
[68] M. Yazawa and R. E. Dolmetsch, “Modeling Timothy syndrome with iPS cells,” *J Cardiovasc. Transl. Res.*, vol. 6, no. 1, pp. 1–9, Feb. 2013.
[69] F. J. Clubb and S. P. Bishop, “Formation of binucleated myocardial cells in the neonatal rat. An index for growth hypertrophy,” *Lab. Investig. J. Tech. Methods Pathol.*, vol. 50, no. 5, pp. 571–577, May 1984.
[70] F. Li, X. Wang, J. M. Capasso, and A. M. Gerdes, “Rapid transition of cardiac myocytes from hyperplasia to hypertrophy during postnatal development,” *J. Mol. Cell. Cardiol.*, vol. 28, no. 8, pp. 1737–1746, Aug. 1996.
[71] G. Hasenfuss *et al.*, “Energetics of isometric force development in control and volume-overload human myocardium. Comparison with animal species.,” *Circ. Res.*, vol. 68, no. 3, pp. 836–846, Mar. 1991.
[72] K. Dolnikov *et al.*, “Functional Properties of Human Embryonic Stem Cell–Derived Cardiomyocytes: Intracellular Ca2+ Handling and the Role of Sarcoplasmic Reticulum in the Contraction,” *STEM CELLS*, vol. 24, no. 2, pp. 236–245.
[73] C. P. Jackman, A. L. Carlson, and N. Bursac, “Dynamic culture yields engineered myocardium with near-adult functional output,” *Biomaterials*, vol. 111, pp. 66–79, Dec. 2016.
[74] P. Razeghi, M. E. Young, J. L. Alcorn, C. S. Moravec, O. H. Frazier, and H. Taegtmeyer, “Metabolic Gene Expression in Fetal and Failing Human Heart,” *Circulation*, vol. 104, no. 24, pp. 2923–2931, Dec. 2001.
[75] P. Rana, B. Anson, S. Engle, and Y. Will, “Characterization of Human-Induced Pluripotent Stem Cell–Derived Cardiomyocytes: Bioenergetics and Utilization in Safety Screening,” *Toxicol. Sci.*, vol. 130, no. 1, pp. 117–131, Nov. 2012.
[76] M. Gherghiceanu *et al.*, “Cardiomyocytes derived from human embryonic and induced pluripotent stem cells: comparative ultrastructure,” *J. Cell. Mol. Med.*, vol. 15, no. 11, pp. 2539–2551, Nov. 2011.
[77] F. B. Bedada *et al.*, “Acquisition of a Quantitative, Stoichiometrically Conserved Ratiometric Marker of Maturation Status in Stem Cell-Derived Cardiac Myocytes,” *Stem Cell Rep.*, vol. 3, no. 4, pp. 594–605, Oct. 2014.
[78] N. M. Hunkeler, J. Kullman, and A. M. Murphy, “Troponin I isoform expression in human heart.,” *Circ. Res.*, vol. 69, no. 5, pp. 1409–1414, Nov. 1991.
[79] J. T. Koivumäki *et al.*, “Structural Immaturity of Human iPSC-Derived Cardiomyocytes: In Silico Investigation of Effects on Function and Disease Modeling,” *Front. Physiol.*, vol. 9, Feb. 2018.
[80] J. J. Kim *et al.*, “Mechanism of automaticity in cardiomyocytes derived from human induced pluripotent stem cells,” *J. Mol. Cell. Cardiol.*, vol. 81, pp. 81–93, Apr. 2015.
[81] A. M. Gerdes, J. Kriseman, and S. P. Bishop, “Changes in myocardial cell size and number during the development and reversal of hyperthyroidism in neonatal rats,” *Lab. Investig. J. Tech. Methods Pathol.*, vol. 48, no. 5, pp. 598–602, May 1983.
[82] K. Rakusan and B. Korecky, “Regression of cardiomegaly induced in newborn rats,” *Can. J. Cardiol.*, vol. 1, no. 3, pp. 217–222, Jun. 1985.
[83] E. Kardami, “Stimulation and inhibition of cardiac myocyte proliferation <Emphasis Type="Italic">in vitro</Emphasis>,” *Mol. Cell. Biochem.*, vol. 92, no. 2, pp. 129–135, Feb. 1990.

[84] T. G. Parker and M. D. Schneider, “Growth factors, proto-oncogenes, and plasticity of the cardiac phenotype,” *Annu. Rev. Physiol.*, vol. 53, pp. 179–200, 1991.
[85] T. J. Kolanowski, C. L. Antos, and K. Guan, “Making human cardiomyocytes up to date: Derivation, maturation state and perspectives,” *Int. J. Cardiol.*, Mar. 2017.
[86] S. Kadota, L. Pabon, H. Reinecke, and C. E. Murry, “In Vivo Maturation of Human Induced Pluripotent Stem Cell-Derived Cardiomyocytes in Neonatal and Adult Rat Hearts,” *Stem Cell Rep.*, vol. 8, no. 2, pp. 278–289, Feb. 2017.
[87] J. Ma *et al.*, “High purity human-induced pluripotent stem cell-derived cardiomyocytes: electrophysiological properties of action potentials and ionic currents,” *Am. J. Physiol. Heart Circ. Physiol.*, vol. 301, no. 5, pp. H2006-2017, Nov. 2011.
[88] Ishihara Keiko, Yan Ding-Hong, Yamamoto Shintaro, and Ehara Tsuguhisa, “Inward rectifier K+ current under physiological cytoplasmic conditions in guinea-pig cardiac ventricular cells,” *J. Physiol.*, vol. 540, no. 3, pp. 831–841, Jul. 2004.
[89] M. Paci, J. Hyttinen, K. Aalto-Setälä, and S. Severi, “Computational models of ventricular- and atrial-like human induced pluripotent stem cell derived cardiomyocytes,” *Ann. Biomed. Eng.*, vol. 41, no. 11, pp. 2334–2348, Nov. 2013.
[90] G. C. L. Bett *et al.*, “Electronic ‘expression’ of the inward rectifier in cardiocytes derived from human-induced pluripotent stem cells,” *Heart Rhythm*, vol. 10, no. 12, pp. 1903–1910, Dec. 2013.
[91] K. Blinova *et al.*, “Comprehensive Translational Assessment of Human-Induced Pluripotent Stem Cell Derived Cardiomyocytes for Evaluating Drug-Induced Arrhythmias,” *Toxicol. Sci. Off. J. Soc. Toxicol.*, vol. 155, no. 1, pp. 234–247, Jan. 2017.
[92] H. Ando *et al.*, “A new paradigm for drug-induced torsadogenic risk assessment using human iPS cell-derived cardiomyocytes,” *J. Pharmacol. Toxicol. Methods*, vol. 84, pp. 111–127, Mar. 2017.
[93] W. J. Crumb, J. Vicente, L. Johannesen, and D. G. Strauss, “An evaluation of 30 clinical drugs against the comprehensive in vitro proarrhythmia assay (CiPA) proposed ion channel panel,” *J. Pharmacol. Toxicol. Methods*, vol. 81, pp. 251–262, Sep. 2016.
[94] S. Scott, “Scott S. State University of New York at Buffalo; 1979. Stimulation simulations of young yet cultured beating hearts. PhD Thesis.”
[95] R. C. Tan and R. W. Joyner, “Electrotonic influences on action potentials from isolated ventricular cells,” *Circ. Res.*, vol. 67, no. 5, pp. 1071–1081, Nov. 1990.
[96] R. C. Tan, T. Osaka, and R. W. Joyner, “Experimental model of effects on normal tissue of injury current from ischemic region,” *Circ. Res.*, vol. 69, no. 4, pp. 965–974, Oct. 1991.
[97] J. R. al et, “Unidirectional block between isolated rabbit ventricular cells coupled by a variable resistance. - PubMed - NCBI.” [Online]. Available: https://www.ncbi.nlm.nih.gov/pubmed/1760503/. [Accessed: 30-Apr-2018].
[98] A. A. Prinz, L. F. Abbott, and E. Marder, “The dynamic clamp comes of age,” *Trends Neurosci.*, vol. 27, no. 4, pp. 218–224, Apr. 2004.
[99] R. C. Ahrens-Nicklas and D. J. Christini, “Anthropomorphizing the Mouse Cardiac Action Potential via a Novel Dynamic Clamp Method,” *Biophys. J.*, vol. 97, no. 10, pp. 2684–2692, Nov. 2009.
[100] T. R. Brown, T. Krogh-Madsen, and D. J. Christini, “Illuminating Myocyte-Fibroblast Homotypic and Heterotypic Gap Junction Dynamics Using Dynamic Clamp,” *Biophys. J.*, vol. 111, no. 4, pp. 785–797, Aug. 2016.

[101] F. A. Ortega, R. J. Butera, D. J. Christini, J. A. White, and A. D. Dorval, “Dynamic clamp in cardiac and neuronal systems using RTXI,” *Methods Mol. Biol. Clifton NJ*, vol. 1183, pp. 327–354, 2014.
[102] B. Goversen *et al.*, “A Hybrid Model for Safety Pharmacology on an Automated Patch Clamp Platform: Using Dynamic Clamp to Join iPSC-Derived Cardiomyocytes and Simulations of Ik1 Ion Channels in Real-Time,” *Front. Physiol.*, vol. 8, 2018.
[103] J.-M. Goaillard and E. Marder, “Dynamic Clamp Analyses of Cardiac, Endocrine, and Neural Function,” *Physiology*, vol. 21, no. 3, pp. 197–207, Jun. 2006.
[104] A. O. Verkerk, C. C. Veerman, J. G. Zegers, I. Mengarelli, C. R. Bezzina, and R. Wilders, “Patch-Clamp Recording from Human Induced Pluripotent Stem Cell-Derived Cardiomyocytes: Improving Action Potential Characteristics through Dynamic Clamp,” *Int. J. Mol. Sci.*, vol. 18, no. 9, Aug. 2017.
[105] R. A. Devenyi, F. A. Ortega, W. Groenendaal, T. Krogh-Madsen, D. J. Christini, and E. A. Sobie, “Differential roles of two delayed rectifier potassium currents in regulation of ventricular action potential duration and arrhythmia susceptibility,” *J. Physiol.*, vol. 595, no. 7, pp. 2301–2317, Apr. 2017.
[106] A. S. Dhamoon and J. Jalife, “The inward rectifier current (IK1) controls cardiac excitability and is involved in arrhythmogenesis,” *Heart Rhythm*, vol. 2, no. 3, pp. 316–324, Mar. 2005.
[107] R. M. E. Meijer van Putten *et al.*, “Ion channelopathies in human induced pluripotent stem cell derived cardiomyocytes: a dynamic clamp study with virtual IK1,” *Front. Physiol.*, vol. 6, p. 7, 2015.
[108] C. C. Veerman *et al.*, “hiPSC-derived cardiomyocytes from Brugada Syndrome patients without identified mutations do not exhibit clear cellular electrophysiological abnormalities,” *Sci. Rep.*, vol. 6, p. 30967, Aug. 2016.
[109] B. Goversen *et al.*, “A Hybrid Model for Safety Pharmacology on an Automated Patch Clamp Platform: Using Dynamic Clamp to Join iPSC-Derived Cardiomyocytes and Simulations of Ik1 Ion Channels in Real-Time,” *Front. Physiol.*, vol. 8, 2018.
[110] M. Rocchetti *et al.*, “Elucidating arrhythmogenic mechanisms of long-QT syndrome CALM1-F142L mutation in patient-specific induced pluripotent stem cell-derived cardiomyocytes,” *Cardiovasc. Res.*, vol. 113, no. 5, pp. 531–541, Apr. 2017.
[111] M. Li *et al.*, “Overexpression of KCNJ2 in induced pluripotent stem cell-derived cardiomyocytes for the assessment of QT-prolonging drugs,” *J. Pharmacol. Sci.*, vol. 134, no. 2, pp. 75–85, Jun. 2017.
[112] J. E. González, K. Oades, Y. Leychkis, A. Harootunian, and P. A. Negulescu, “Cell-based assays and instrumentation for screening ion-channel targets,” *Drug Discov. Today*, vol. 4, no. 9, pp. 431–439, Sep. 1999.
[113] W. Zheng, R. H. Spencer, and L. Kiss, “High Throughput Assay Technologies for Ion Channel Drug Discovery,” *ASSAY Drug Dev. Technol.*, vol. 2, no. 5, pp. 543–552, Oct. 2004.
[114] “Electrophysiological analysis instruments based on the patch clamp technology for ion channel screening, SSM-based electrophysiology for electrogenic transporter research, impedance-based analysis for toxicology assays and bilayer recording technology for single channel analysis, used for drug development as cardiac safety, efficacy and HTS screening, SAR studies, as well as for basic research.” [Online]. Available: https://www.nanion.de/en/. [Accessed: 02-May-2018].

[115] I. Inc, “Automated Patch Clamp :: Icagen, Inc.” [Online]. Available: http://www.icagen.com/tools-technologies/biology/automated-patch-clamp. [Accessed: 02-May-2018].
[116] “IonFlux High Throughput Automated Patch Clamp Systems | Molecular Devices.” [Online]. Available: https://www.moleculardevices.com/en/assets/app-note/dd/cns/ionflux-high-throughput-automated-patch-clamp-systems. [Accessed: 02-May-2018].
[117] A. Klimas, C. M. Ambrosi, J. Yu, J. C. Williams, H. Bien, and E. Entcheva, “OptoDyCE as an automated system for high-throughput all-optical dynamic cardiac electrophysiology,” *Nat. Commun.*, vol. 7, p. ncomms11542, May 2016.
[118] F. St-Pierre, M. Chavarha, and M. Z. Lin, “Designs and sensing mechanisms of genetically encoded fluorescent voltage indicators,” *Curr. Opin. Chem. Biol.*, vol. 27, pp. 31–38, Aug. 2015.
[119] G. T. Dempsey *et al.*, “Cardiotoxicity screening with simultaneous optogenetic pacing, voltage imaging and calcium imaging,” *J. Pharmacol. Toxicol. Methods*, vol. 81, pp. 240–250, Sep. 2016.
[120] A. Ahola, R.-P. Pölönen, K. Aalto-Setälä, and J. Hyttinen, “Simultaneous Measurement of Contraction and Calcium Transients in Stem Cell Derived Cardiomyocytes,” *Ann. Biomed. Eng.*, vol. 46, no. 1, pp. 148–158, Jan. 2018.
[121] M. Maddah *et al.*, “A Non-invasive Platform for Functional Characterization of Stem-Cell-Derived Cardiomyocytes with Applications in Cardiotoxicity Testing,” *Stem Cell Rep.*, vol. 4, no. 4, pp. 621–631, Mar. 2015.
[122] N. Huebsch *et al.*, “Automated Video-Based Analysis of Contractility and Calcium Flux in Human-Induced Pluripotent Stem Cell-Derived Cardiomyocytes Cultured over Different Spatial Scales,” *Tissue Eng. Part C Methods*, vol. 21, no. 5, pp. 467–479, May 2015.
[123] H. Mutoh and T. Knöpfel, “Probing neuronal activities with genetically encoded optical indicators: from a historical to a forward-looking perspective,” *Pflüg. Arch. - Eur. J. Physiol.*, vol. 465, no. 3, pp. 361–371, Mar. 2013.
[124] N. Huebsch *et al.*, “Miniaturized iPS-Cell-Derived Cardiac Muscles for Physiologically Relevant Drug Response Analyses,” *Sci. Rep.*, vol. 6, p. 24726, Apr. 2016.
[125] X. Han *et al.*, “A High-Light Sensitivity Optical Neural Silencer: Development and Application to Optogenetic Control of Non-Human Primate Cortex,” *Front. Syst. Neurosci.*, vol. 5, Apr. 2011.
[126] B. Y. Chow, X. Han, and E. S. Boyden, “Genetically encoded molecular tools for light-driven silencing of targeted neurons,” *Prog. Brain Res.*, vol. 196, pp. 49–61, 2012.
[127] J. Mattis *et al.*, “Principles for applying optogenetic tools derived from direct comparative analysis of microbial opsins,” *Nat. Methods*, vol. 9, no. 2, pp. 159–172, Feb. 2012.
[128] G. T. Dempsey *et al.*, “Cardiotoxicity screening with simultaneous optogenetic pacing, voltage imaging and calcium imaging,” *J. Pharmacol. Toxicol. Methods*, vol. 81, pp. 240–250, Sep. 2016.
[129] D. R. Hochbaum *et al.*, “All-optical electrophysiology in mammalian neurons using engineered microbial rhodopsins,” *Nat. Methods*, vol. 11, no. 8, pp. 825–833, Aug. 2014.

[130] F. St-Pierre, J. D. Marshall, Y. Yang, Y. Gong, M. J. Schnitzer, and M. Z. Lin, "High-fidelity optical reporting of neuronal electrical activity with an ultrafast fluorescent voltage sensor," *Nat. Neurosci.*, vol. 17, no. 6, pp. 884–889, Jun. 2014.
[131] C. Cosentino *et al.*, "Engineering of a light-gated potassium channel," *Science*, vol. 348, no. 6235, pp. 707–710, May 2015.
[132] D. L. Fortin *et al.*, "Optogenetic photochemical control of designer K+ channels in mammalian neurons," *J. Neurophysiol.*, vol. 106, no. 1, pp. 488–496, Jul. 2011.
[133] E. Entcheva and J. C. Williams, "Channelrhodopsin2 Current During the Action Potential: 'Optical AP Clamp' and Approximation," *Sci. Rep.*, vol. 4, p. srep05838, Jul. 2014.
[134] J. C. Williams *et al.*, "Computational Optogenetics: Empirically-Derived Voltage- and Light-Sensitive Channelrhodopsin-2 Model," *PLOS Comput. Biol.*, vol. 9, no. 9, p. e1003220, Sep. 2013.
[135] T. V. Karathanos, P. M. Boyle, and N. A. Trayanova, "Optogenetics-enabled dynamic modulation of action potential duration in atrial tissue: feasibility of a novel therapeutic approach," *Eur. Eur. Pacing Arrhythm. Card. Electrophysiol. J. Work. Groups Card. Pacing Arrhythm. Card. Cell. Electrophysiol. Eur. Soc. Cardiol.*, vol. 16 Suppl 4, pp. iv69–iv76, Nov. 2014.
[136] E. G. Govorunova, S. R. Cunha, O. A. Sineshchekov, and J. L. Spudich, "Anion channelrhodopsins for inhibitory cardiac optogenetics," *Sci. Rep.*, vol. 6, Sep. 2016.
[137] S. A. Park, S.-R. Lee, L. Tung, and D. T. Yue, "Optical mapping of optogenetically shaped cardiac action potentials," *Sci. Rep.*, vol. 4, p. 6125, Aug. 2014.
[138] M. L. Huff, R. L. Miller, K. Deisseroth, D. E. Moorman, and R. T. LaLumiere, "Posttraining optogenetic manipulations of basolateral amygdala activity modulate consolidation of inhibitory avoidance memory in rats," *Proc. Natl. Acad. Sci.*, vol. 110, no. 9, pp. 3597–3602, Feb. 2013.
[139] U. Nussinovitch, R. Shinnawi, and L. Gepstein, "Modulation of cardiac tissue electrophysiological properties with light-sensitive proteins," *Cardiovasc. Res.*, vol. 102, no. 1, pp. 176–187, Apr. 2014.
[140] B. Li, X. Yang, F. Qian, M. Tang, C. Ma, and L.-Y. Chiang, "A novel analgesic approach to optogenetically and specifically inhibit pain transmission using TRPV1 promoter," *Brain Res.*, vol. 1609, pp. 12–20, Jun. 2015.
[141] T. Tsunematsu and A. Yamanaka, "Elucidation of Neuronal Circuitry Involved in the Regulation of Sleep/Wakefulness Using Optogenetics," in *Optogenetics*, H. Yawo, H. Kandori, and A. Koizumi, Eds. Springer Japan, 2015, pp. 249–263.
[142] V. Lux, O. A. Masseck, S. Herlitze, and M. M. Sauvage, "Optogenetic Destabilization of the Memory Trace in CA1: Insights into Reconsolidation and Retrieval Processes," *Cereb. Cortex*, vol. 27, no. 1, pp. 841–851, Jan. 2017.
[143] C. M. Ambrosi and E. Entcheva, "Optogenetic Control of Cardiomyocytes via Viral Delivery," *Methods Mol. Biol. Clifton NJ*, vol. 1181, pp. 215–228, 2014.
[144] J. Yu and E. Entcheva, "Inscribing Optical Excitability to Non-Excitable Cardiac Cells: Viral Delivery of Optogenetic Tools in Primary Cardiac Fibroblasts," *Methods Mol. Biol. Clifton NJ*, vol. 1408, pp. 303–317, 2016.
[145] E. P. Lukashev, R. Govindjee1, M. Kono1, 1 Ebrey† T. G., Y. Sugiyama2, and Y. Mukohata2, "pH DEPENDENCE OF THE ABSORPTION SPECTRA AND PHOTOCHEMICAL TRANSFORMATIONS OF THE ARCHAERHODOPSINS," *Photochem. Photobiol.*, vol. 60, no. 1, pp. 69–75, Jul. 1994.

[146] M. Ming, M. Lu, S. P. Balashov, T. G. Ebrey, Q. Li, and J. Ding, “pH Dependence of Light-Driven Proton Pumping by an Archaerhodopsin from Tibet: Comparison with Bacteriorhodopsin,” *Biophys. J.*, vol. 90, no. 9, pp. 3322–3332, May 2006.
[147] E. C. Saint Clair, J. I. Ogren, S. Mamaev, D. Russano, J. M. Kralj, and K. J. Rothschild, “Near-IR Resonance Raman Spectroscopy of Archaerhodopsin 3: Effects of Transmembrane Potential,” *J. Phys. Chem. B*, vol. 116, no. 50, pp. 14592–14601, Dec. 2012.
[148] R. S. Bedlack Jr., M. Wei, S. H. Fox, E. Gross, and L. M. Loew, “Distinct electric potentials in soma and neurite membranes,” *Neuron*, vol. 13, no. 5, pp. 1187–1193, Nov. 1994.
[149] K. Beppu *et al.*, “Optogenetic Countering of Glial Acidosis Suppresses Glial Glutamate Release and Ischemic Brain Damage,” *Neuron*, vol. 81, no. 2, pp. 314–320, Jan. 2014.
[150] M. El-Gaby, Y. Zhang, K. Wolf, C. J. Schwiening, O. Paulsen, and O. A. Shipton, “Archaerhodopsin Selectively and Reversibly Silences Synaptic Transmission through Altered pH,” *Cell Rep.*, vol. 16, no. 8, pp. 2259–2268, Aug. 2016.
[151] Y. Kato, H. Masumiya, N. Agata, H. Tanaka, and K. Shigenobu, “Developmental Changes in Action Potential and Membrane Currents in Fetal, Neonatal and Adult Guinea-pig Ventricular Myocytes,” *J. Mol. Cell. Cardiol.*, vol. 28, no. 7, pp. 1515–1522, Jul. 1996.
[152] O. Caspi *et al.*, “In Vitro Electrophysiological Drug Testing Using Human Embryonic Stem Cell Derived Cardiomyocytes,” *Stem Cells Dev.*, vol. 18, no. 1, pp. 161–172, May 2008.
[153] A. Haase *et al.*, “Generation of Induced Pluripotent Stem Cells from Human Cord Blood,” *Cell Stem Cell*, vol. 5, no. 4, pp. 434–441, Oct. 2009.
[154] G. C. L. Bett *et al.*, “Electronic ‘expression’ of the inward rectifier in cardiocytes derived from human-induced pluripotent stem cells,” *Heart Rhythm*, vol. 10, no. 12, pp. 1903–1910, Dec. 2013.
[155] H. Itoh, *Electrophysiological Simulation of Developmental Changes in Action Potentials of Cardiomyocytes*. Landes Bioscience, 2013.
[156] O. Scheel, S. Frech, B. Amuzescu, J. Eisfeld, K.-H. Lin, and T. Knott, “Action Potential Characterization of Human Induced Pluripotent Stem Cell–Derived Cardiomyocytes Using Automated Patch-Clamp Technology,” *ASSAY Drug Dev. Technol.*, vol. 12, no. 8, pp. 457–469, Oct. 2014.
[157] X. Lian *et al.*, “Chemically defined, albumin-free human cardiomyocyte generation,” *Nat. Methods*, vol. 12, no. 7, pp. 595–596, Jul. 2015.
[158] A. E. Cohen and V. Venkatachalam, “Bringing Bioelectricity to Light,” *Annu. Rev. Biophys.*, vol. 43, no. 1, pp. 211–232, 2014.
[159] G. T. Dempsey *et al.*, “Cardiotoxicity screening with simultaneous optogenetic pacing, voltage imaging and calcium imaging,” *J. Pharmacol. Toxicol. Methods*, vol. 81, pp. 240–250, Sep. 2016.
[160] A. Cohen and D. Hochbaum, “Measuring Membrane Voltage with Microbial Rhodopsins,” in *Fluorescent Protein-Based Biosensors*, J. Zhang, Q. Ni, and R. H. Newman, Eds. Humana Press, 2014, pp. 97–108.
[161] J. H. Hou, V. Venkatachalam, and A. E. Cohen, “Temporal Dynamics of Microbial Rhodopsin Fluorescence Reports Absolute Membrane Voltage,” *Biophys. J.*, vol. 106, no. 3, pp. 639–648, Feb. 2014.

[162] M. Suhaeri *et al.*, “Novel Platform of Cardiomyocyte Culture and Coculture via Fibroblast-Derived Matrix-Coupled Aligned Electrospun Nanofiber,” *ACS Appl. Mater. Interfaces*, vol. 9, no. 1, pp. 224–235, Jan. 2017.
[163] A. Marsano *et al.*, “Beating heart on a chip: a novel microfluidic platform to generate functional 3D cardiac microtissues,” *Lab. Chip*, vol. 16, no. 3, pp. 599–610, Feb. 2016.
[164] A. H. Fong *et al.*, “Three-Dimensional Adult Cardiac Extracellular Matrix Promotes Maturation of Human Induced Pluripotent Stem Cell-Derived Cardiomyocytes,” *Tissue Eng. Part A*, vol. 22, no. 15–16, pp. 1016–1025, 2016.
[165] M. D. Lemoine *et al.*, “Human iPSC-derived cardiomyocytes cultured in 3D engineered heart tissue show physiological upstroke velocity and sodium current density,” *Sci. Rep.*, vol. 7, no. 1, p. 5464, Jul. 2017.
[166] S. Sakai, K. Ueno, T. Ishizuka, and H. Yawo, “Parallel and patterned optogenetic manipulation of neurons in the brain slice using a DMD-based projector,” *Neurosci. Res.*, vol. 75, no. 1, pp. 59–64, Jan. 2013.
[167] R. A. B. Burton *et al.*, “Optical control of excitation waves in cardiac tissue,” *Nat. Photonics*, vol. 9, no. 12, pp. 813–816, Dec. 2015.
[168] E. Entcheva and G. Bub, “All-optical control of cardiac excitation: combined high-resolution optogenetic actuation and optical mapping,” *J. Physiol.*, vol. 594, no. 9, pp. 2503–2510, May 2016.
[169] J. Mattis *et al.*, “Principles for applying optogenetic tools derived from direct comparative analysis of microbial opsins,” *Nat. Methods*, vol. 9, no. 2, pp. 159–172, Feb. 2012.
[170] E. G. Govorunova, O. A. Sineshchekov, R. Janz, X. Liu, and J. L. Spudich, “Natural light-gated anion channels: A family of microbial rhodopsins for advanced optogenetics,” *Science*, vol. 349, no. 6248, pp. 647–650, Aug. 2015.
[171] C. M. Ambrosi, A. Klimas, J. Yu, and E. Entcheva, “Cardiac applications of optogenetics,” *Prog. Biophys. Mol. Biol.*, vol. 115, no. 2–3, pp. 294–304, Aug. 2014.
[172] E. Entcheva, “Cardiac optogenetics,” *Am. J. Physiol. - Heart Circ. Physiol.*, vol. 304, no. 9, pp. H1179–H1191, May 2013.
[173] I. P. Clements *et al.*, “Optogenetic stimulation of multiwell MEA plates for neural and cardiac applications,” 2016, vol. 9690, pp. 96902C-96902C–10.
[174] J. K. Gibson, Y. Yue, J. Bronson, C. Palmer, and R. Numann, “Human stem cell-derived cardiomyocytes detect drug-mediated changes in action potentials and ion currents,” *J. Pharmacol. Toxicol. Methods*, vol. 70, no. 3, pp. 255–267, Nov. 2014.
[175] L. Guo *et al.*, “Estimating the Risk of Drug-Induced Proarrhythmia Using Human Induced Pluripotent Stem Cell–Derived Cardiomyocytes,” *Toxicol. Sci.*, vol. 123, no. 1, pp. 281–289, Sep. 2011.
[176] G. Thomas, M. Chung, and C. J. Cohen, “A dihydropyridine (Bay k 8644) that enhances calcium currents in guinea pig and calf myocardial cells. A new type of positive inotropic agent,” *Circ. Res.*, vol. 56, no. 1, pp. 87–96, Jan. 1985.
[177] M. Bechem and H. Hoffmann, “The molecular mode of action of the Ca agonist (-) BAY K 8644 on the cardiac Ca channel,” *Pflugers Arch.*, vol. 424, no. 3–4, pp. 343–353, Aug. 1993.
[178] I. R. Josephson and N. Sperelakis, “Fast activation of cardiac Ca++ channel gating charge by the dihydropyridine agonist, BAY K 8644.,” *Biophys. J.*, vol. 58, no. 5, pp. 1307–1311, Nov. 1990.

[179] J. Woodcock, “Hoechst Marion Roussel, Inc., and Baker Norton Pharmaceuticals, Inc.; Terfenadine; Withdrawal of Approval of Two New Drug Applications and One Abbreviated New Drug Application,” Federal Register, Sep. 1998.
[180] R. L. Woosley, Y. Chen, J. P. Freiman, and R. A. Gillis, “Mechanism of the Cardiotoxic Actions of Terfenadine,” *JAMA*, vol. 269, no. 12, pp. 1532–1536, Mar. 1993.
[181] J. J. Salata, N. K. Jurkiewicz, A. A. Wallace, R. F. Stupienski, P. J. Guinosso, and J. J. Lynch, “Cardiac electrophysiological actions of the histamine H1-receptor antagonists astemizole and terfenadine compared with chlorpheniramine and pyrilamine,” *Circ. Res.*, vol. 76, no. 1, pp. 110–119, Jan. 1995.
[182] M. Roy, R. Dumaine, and A. M. Brown, “HERG, a primary human ventricular target of the nonsedating antihistamine terfenadine,” *Circulation*, vol. 94, no. 4, pp. 817–823, Aug. 1996.
[183] D. Fernandez, A. Ghanta, G. W. Kauffman, and M. C. Sanguinetti, “Physicochemical features of the HERG channel drug binding site,” *J. Biol. Chem.*, vol. 279, no. 11, pp. 10120–10127, Mar. 2004.
[184] W. G. Nayler and J. S. Dillon, “Calcium antagonists and their mode of action,” *Br. J. Clin. Pharmacol.*, vol. 21, no. Suppl 2, pp. 97S-107S, 1986.
[185] G. R. Lewis, K. D. Morley, B. M. Lewis, and P. J. Bones, “The treatment of hypertension with verapamil,” *N. Z. Med. J.*, vol. 87, no. 612, pp. 351–354, May 1978.
[186] W. Frishman *et al.*, “Twice-Daily Administration of Oral Verapamil in the Treatment of Essential Hypertension,” *Arch. Intern. Med.*, vol. 146, no. 3, pp. 561–565, Mar. 1986.
[187] B. D. Johnson, G. H. Hockerman, T. Scheuer, and W. A. Catterall, “Distinct effects of mutations in transmembrane segment IVS6 on block of L-type calcium channels by structurally similar phenylalkylamines,” *Mol. Pharmacol.*, vol. 50, no. 5, pp. 1388–1400, Nov. 1996.
[188] P. Bergson, G. Lipkind, S. P. Lee, M.-E. Duban, and D. A. Hanck, “Verapamil Block of T-Type Calcium Channels,” *Mol. Pharmacol.*, vol. 79, no. 3, pp. 411–419, Mar. 2011.
[189] L. X. Cubeddu *et al.*, “A Comparison of Verapamil and Propranolol for the Initial Treatment of Hypertension: Racial Differences in Response,” *JAMA*, vol. 256, no. 16, pp. 2214–2221, Oct. 1986.
[190] K. Midtbø, O. Hals, O. Lauve, J. van der Meer, and L. Storstein, “Studies on verapamil in the treatment of essential hypertension: a review,” *Br. J. Clin. Pharmacol.*, vol. 21 Suppl 2, pp. 165S-171S, 1986.
[191] A. Bril *et al.*, “Combined potassium and calcium channel blocking activities as a basis for antiarrhythmic efficacy with low proarrhythmic risk: experimental profile of BRL-32872,” *J. Pharmacol. Exp. Ther.*, vol. 276, no. 2, pp. 637–646, Feb. 1996.
[192] G. H. Dersham and J. Han, “Effects of verapamil on action potentials of Purkinje fibers,” *J. Electrocardiol.*, vol. 13, no. 1, pp. 67–71, Jan. 1980.
[193] R. S. Kass and R. W. Tsien, “Multiple effects of calcium antagonists on plateau currents in cardiac Purkinje fibers,” *J. Gen. Physiol.*, vol. 66, no. 2, pp. 169–192, Aug. 1975.
[194] S. Zhang, T. Sawanobori, Y. Hirano, and M. Hiraoka, “Multiple modulations of action potential duration by different calcium channel blocking agents in guinea pig ventricular myocytes,” *J. Cardiovasc. Pharmacol.*, vol. 30, no. 4, pp. 489–496, Oct. 1997.
[195] K. Blinova *et al.*, “Comprehensive Translational Assessment of Human-Induced Pluripotent Stem Cell Derived Cardiomyocytes for Evaluating Drug-Induced Arrhythmias,” *Toxicol. Sci. Off. J. Soc. Toxicol.*, vol. 155, no. 1, pp. 234–247, Jan. 2017.

[196] D. K. Lieu *et al.*, “Mechanism-based facilitated maturation of human pluripotent stem cell-derived cardiomyocytes,” *Circ. Arrhythm. Electrophysiol.*, vol. 6, no. 1, pp. 191–201, Feb. 2013.
[197] E. A. SOBIE, L.-S. SONG, and W. J. LEDERER, “Restitution of Ca2+ Release and Vulnerability to Arrhythmias,” *J. Cardiovasc. Electrophysiol.*, vol. 17, no. Suppl 1, pp. S64–S70, May 2006.
[198] M. K. B. Jonsson *et al.*, “Application of human stem cell-derived cardiomyocytes in safety pharmacology requires caution beyond hERG,” *J. Mol. Cell. Cardiol.*, vol. 52, no. 5, pp. 998–1008, May 2012.
[199] S. Bedut *et al.*, “High-throughput drug profiling with voltage- and calcium-sensitive fluorescent probes in human iPSC-derived cardiomyocytes,” *Am. J. Physiol.-Heart Circ. Physiol.*, vol. 311, no. 1, pp. H44–H53, May 2016.
[200] G. Rast, J. Weber, C. Disch, E. Schuck, C. Ittrich, and B. D. Guth, “An integrated platform for simultaneous multi-well field potential recording and Fura-2-based calcium transient ratiometry in human induced pluripotent stem cell (hiPSC)-derived cardiomyocytes,” *J. Pharmacol. Toxicol. Methods*, vol. 75, pp. 91–100, Sep. 2015.
[201] J. Kang, X.-L. Chen, J. Ji, Q. Lei, and D. Rampe, “Ca2+ Channel Activators Reveal Differential L-Type Ca2+ Channel Pharmacology between Native and Stem Cell-Derived Cardiomyocytes,” *J. Pharmacol. Exp. Ther.*, vol. 341, no. 2, pp. 510–517, May 2012.
[202] Z. Qu, Y. Xie, A. Garfinkel, and J. N. Weiss, “T-Wave Alternans and Arrhythmogenesis in Cardiac Diseases,” *Front. Physiol.*, vol. 1, 2010.
[203] M. J. Shattock *et al.*, “Restitution slope is principally determined by steady-state action potential duration,” *Cardiovasc. Res.*, vol. 113, no. 7, pp. 817–828, Jun. 2017.
[204] D. T. M. Du, N. Hellen, C. Kane, and C. M. N. Terracciano, “Action Potential Morphology of Human Induced Pluripotent Stem Cell-Derived Cardiomyocytes Does Not Predict Cardiac Chamber Specificity and Is Dependent on Cell Density,” *Biophys. J.*, vol. 108, no. 1, pp. 1–4, Jan. 2015.
[205] Y. Amano *et al.*, “Development of vascularized iPSC derived 3D-cardiomyocyte tissues by filtration Layer-by-Layer technique and their application for pharmaceutical assays,” *Acta Biomater.*, vol. 33, pp. 110–121, Mar. 2016.
[206] J. Pasquier *et al.*, “Coculturing with endothelial cells promotes in vitro maturation and electrical coupling of human embryonic stem cell–derived cardiomyocytes,” *J. Heart Lung Transplant.*, vol. 36, no. 6, pp. 684–693, Jun. 2017.
[207] J. Huo *et al.*, “Evaluation of Batch Variations in Induced Pluripotent Stem Cell-Derived Human Cardiomyocytes from 2 Major Suppliers,” *Toxicol. Sci. Off. J. Soc. Toxicol.*, vol. 156, no. 1, pp. 25–38, Mar. 2017.
[208] S. Lou *et al.*, “Genetically Targeted All-Optical Electrophysiology with a Transgenic Cre-Dependent Optopatch Mouse,” *J. Neurosci. Off. J. Soc. Neurosci.*, vol. 36, no. 43, pp. 11059–11073, Oct. 2016.
[209] B. D. Allen, A. C. Singer, and E. S. Boyden, “Principles of designing interpretable optogenetic behavior experiments,” *Learn. Mem.*, vol. 22, no. 4, pp. 232–238, Apr. 2015.
[210] L. Madisen *et al.*, “A toolbox of Cre-dependent optogenetic transgenic mice for light-induced activation and silencing,” *Nat. Neurosci.*, vol. 15, no. 5, pp. 793–802, May 2012.

[211] K. Beppu *et al.*, "Optogenetic Countering of Glial Acidosis Suppresses Glial Glutamate Release and Ischemic Brain Damage," *Neuron*, vol. 81, no. 2, pp. 314–320, Jan. 2014.
[212] H. Adesnik, W. Bruns, H. Taniguchi, Z. J. Huang, and M. Scanziani, "A neural circuit for spatial summation in visual cortex," *Nature*, vol. 490, no. 7419, pp. 226–231, Oct. 2012.
[213] M. T. Stefanik *et al.*, "Optogenetic inhibition of cocaine seeking in rats," *Addict. Biol.*, vol. 18, no. 1, pp. 50–53, Jan. 2013.
[214] J. V. Raimondo, L. Kay, T. J. Ellender, and C. J. Akerman, "Optogenetic silencing strategies differ in their effects on inhibitory synaptic transmission," *Nat. Neurosci.*, vol. 15, no. 8, pp. 1102–1104, Aug. 2012.
[215] A. B. Arrenberg, D. Y. R. Stainier, H. Baier, and J. Huisken, "Optogenetic control of cardiac function," *Science*, vol. 330, no. 6006, pp. 971–974, Nov. 2010.
[216] Y. Wang *et al.*, "Optogenetic Control of Heart Rhythm by Selective Stimulation of Cardiomyocytes Derived from Pnmt(+) Cells in Murine Heart," *Sci. Rep.*, vol. 7, p. 40687, Jan. 2017.
[217] T. Bruegmann *et al.*, "Optogenetic control of heart muscle in vitro and in vivo," *Nat. Methods*, vol. 7, no. 11, pp. 897–900, Nov. 2010.
[218] H. Zhang, E. Reichert, and A. E. Cohen, "Optical electrophysiology for probing function and pharmacology of voltage-gated ion channels," *eLife*, vol. 5, May 2016.
[219] C. M. Ambrosi, P. M. Boyle, K. Chen, N. A. Trayanova, and E. Entcheva, "Optogenetics-enabled assessment of viral gene and cell therapy for restoration of cardiac excitability," *Sci. Rep.*, vol. 5, p. 17350, Dec. 2015.
[220] M. K. B. Jonsson *et al.*, "Application of human stem cell-derived cardiomyocytes in safety pharmacology requires caution beyond hERG," *J. Mol. Cell. Cardiol.*, vol. 52, no. 5, pp. 998–1008, May 2012.
[221] S. Li, H. Cheng, G. F. Tomaselli, and R. A. Li, "Mechanistic basis of excitation-contraction coupling in human pluripotent stem cell-derived ventricular cardiomyocytes revealed by Ca2+ spark characteristics: Direct evidence of functional Ca2+-induced Ca2+ release," *Heart Rhythm*, vol. 11, no. 1, pp. 133–140, Jan. 2014.
[222] S. Goineau and V. Castagné, "Electrophysiological characteristics and pharmacological sensitivity of two lines of human induced pluripotent stem cell derived cardiomyocytes coming from two different suppliers," *J. Pharmacol. Toxicol. Methods*, vol. 90, pp. 58–66, Mar. 2018.
[223] D. Schocken *et al.*, "Comparative analysis of media effects on human induced pluripotent stem cell-derived cardiomyocytes in proarrhythmia risk assessment," *J. Pharmacol. Toxicol. Methods*, vol. 90, pp. 39–47, Apr. 2018.
[224] M. L. Milstein *et al.*, "Dynamic reciprocity of sodium and potassium channel expression in a macromolecular complex controls cardiac excitability and arrhythmia," *Proc. Natl. Acad. Sci. U. S. A.*, vol. 109, no. 31, pp. E2134-2143, Jul. 2012.
[225] J. Li *et al.*, "Calmodulin kinase II inhibition shortens action potential duration by upregulation of K+ currents," *Circ. Res.*, vol. 99, no. 10, pp. 1092–1099, Nov. 2006.
[226] A. Zaza, M. Rocchetti, A. Brioschi, A. Cantadori, and A. Ferroni, "Dynamic Ca2+-induced inward rectification of K+ current during the ventricular action potential," *Circ. Res.*, vol. 82, no. 9, pp. 947–956, May 1998.
[227] C.-H. Liu, H.-K. Chang, S.-P. Lee, and R.-C. Shieh, "Activation of the Ca2+-sensing receptors increases currents through inward rectifier K+ channels via activation of

phosphatidylinositol 4-kinase," *Pflugers Arch.*, vol. 468, no. 11–12, pp. 1931–1943, 2016.
[228] V. G. Romanenko *et al.*, "Cholesterol sensitivity and lipid raft targeting of Kir2.1 channels," *Biophys. J.*, vol. 87, no. 6, pp. 3850–3861, Dec. 2004.
[229] C. A. Karle *et al.*, "Human cardiac inwardly-rectifying K+ channel Kir(2.1b) is inhibited by direct protein kinase C-dependent regulation in human isolated cardiomyocytes and in an expression system," *Circulation*, vol. 106, no. 12, pp. 1493–1499, Sep. 2002.
[230] C. Munoz, A. Almilaji, I. Setiawan, M. Föller, and F. Lang, "Up-regulation of the inwardly rectifying K^+ channel Kir2.1 (KCNJ2) by protein kinase B (PKB/Akt) and PIKfyve," *J. Membr. Biol.*, vol. 246, no. 3, pp. 189–197, Mar. 2013.
[231] C. Seyler *et al.*, "Role of plasma membrane-associated AKAPs for the regulation of cardiac IK1 current by protein kinase A," *Naunyn. Schmiedebergs Arch. Pharmacol.*, vol. 390, no. 5, pp. 493–503, May 2017.
[232] S. Yoshida *et al.*, "Maturation of Human Induced Pluripotent Stem Cell-Derived Cardiomyocytes by Soluble Factors from Human Mesenchymal Stem Cells," *Mol. Ther.*, Aug. 2018.